LAPPEENRANTA UNIVERSITY OF TECHNOLOGY
LUT School of Engineering Science
Degree Programme in Chemical Engineering

Mikko Äijälä

EFFECT OF PARTICLE FRACTIONATION ON THE VACUUM FILTRATION PERFORMANCE OF MAGNETITE SUSPENSIONS

Examiners: Professor, D.Sc. (Tech.) Antti Häkkinen
Professor, D.Sc. (Tech.) Tuomas Koiranen
Instructors: M.Sc. (Tech.) Janne Kauppi
D.Sc. (Tech.) Teemu Kinnarinen

ABSTRACT

Lappeenranta University of Technology
LUT School of Engineering Science
Degree Programme in Chemical Engineering

Mikko Äijälä

Effect of particle fractionation on the vacuum filtration performance of magnetite suspensions

Master's Thesis

2016

85 pages, 58 figures, 16 tables, 7 appendices

Examiners: Professor, D.Sc. (Tech.) Antti Häkkinen
Professor, D.Sc. (Tech.) Tuomas Koiranen

Keywords: cake filtration, fractionation, slurry, particle size distribution, pre-coating, filtrate flow, filtration capacity

Cake filtration is one of the most commonly used solid-liquid separation techniques in different sectors of chemical industry. Mining industry produces vast amount of slurries that are dewatered, for example, by continuous horizontal vacuum belt filtration. The slurries typically include large amount of fine particles of different sizes. Filtration capacity and filtrate flow rate through the cake are strongly dependent on the size and the accumulation order of the slurry particles on top of the filter medium. In case the coarser particles formed the lower layer of the cake, the filtration capacity and the filtrate flow rate could be possibly improved.

In this work, it was investigated how the fractionation of fine and coarse magnetite particles into separate layers affects the filtration capacity, the filtrate flow rate and the cake moisture content. Three sieves of different sizes were used in particle fractionation and the filtration experiments were carried out by filtering both non-fractionated and fractionated magnetite slurry batches with Büchner vacuum filtration equipment. Four different weight ratios between fine and coarse particle layer were used in the batch filtration tests with the fractionated suspensions. The experiments contained filtration tests with and without settling of the slurry. Separate sedimentation experiments were also carried out in order to produce data for possible future studies regarding particle fractionation in a horizontal pipe flow.

The filtration experiments revealed that by using the chosen fractionation methods only minor improvements in terms of filtration capacity were achieved. The average filtrate flow rates were lower when fractionation was used, and the moisture contents of the cakes did not significantly change. It was observed that by optimizing the volumetric size distribution width ratio between fine and coarse particles in a narrow scale, minor improvements in terms of filtration capacity could be achieved.

TIIVISTELMÄ

Lappeenrannan teknillinen yliopisto
LUT School of Engineering Science
Kemiantekniikan koulutusohjelma

Mikko Äijälä

Partikkelifraktioinnin vaikutus magnetiittisuspensioiden vakuumisuodatusprosessiin

Diplomityö

2016

85 sivua, 58 kuvaa, 16 taulukkoa, 7 liitettä

Työn tarkastajat: Professori, TkT Antti Häkkinen
Professori, TkT Tuomas Koiranen

Hakusanat: kakkusuodatus, fraktiointi, liete, partikkelikokojakauma, pre-coating, suodoksen läpivirtaus, suodatuskapasiteetti

Kakkusuodatus on yksi yleisimmin käytetyistä neste-kiintoaine –erotusmenetelmistä eri kemianteollisuuden aloilla. Kaivosteollisuus tuottaa valtavia määriä lietteitä, joista poistetaan vettä esimerkiksi jatkuvatoimisella horisontaalivakuuminauhasuodatuksella. Lietemassat sisältävät tyypillisesti suuria määriä erikokoisia hienojakoisia partikkeleita. Suodatuskapasiteetti ja suodoksen läpivirtaus muodostuneen kakun läpi ovat pitkälti riippuvaisia partikkelien koosta sekä niiden asettumisjärjestyksestä suodinmateriaalin päälle. Isompien partikkelien muodostaessa alimman kakkukerroksen, suodatuskapasiteettia ja suodoksen läpivirtausta voitaisiin mahdollisesti parantaa.

Tässä työssä tutkittiin, miten hienojakoisten ja karkeiden magnetiittipartikkelien fraktiointi erillisiin kerroksiin vaikuttaa suodatuskapasiteettiin, suodoksen läpivirtaukseen ja kakun kosteuspitoisuuteen. Partikkelien fraktioinnissa käytettiin kolmea eri seulakokoa ja suodatuskokeet suoritettiin fraktioimattomilla ja fraktioiduilla magnetiittilietteillä Büchner-vakuumisuodatuslaitteella. Fraktiointisuodatuksissa käytettiin neljää eri painosuhdetta hienojakoisen ja karkean partikkelikerroksen välillä. Suodatuskokeita tehtiin ilman lietteen laskeutusta sekä laskeutuksen kanssa. Liete-erillä tehtiin myös laskeutuskokeita joista saatiin tutkimustietoa mahdollisia jatkotutkimuksia varten.

Suodatuskokeet osoittivat että valittu fraktiointitapa parantaa vain hieman suodatuskapasiteettia. Suodoksen keskimääräinen läpivirtaus jäi alhaisemmaksi verrattuna fraktioimattomaan lietteeseen, ja muodostuneen kakun kosteuspitoisuus ei merkittävästi muuttunut. Kokeet osoittivat, että suodatuskapasiteettia voitiin parantaa hieman optimoimalla hienojakoisten ja karkeiden partikkelien tilavuuskokojakauman suhdetta kapealla välillä.

SYMBOLS

A	Cross-sectional area of the bed, m^2
A_B	Area of particles, m^2
A_F	Flow area, m^2
A_p	Particle area, m^2
A_s	Sedimentation area, m^2
Ar	Archimedes number, -
a	Small particle fraction in SPLITT process, -
a'	Initial sample containing small and large particles in SPLITT process, -
b	Fraction containing large and small particles in SPLITT process, -
C	Solid volume fraction, -
c	Filtration concentration, kg/m^3
C_D	Drag coefficient, -
C_s	Volume fraction of particles, -
$D[3;2]$	Sauter mean diameter, m
D, d	Particle diameter, m
$D[4;3]$	Volume mean diameter, m
$Dx(10)$	Particle diameter, below which are 10 % of the particles in the sample, µm
$Dx(50)$	Particle diameter, below which are 50 % of the particles in the sample, µm
$Dx(90)$	Particle diameter, below which are 90 % of the particles in the sample, µm
e_a	The unit vector of the major axis of the spheroid, m
e_b	The unit vector of the minor axis of the spheroid, m
e_f	The unit vector of the frictional force, m
e_n	The unit normal contact vector, m
e_t	The unit tangential contact vector, m
e_x	The unit vector of the abscissa of the filter, m
e_y	The unit vector of the coordinate of the filter, m
F_A	Buoyancy force, kgm/s^2
F_c	Coarse material description in a separator mass balance calculations, -
F_D	Drag force during particle settling in a gravitational field, kgm/s^2
F_d	The frictional drag force due to fluid flow during particle packing on a filter medium, kgm/s^2
F_f	The frictional force, kgm/s^2 OR fine material description in a separator mass balance calculations, -
$F_{p,g}$	Gravitational force for a spherical particle, kgm/s^2
F_n	The normal force, kgm/s^2
F_o	The sum of F_d and F_g, kgm/s^2
F_R	Hydrodynamic force, kgm/s^2
g	Gravitational constant, m/s^2
h_L	Hold-up of the liquid, -
h_s	Hold-up of the solids, -
h	Slurry height, m
K	Kozeny constant, -
k	Permeability, m^2

L	Bed depth, m
M	Mass flow rate, kg/s
M_c	Mass flow rate of the coarse material in the underflow, kg/s
M_f	Mass flow rate of the fine material in the overflow, kg/s
m	The centroid of particle *m*, -
m_f	Filtrate mass, g
n	Compressibility index, -
o	The centroid of particle *o*, -
O	Volumetric flow rate of the overflow suspension, m^3/s
P	Pressure, Pa
Q	Flow rate, m^3/s
q	The filtration velocity, m^3/m^2s
R	Medium resistance, 1/m
r	Radius of the inner surface of the liquid in a centrifugal field, m
R_c	Cake resistance, 1/m
Re	Reynolds number, -
Re_p	Particle Reynolds number, -
S	Cake saturation, -
S_B	Solid cake layer specific surface area, m^2/m^3
S_p	Particle specific surface area, m^2/m^3
S_0	Spherical particle specific surface area, m^{-1}
t	Time, s
t_s	Constant pressure filtration starting time, s
U	Volumetric flow rate of the underflow suspension, m^3/s
u	Particle-fluid relative velocity (slip velocity), m/s
u_d	Terminal settling velocity of the particle, m/s
u_m	Mixture velocity, m/s
u'_L	Absolute linear velocity of the liquid, m/s
u'_S	Absolute linear velocity of the particle, m/s
V	Volume, m^3
v	Proportion of particles in the size fraction, -
V_B	Solid cake layer volume, m^3
V_l	Volume of liquid in the cake, m^3
V_p	Particle volume, m^3
V_s	Volume of filtrate obtained before achieving the desired constant pressure, m^3
V_T	Total bed volume, m^3
V_v	Volume of voids, m^3
W_c	Constant fall velocity, m/s
w	Mass of cake deposited per unit area, kg/m^2
x	Particle size in a separator mass balance calculations, -
z	Richardson-Zaki index, -
α	Specific cake resistance, m/kg
α_{av}	Average cake specific resistance, m/kg
α_0	Resistance at unit applied pressure difference, m/kg
Δ	Difference, -
ε	Cake porosity, -
ε_B	Bed voidage, -
θ	Angle, °
μ	Viscosity, kg/ms

ν	Kinematic viscosity, m^2/s
π	Constant, -
ρ	Density, kg/m^3
σ	Standard deviation of size distribution, m
Ψ	Sedimentation flux, kg/m^2s
ω	Angular velocity in a centrifugal field, rad/s

TABLE OF CONTENTS

INTRODUCTION

Vacuum belt filtration is a typical process employed to treat vast amount of slurries produced by the mining industry. In order to improve the filtration capacity of the process, pre-treatment of the slurry is essential. One possible pre-treatment techniques is fractionation of the slurry particles into coarse and fine fractions before the slurry is dewatered. It is assumed that separating the coarser particles to form the lower layer of the cake, filtration capacity of the process could possibly be improved by decreasing the average specific cake resistance. Different types of classifiers are commonly employed for particle fractionation. However, more energy efficient fractionation techniques are still being developed. Using horizontal pipe flow fractionation of the slurry particles in an industrial scale is one of the options that has not yet been used and investigated much.

Objective of this work was to study how fractionation of particles into separate fine and coarse fractions affects the filtrate flow rate during filtration, filtration capacity of the process and the final moisture content of the magnetite cake. It was hypothesized that fractionation of particles improves the filtration performance.

Literature part of this thesis reviews the background of solid-liquid separation and cake filtration processes. The basic theory of cake formation and particle settling are introduced. The basics of particle properties, particle deposition in packed beds and the most used classification equipment are presented. Fluid mechanics and basics of multiphase flow phenomena are also reviewed.

The experimental part focuses on carrying out filtration experiments with non-fractionated and fractionated magnetite slurry batches by using Büchner vacuum filtration equipment. In order to study the effect of particle fractionation on the filtrate flow rate, filtration capacity and cake moisture content, the values gained from the non-fractionated cake filtration tests were compared with the ones from the fractionated cake filtration tests. Cake compressibility was determined by filtering several non-fractionated slurry batches at different vacuum pressures. The fine and coarse particle fractions were obtained by using three sieves of different sizes. The volumetric particle size distributions of the fractions and the cake layers were determined by using laser diffraction technique and scanning electron microscope was employed to investigate particle deposition in the cake layers. Also sedimentation experiments were conducted in order to find out settling behavior of the magnetite slurry and to gain data for possible fractionation studies in the future.

LITERATURE PART

1 SOLID-LIQUID FILTRATION

1.1 Background

Filtration processes in solid-liquid separation have been used in mining industry for several purposes already for decades. Due to the current global trend, more effective, environmentally friendly and sustainable filtration processes are being designed to meet even tightening demands and regulations. This means that processes should be more energy intensive and consume less natural resources in the future.

Generally, solid-liquid separation processes are used to serve several purposes in industrial scale that mainly include recovery of valuable solid component, liquid or both solid and liquid phases and cleaning the liquid phase in order to prevent water pollution. The processes can be used either continuously or batchwise, depending on the chosen equipment. Solid-liquid separation con be considered to consist of four consecutive stages, including pre-treatment, solids concentration, solids separation and post-treatment of the cake or the liquid. [1]

Slurry dewatering by vacuum belt filtration is one of the most essential areas in solid-liquid filtration. Slurry is considered as a mass containing suspended solids and fluid and slurries are produced by many industrial segments in a large scale worldwide. A lot of attention has recently been paid on utilizing the slurries, since they could be re-processed into other useful products. Useful components of the slurry could be beneficial for example in agriculture. [2]

1.2 Vacuum belt filtration process

The main purpose of vacuum filtration is to form a solid cake on top of a filter medium. Vacuum filtration is based on a pressure suction on the filtrate side of the filter medium. The pressure suction is the driving force that removes water from the solid mass. Vacuum filtration processes are divided mainly into batch-operated and continuous. [3]

The main function of the vacuum belt filtration process is based on a continuously moving belt affected by a constant vacuum pressure underneath. The feed stream is fed onto the belt, where it is immediately exposed to the pressure difference. The separated liquid, filtrate, is transferred through the filter medium by the pressure difference. As the solid mass moves along the belt onwards, the moisture content decreases, and the solid cake is formed during the movement. At the end of the belt the formed cake is collected and stored, or passed on to further treatment. The cake can also be washed during the process, and some part of the filtrate can be recycled back either to the feed stream or for the washing purposes. The basic structure and operating principle of a horizontal belt filter is described in Figure 1.

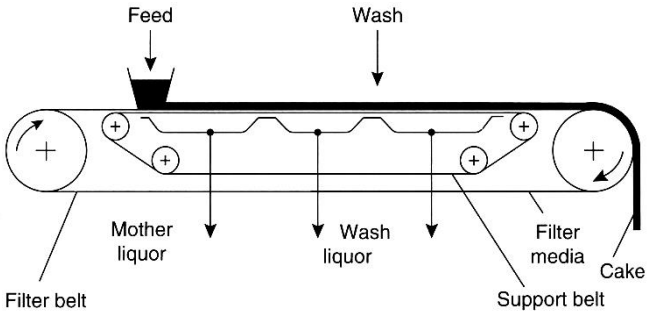

Figure 1. Horizontal vacuum belt filter [4].

Horizontal vacuum belt filters are capable to treat many different types of slurries. Separation characteristics of slurries vary a lot, for example in terms of cake formation rate, normal concentration and settling rate [4]. The process is able to treat large capacities of sludge with filtration areas up to more than 200 m^2 at fast belt speeds up to 30 meters per minute [3]. High belt speeds are used to treat fast-filtering materials like mineral slurries, and the process can be applied to both fast and slowly draining solids [5]. Generally, the practical pressure difference used in vacuum filters is limited to 70 or 80 kPa or even below that [3, 5].

Generally, the position of the filtration area with respect to gravity brings many advantages to vacuum filtration [3, 6]. For example, substantial blinding of the filter medium can be prevented by the formation of a pre-coat layer consisting of the coarser particles due to gravity settling before the vacuum is applied [3], and the feed slurry can be delivered onto the filter medium by gravity flow [6]. As the applied pressure in the process is quite low, the structure of the equipment is not significantly stressed. This makes it possible to use a wide range of materials for manufacturing of the equipment [6]. One of the most notable advantages in vacuum filtration is also the fact that the formed cake can be easily washed and removed after dewatering [6]. However, vacuum filtration has also a few drawbacks, for example larger filtration areas are needed and that requires higher capital costs [3].

Horizontal belt vacuum filters are suitable for fast-filtering materials such as mineral slurries and both fast and slowly draining solids where washing requirements are essential. The filters are able to treat solids that form cakes with the thickness ranging from 3 to 150 mm, solids capacity ranging between 10 – 500 kg of solids per square meter of filtration area per hour. [3] Depending on the type of the filtered slurry, filtration velocity and dry cake production rate can vary from 0.25 to 10 m^3/m^2h and from 6.8 to 678 g/m^2s respectively [3].

Better washing of the formed cake can sometimes be achieved if dewatering is performed before the washing [3]. Countercurrent washing of the cake is generally employed in horizontal vacuum filters. Wash liquor is first applied to the final stage of the filtration, after which the wash effluent is used as the wash liquor for the preceding stage. [7] It has been presented by Wakeman and Tarleton [7], that lower belt speed results in a thicker cake and may improve the washing characteristics. This leads to an increased cake resistance, reducing the air flux during dewatering thus leading to a higher moisture content of the discharged cake. [7]

According to Tsang and Vesilind [8], moisture in slurries can be distributed in four different forms: free moisture that is not attached to the particles of the slurry, interstitial moisture that is located between the solids, surface moisture on the surface of the particles and intracellular and chemically bound moisture. The status of the water in the slurry and the type of the dewatering process define the amount of water that can be removed. Free water, as described in Figure 2, can be removed by mechanical dewatering. The remaining bound water (Figure 2), including both chemically bound moisture and the partial surface moisture, is considered as the theoretical limit of mechanical dewatering. [8, 9]

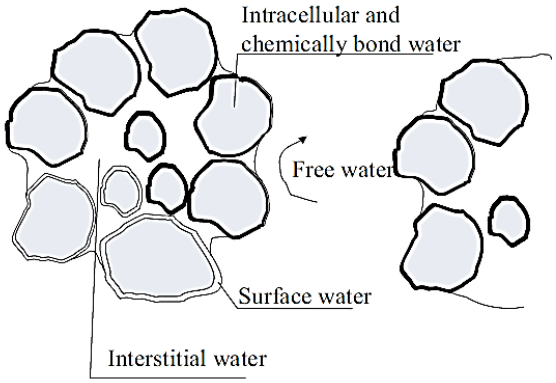

Figure 2. Water distribution in a slurry [8].

The moisture content of the formed cake can be reduced by dewatering, which in the case of horizontal vacuum filters occurs by displacement of liquid by air under vacuum pressure [3]. Increase of the applied vacuum pressure and wash liquor temperature are known to decrease the moisture content of the discharged cake in horizontal belt filtration process. According to Wakeman and Tarleton [7], when the applied vacuum pressure ranges between 20 – 80 kPa and wash liquor temperature ranges between 5 – 35 °C, the moisture content of the discharged cake ranges between 39 – 48 %. This, however, depends on the material being filtered.

2 FILTER CAKE

2.1 Cake formation and cake layer

Cake filtration is considered when particles form a deposit on the filter medium surface. As described in Figure 3, filter cake is formed basically by two primary mechanisms, complete blocking and bridging. [1] Complete blocking typically refers to a situation where the filter medium is blinded by the solid particles, due to too low solids concentration, for example, and this normally results in failure of the filtration process. Thus the aim is always to achieve successful bridging process to take place in the beginning of filtration.

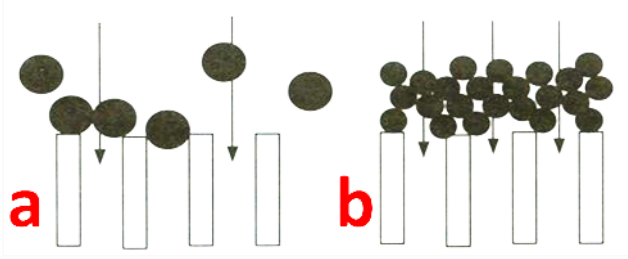

Figure 3. Cake formation on a filter medium by complete blocking (a) and bridging (b) [1].

Filter cake is formed when the solid particles within the slurry start to accumulate on a filter medium. It is known that the cake is formed mainly because of the bridging mechanism of particles over the surface pores. The type of filter medium has an essential role in initiating the filtration and on the properties and structure of the filter cake. [10] The cake starts to form due to the pressure difference across the filter medium and pressure difference can be generated by four different types of driving forces: gravity, vacuum, pressure and centrifugal. [3] Cake formation on a filter medium is illustrated in Figure 4.

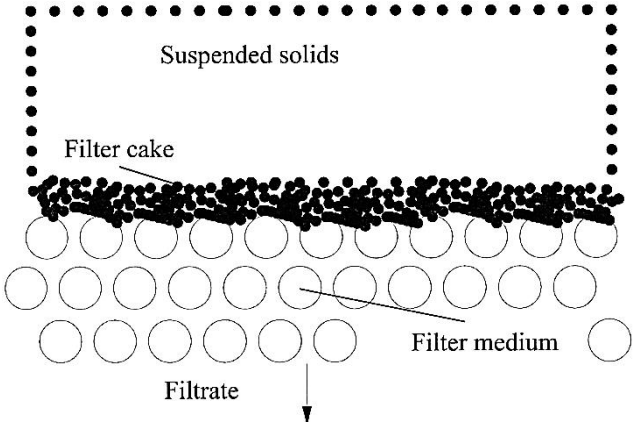

Figure 4. Cake formation on a filter medium [10].

Total volume of a porous medium is formed by voids and solid structures. Porosity ε, the volume fraction of the bed available for fluid flow, is an essential quantity and is defined as [10]:

$$\varepsilon = \frac{V_v}{V_T} \tag{1}$$

where V_v Volume of voids in the cake, m^3

V_T Total bed volume, m^3

Total volume fraction in a porous medium is the sum of void (ε) and solid (C) fractions [10]:

$$\varepsilon + C = 1 \tag{2}$$

Thus, solid volume fraction concentration is calculated [10]:

$$C = 1 - \varepsilon \tag{3}$$

Each particle has the specific surface area that is defined as [11]:

$$S_p = \frac{A_p}{V_p} \tag{4}$$

where S_p Particle specific surface area, m^2/m^3

A_p Area of the particle, m^2

V_p Volume of the particle, m^3

For a spherical particle the specific surface area is [1]:

$$S_0 = \frac{6}{d} \tag{5}$$

where S_0 Specific surface area of a spherical particle, m^{-1}

d Diameter of the particle, m

The specific surface for the whole solid cake layer is defined as [11]:

$$S_B = \frac{A_B}{V_B} \tag{6}$$

where S_B Specific surface area of the solid cake layer, m^2/m^3

A_B Area of the particles, m^2

V_B Volume of the solid cake layer, m^3

In case the where the solid layer is formed completely by particles of the same size and shape, the specific surface area can be defined as [12]:

$$S_B = S_p(1-\varepsilon) \tag{7}$$

In order to define particle size, the so-called surface mean diameter, Sauter mean diameter D[3;2] is often used. This particle size is obtained by converting the volumetric distribution to surface area distribution [13]:

$$D[3;2] = \frac{\sum_{i=1}^{n} D_i^3 v_i}{\sum_{i=1}^{n} D_i^2 v_i} \tag{8}$$

where *D[3;2]* Sauter mean diameter, m

D Diameter of a particle, m

v Proportion of particles in the size fraction, -

The volume mean diameter D[4;3] is calculated as [13]:

$$D[4;3] = \frac{\sum_{i=1}^{n} D_i^4 v_i}{\sum_{i=1}^{n} D_i^3 v_i} \tag{9}$$

where *D[4;3]* Volume mean diameter, m

D Diameter of a particle, m

v Proportion of particles in the size fraction, -

As presented by Jankovic and Sinclair [14], the width of particle size distribution can be defined as:

$$\frac{Dx(90) - Dx(10)}{Dx(50)} \tag{10}$$

where *Dx(90)* Diameter of a particle, below which are 90 % of the particles in the sample, µm

Dx(50) Diameter of a particle, below which are 50 % of the particles in the sample, µm

Dx(10) Diameter of a particle, below which are 10 % of the particles in the sample, µm

2.2 Fluid flow through porous media

In order to gain deeper understanding of cake filtration, it is essential to take a look on some basic characteristics of fluid flow through porous media. According to Darcy's law there is a fundamental relation between the pressure difference and the flow rate of liquid through porous media. [10]

Darcy's law is defined as

$$\frac{\Delta P}{L} = \frac{\mu Q}{kA} \tag{11}$$

where ΔP Pressure difference across the cake layer, Pa

L Bed depth, m

μ Liquid dynamic viscosity, kg/ms

Q Volumetric flow rate, m^3/s

k Permeability, m^2

A Cross-sectional area of the bed, m^2

In Equation (11) the filter medium resistance has been neglected. The volumetric flow rate Q through porous media can also be stated as

$$Q = \frac{dV}{dt} \tag{12}$$

where dV is the filtrate volume in time dt.

When a fluid flows through a porous medium, including filter cake, the parameter describing the ease of this flow is called permeability. The permeability is affected by the porosity and the properties of the particles of the porous medium. Equation describing the permeability is defined as [10]:

$$k = \frac{\varepsilon^3}{K(1-\varepsilon)^2 S_p^2} \tag{13}$$

k	Permeability, m^2
ε	Porosity, -
K	Kozeny constant, -
S_p	Specific surface area per unit volume of the particles, m^2/m^3

The permeability equation can be placed into Darcy's law. With these, combined Kozeny-Carman equation is presented as follows [10]:

$$\frac{\Delta P}{L} = \mu \left(\frac{K(1-\varepsilon)^2 S_p^2}{\varepsilon^3} \right) \frac{Q}{A} \tag{14}$$

As the cake starts to build up on a filter medium, the resistance force is caused by the medium itself and the cake layer, the latter of which increases with time. This eventually leads to a gradual decrease of the flow rate. When the slurry is being fed on a filter medium, the following equation applies [3]:

$$Q = \frac{A_F \Delta P}{\mu(R + R_c)} \tag{15}$$

where

Q	Filtrate flow rate, m^3/s
A_F	Flow area, m^2
ΔP	Pressure difference across the cake layer, Pa
μ	Filtrate viscosity, kg/ms
R	Medium resistance, 1/m
R_c	Cake resistance, 1/m

Incompressible cakes create the resistance that is directly proportional to the amount of which they are deposited on a filter medium. The resistance can be stated as follows [3]:

$$R_c = \alpha w \tag{16}$$

where

w	Mass of cake deposited per unit area, kg/m^2
α	Specific cake resistance, m/kg

Thus, Equation (15) can be presented as [3]:

$$Q = \frac{A_F \Delta P}{\mu R + \alpha \mu w} \tag{17}$$

With this equation, the pressure difference can be presented as follows [3]:

$$\Delta P = \frac{Q(\mu R + \alpha \mu w)}{A_F} \tag{18}$$

According to Svarovsky [3], the specific cake resistance is equal to

$$\alpha = \left(\frac{KS_p^2}{\rho_s} \right) \left(\frac{(1-\varepsilon)}{\varepsilon^3} \right) \tag{19}$$

where α Cake specific resistance, m/kg

K Kozeny constant, -

S_p Specific surface of the particles, m^2/m^3

ρ_s Solids density, kg/m^3

ε Porosity, -

To determine the specific cake resistance in constant pressure filtration, a graph where time per volume of filtrate (t/V) is plotted against the volume of filtrate (V) is used [10]:

$$\int_0^t dt = \frac{\mu c \alpha}{A^2 \Delta P} \int_0^V V dV + \frac{\mu R}{A} \int_0^V dV \tag{20}$$

V Volume of filtrate, m^3

The integrated version of Equation (20) gives the form

$$\frac{t}{V} = \frac{\mu c \alpha}{2A^2 \Delta P} V + \frac{\mu R}{A \Delta P} \tag{21}$$

where c Filtration concentration, kg/m^3

As the obtained plots have been placed, the slope

$$\frac{\mu c \alpha}{2A^2 \Delta P} \tag{22}$$

and the intercept

$$\frac{\mu R}{A\Delta P} \tag{23}$$

are determined [10]. The intercept value defines the filter medium resistance, and the cake specific resistance can be calculated by using the value of the slope [3]. According to Svarovsky [3], the simplified version of Equation (21) can be expressed as

$$\frac{t}{V} = aV + b \tag{24}$$

where a is equal to Equation (22) and b is equal to Equation (23).

In case the desired constant filtration pressure is not immediately achieved, it is taken into account by using Equation (25) [3]:

$$\frac{t - t_s}{V - V_s} = \frac{\mu c \alpha}{2A^2 \Delta P}(V + V_s) + \frac{\mu R}{A\Delta P} \tag{25}$$

t_s Constant pressure filtration starting time, s

V_s Volume of filtrate obtained before achieving the desired constant pressure, m^3

Compressibility of the filter cake can be defined by the power coefficient n obtained from Equation (26) presented by Svarovsky [3]:

$$\alpha_{av} = (1 - n)\alpha_0 (\Delta P)^n \tag{26}$$

where α_{av} Average cake specific resistance, m/kg

n Compressibility index, -

α_0 Resistance at unit applied pressure difference, m/kg

ΔP Pressure difference across the cake, Pa

In practice, compressibility occurs in all filter cakes [10]. According to Mendret *et al.* [15] and Le-Clech *et al.* [16], the higher the power coefficient n, the more compressible the formed cake is. According to Wakeman and Tarleton [1], the formed cake is considered either very compressible, moderately compressible or almost incompressible when the power coefficient n in Equation (26) is ~ 1, ~ 0.5 or less than 0.2 respectively.

According to Wakeman and Tarleton [7], the extent of saturation together with the presence of the liquid modify the shape of the flow channels in the cake. Cake saturation S is defined as [7]:

$$S = \frac{V_l}{V_v} \tag{27}$$

where V_l Volume of liquid in the cake, m^3

V_v Volume of voids in the cake, m^3

3 SETTLING OF SOLIDS

3.1 Introduction

Settling, also considered as thickening, is a typical pre-treatment process in solid-liquid filtration to improve the structure of the formed cake and the performance of the cake filtration equipment itself. The process is meant to remove the bulk of water from streams, leading to a product containing usually 55-65 % solids. The benefits of pre-thickening apply to the lower resistance of the formed cake and the filter medium and the increased filtration capacity. The process also improves the filtrate clarity because it prevents the penetration of solids into the filter cloth. [5]

During the process of settling, downward movement of solid particles happens in such a way that the larger particles form the lower layer of the cake with the smaller ones accumulated on top of these. Settling process can be performed in chemical, physical or mechanical way. The particles can be treated with different types of coagulants and flocculants that combine several particles to form larger ones. Particles of different sizes can also be separated from one another by controlling behavior of the fluid. Settling phenomenon is based on the interaction between the particles, the carrier fluid and gravitational forces. [3, 6, 17]

3.2 Theory

As the particles settle within the gravity field, laminar, intermediate and turbulent settling regimes can be distinguished. During settling, the particles are affected by gravitational, buoyancy and hydrodynamic drag forces. [17]

Particles in a fluid are affected by a drag force whenever relative motion occurs between the surrounding fluid and the particles [18]. Stokes' law describes drag force affecting the spherical particles of very small sizes, and it applies when the flow is laminar and viscous forces prevail [3]. Stokes' law is defined as [4]:

$$u_d = \frac{d_d^2 g(\rho_d - \rho_c)}{18\mu_c} \tag{28}$$

where u_d Terminal settling velocity of the particle, m/s

d_d Particle diameter, m

ρ_c Density of the continuous phase, kg/m^3

ρ_d Density of the particle, kg/m^3

μ_c Viscosity of the continuous phase, Ns/m^2

g Gravitational constant, 9,81 m/s^2

Stokes' law can also be presented in the form [3]:

$$F_D = 3\pi\mu u d \tag{29}$$

where F_D Drag force, kgm/s^2

μ Viscosity of the fluid, kg/ms

d Diameter of the particle, m

u Particle-fluid relative velocity, m/s

The drag coefficient C_D for spherical particles can be presented as a function of the particle Reynolds number. When laminar flow conditions prevail it is connected to Stokes' law that can be stated also as follows [3]:

$$C_D = \frac{24}{\mathrm{Re}_p} (Re_p < 0{,}2) \tag{30}$$

where C_D Drag coefficient, -

Re_p Particle Reynolds number, -

Related to Stokes' law, particle relaxation time describes spherical reaction of spherical particles to changes in the fluid phase velocity within a timescale [3]. Drag

coefficient as the function of particle Reynolds number for spherical particles is described in Figure 5.

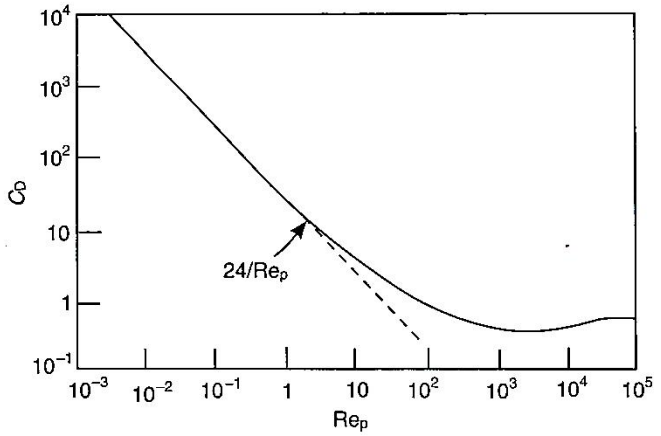

Figure 5. Drag coefficient as the function of particle Reynolds number for spherical particles [3].

Depending on the density of a particle, its relative movement within the gravity field of a fluid can be either upward or downward. According to the Stokes experiment, the main parameters affecting a spherical particle in a fluid at rest are constant fall velocity, diameter and density of the particle, and viscosity of the surrounding fluid. At the point where the particle reaches steady-state velocity, equilibrium between the reduced weight and the hydrodynamic drag force apply. [17]

Very fine particles with the diameter of less than 1 μm are affected by Brownian motion [6], and thus Stokes' law cannot be assumed to apply when particle settles in a gravity field [3]. This phenomenon creates dispersive forces between particles and leads to irregular motion behavior of the particles in the gravitational field [6].

There are three forces that affect the movement of a particle [17]:

1. The gravitational force (downwards)
2. The buoyancy force exerted by the fluid (upwards)
3. The hydrodynamic force exerted by the fluid on the particle (upwards)

For a spherical particle, the gravitational force is defined as [17]:

$$F_P = \rho_p \frac{\pi D^3}{6} g \qquad (31)$$

where F_P The gravitational force for a spherical particle, kgm/s^2

ρ_p Density of the particle, kg/m^3

D Diameter of the particle, m

g The gravitational constant, 9,81 m/s^2

The buoyancy force is defined as [17]:

$$F_A = \rho_f \frac{\pi D^3}{6} g \tag{32}$$

where F_A The buoyancy force, kgm/s^2

ρ_f Density of the fluid, kg/m^3

The hydrodynamic force results from the flow of the fluid past the particle and depends indirectly on the particle density through constant fall velocity. The dependence between these two is defined as [17]:

$$F_R(W_c, D, \rho_f, \upsilon) \tag{33}$$

where F_R The hydrodynamic force, kgm/s^s

W_c Constant fall velocity, m/s

D Diameter of the particle, m

ρ_f Density of the fluid, kg/m^3

v Kinematic viscosity, m^2/s

The kinematic viscosity (ν) is the ratio of the dynamic viscosity to the density of the fluid [19]:

$$\upsilon = \frac{\mu}{\rho_f} \tag{34}$$

where μ Dynamic viscosity of the fluid, kg/ms

When the particle falls at a constant velocity, the sum of all aforementioned forces equals to zero [17]:

$$F_P - F_A - F_R = (\rho_p - \rho_f)\frac{\pi D^3}{6} g - F_R = 0 \tag{35}$$

where F_P The gravitational force, kgm/s^2

F_A The buoyancy force, kgm/s^2

F_R The hydrodynamic force, kgm/s^2

Because of the complex dependency of the hydrodynamic force on the particle density through constant fall velocity, the latter can be defined by linking two dimensionless numbers, Reynolds number and the Archimedes number [17]. According to White [19], the Reynolds number is the primary parameter that correlates the viscous behavior of all Newtonian fluids. As the fluid properties change, the Reynolds number value is directly linked to the flow pattern. When the flow pattern changes from a creeping motion to a laminar and further up to a chaotic and unpredictable turbulent flow, the Reynolds number value increases. [19, 20] Also, the Archimedes number value increases when the flow pattern changes from laminar to turbulent flow [17].

In this context, the Reynolds number is defined as [17]:

$$\mathrm{Re} = \frac{W_c D}{\nu} \tag{36}$$

where

Re	The Reynolds number, -
W_c	Fall velocity, m/s
D	Diameter of the particle, m
ν	Kinematic viscosity, m^2/s

As the particles settle within the gravity field, laminar, intermediate and turbulent settling regimes can be defined by the Archimedes' number which characterizes the physical properties of the fluid and particle. It is used to find the connection between the aforementioned properties and the particle fall velocity. [17]

Archimedes number is defined as [17]:

$$Ar = \frac{(\rho_p - \rho_f) g D^3}{\rho_f \nu^2} \tag{37}$$

where

Ar	Archimedes number, -
ρ_p	Density of the particle, kg/m^3
ρ_f	Density of the fluid, kg/m^3
g	Gravitational constant, 9,81 m/s^2
D	Diameter of the particle, m
ν	Kinematic viscosity, m^2/s

Mory [17] presents that the fall velocity can be determined by a relation between these two dimensionless numbers, where the Reynolds number is the function of Archimedes number as follows:

$$\mathrm{Re} = f(Ar) \tag{38}$$

Richardson-Zaki Equation is often used for hindered settling velocity for uniform sized particles as [21]:

$$\frac{u}{u_d} = \varepsilon_B^{z-1} = (1-C)^{z-1} \tag{39}$$

where u The velocity of a particle relative to the liquid (slip velocity), m/s

u_d The terminal settling velocity of a particle, m/s

ε_B The bed voidage, -

z Richardson-Zaki index, -

C The particle concentration in volume fraction, -

3.3 Settling progress

Settling process takes place when a suspension consisting of liquid and solid particles is turned into a solid sediment bed. The final result is the clearly formed interface between solid mass and liquid phase. Suspensions include particles in different shapes and sizes, thus their settling velocities may greatly differ from one another. Before the final sedimentation bed is formed, separate particle settling zones are formed because of this. As long as the settling phenomenon is in progress, it fractionates particles according to their properties. [6, 22-24]

Two ways of settling can be distinguished in concentrated suspension sedimentation. The zones during the process can be of four or three types. They are divided into clear liquid, two suspension concentration and sediment zones. Generally, in the first suspension zone the concentration is constant before it starts to increase rapidly before the sediment is formed. The less common type of settling process does not include the constant concentration zone, which happens in the case when the particle size range within suspension is wide. [6]

The separated zones have been observed for example by Krishnamoorthy [22], when settling of suspension including two particle sizes in the Stokes region was investigated. In the experiment clear liquid zone, upper and lower settling zones and sediment zone were obtained. It was noticed, that in the upper settling zone

only small particles settle, whereas both particle sizes were present in the lower settling zone. [22] Franca *et al.* [23] described two main zones below the clear zone during sedimentation: free settling zone and compression zone.

Holdich and Butt [24] describe the behavior of different zones during sedimentation. It is stated, that in the clear liquid zone the particles are settling freely and hindrance does not occur. The interface between the clear liquid and the settling suspension can be observed when the sedimentation progresses and particle concentration increases. This phenomenon occurs when particles settle as a compact mass instead of settling individually. [24]

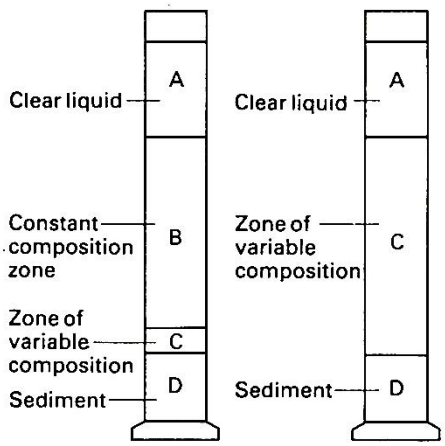

Figure 6. Two different types of settling of a suspension [6].

Separated zones formed during settling and two different types of settling are described in Figure 6. When a suspension is affected by gravitational settling, the larger particles settle faster than the smaller ones. When the particles are moving downwards, they cause volume displacement of the fluid. As the area and shape of the fluid flow changes during the process, the effective density and viscosity of the fluid increase. As the result of this, the particles are affected by the increased velocity gradients. The motion of small particles is accelerated and they are dragged downwards by the motion of large particles. In the case where the settling velocity is greater for larger particles, the settling type is called selective. [6]

In the case where the sizes of particles in the slurry are above 1µm and Stokes' law (Equation 28) can be used to predict the terminal settling velocity of particles [3], gravitational settling divides the particles of different sizes into separated fractions [22]. Disadvantage in gravity settling is relatively weak acceleration field. This is not a problem for most minerals where the particle size is at least 30 or 40 µm, but for very fine particles this can be a drawback. [3]

During sedimentation progress, the distinguished zones become visible as the upper and lower interface of the zones form. The falling speeds of these interfaces depend on the size and volume fraction concentration of particles in suspension. [22, 25] Sedimentation evolution for slurries containing several particle sizes is described in Figure 7.

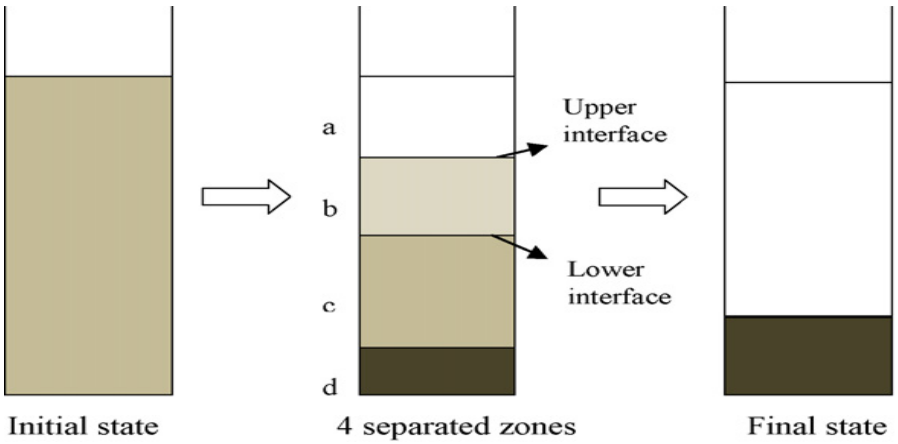

Figure 7. Sedimentation evolution for slurries containing several particle sizes [25].

Krishnamoorthy [22] developed a model to predict the settling velocity in suspensions of particles of two different sizes. In the experiments, the retarding phenomenon created by the smaller particles on the settling velocity of the larger particles was taken into account. It was observed, that when total concentration of small particles in volume fraction was kept constant, the increase in the volume fraction of the large particles decreases both the lower and upper interface velocity. The lower interface velocity decreased also in the case when total concentration of large particles in volume fraction was kept constant and the volume fraction of the small particles was increased. The lower and upper interface velocities were observed to increase with the increase in bed porosity. [22]

A number of experiments on the behavior and characteristics of different types of suspensions has been carried out. In the experiments a lot of data about the correlation between important parameters has been obtained.

According to Coulson *et al.* [6], the increase of suspension concentration results in the lower settling rate of suspended solids. Thus the velocity gradients in the fluid are steeper, caused by the increased upward velocity of the displaced fluid. [6] A clear and often used experiment to explore the settling velocity of a suspension is to measure the change of height of its interfaces as the function of time [26-29]. Davis and Maffia [26] used laboratory scale settling column to investigate the settling rate of alum slurry in gravitational field. The experiments showed a substantial increase of the slurry settling velocity from 0,03 cm/min to 1,2 cm/min as the initial solids content of the slurry was decreased from 0,60% to 0,10% respectively.

Bux *et al.* [27] carried out experiments to characterize a concentrated colloidal titanium dioxide (TiO_2) settling suspension. They compared the settling rates of three TiO_2 suspensions in three different concentrations. It was found out that the increased concentration of suspension lowered the settling rate. [27] Suspension interface demarcation as the function of time with different suspension concentrations is described in Figure 8.

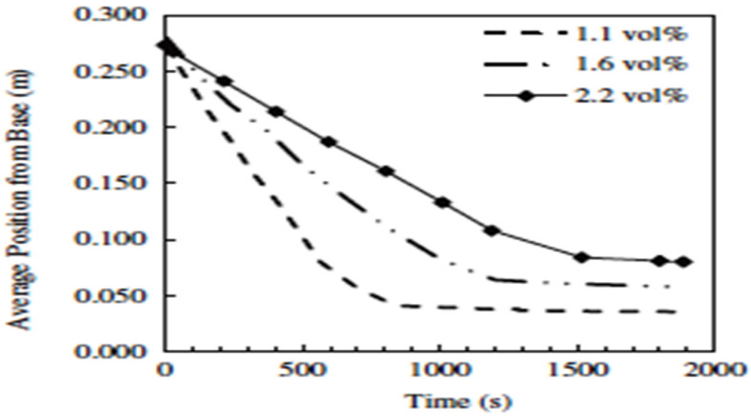

Figure 8. Suspension interface demarcation as the function of time with different suspension concentrations, graph obtained by Bux *et al.* [27].

Suspensions including very fine particles have also been investigated. The gravity-settling behavior of aqueous barium titanate ($BaTiO_3$) suspensions with various solids contents was observed by Tseng and Li [28]. In their experiments, similar trend for settling velocities of the suspensions was reported as mentioned in the theory [6] and other experiments [26, 27]. Experiments of the gravity-settling behavior of aqueous alumina (Al_2O_3) suspensions have also been carried out by Tseng and Wu [29]. The results indicated the similar trend to the experiments made with $BaTiO_3$ suspensions [28].

Suspension sedimentation by horizontal movement has been investigated by Yoshida *et al.* [30]. They conducted both experimental and numerical studies about the sedimentation velocity of nearly monodispersed particles in ion-exchanged water, using rectangular container placed on a moving plate. The experiments showed that the increased horizontal movement lowers the sedimentation velocity of the particles and also affects the distribution of particles in a suspension. [30]

3.4 Hindered settling

The settling behavior of particles changes with increasing concentration as the particles do not settle as individuals [10]. Hindered settling occurs when a set of several particles is in question. In this case, the laws affecting to a single particle in a fluid do not apply [17]. The regions of hindered settling are described in Figure 9.

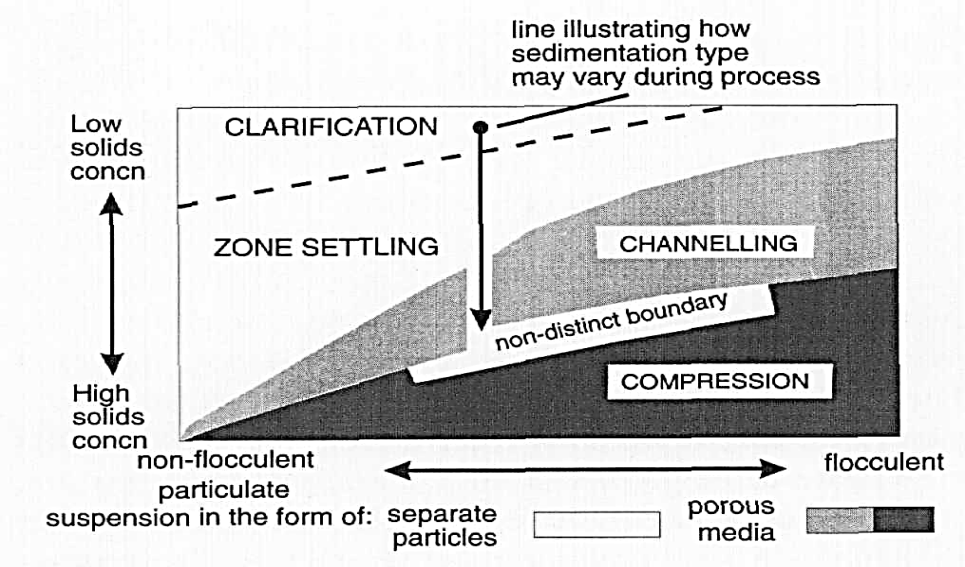

Figure 9. Hindered settling regions described by Fitch [31].

When the treated suspension has higher concentration of particles, they easily begin to interfere with each other. Thus, a cluster consisting of several particles is formed. [3] Within a cluster, particles are affected by attractive and repulsive inter-particular forces, the Van der Waals and electrostatic force respectively [17]. However, the formed cluster structures usually do not last, breaking into several smaller pieces. As the result of this phenomenon, volume displacing return flow distributes more uniformly and declines the settling rate because of the proximity of particles to one another [3, 17, 18]. Figure 10 describes uniform flow with respect to cluster pieces during hindered settling.

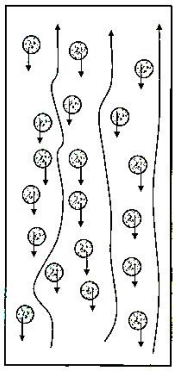

Figure 10. Uniform flow with respect to cluster pieces during hindered settling [17].

Hindered settling occurs in sedimentation and transport of concentrated slurries. Thus the viscosity of the suspension is increased. Settling velocity is decreased less than 1 percent when the volumetric particle concentration is below 0.1 percent. [18] Hindered settling can be calculated by Richardson-Zaki Equation (Equation 39) that shows the connection between the terminal settling velocity of the particles calculated by Stokes' law and the voidage or porosity of the suspension. The latter is raised to a power that is a function of the particle Reynolds number. [10]

According to Svarovsky [3], Richardson-Zaki Equation is used to describe hindered settling of concentrated suspensions and it correlates with the shape of the settling particles. Regarding the settling behavior of coarse particles, the sedimentation exponent of the equation is substantially larger for irregular particles than for particles of regular shape [3].

Heath *et al.* [32] studied the initial hindered settling velocities of flocculated calcite suspensions under various process conditions. They reported that higher hindered settling velocity correlates with larger aggregate sizes and decreased suspension concentration [32]. Similar findings were obtained also by Turian *et al.* [33], when they investigated the settling behavior of fine particulate slurries.

Tomkins [34] analysed the former research results by comparing the behavior of particulate systems involving sand, where the average particle size was 61µm or larger, with Richardson-Zaki Equation. The sedimentation exponent was found to be similarly dependent on the particle shape than mentioned by Svarovsky [3]. It was also found out that the particle Reynolds number increases as the sedimentation exponent decreases, but the practical experiments showed greater values for the exponent than theoretical ones. Also it was pointed out that greater average particle size correlates with greater particle Reynolds number value. [34] Chen *et al.* [35] investigated the zone settling of the waste activated slurries as the solid concentration varied. It was found out that the Richardson-Zaki type correlation was adequate only in the intermediate concentration range [35].

Lu *et al.* [36] made a theoretical analysis on the effect of hindered settling on the local cake structure formed under gravity filtration. They found out the correlation between theoretical and experimental results according to which decreasing the relative settling velocity between large and fine particles results in better uniformity of particle size distribution in the filter cake.

4 PARTICLE PROPERTIES AND FILTRATION PERFORMANCE

4.1 Background

There are three parameter types that are the primary properties describing a solid/liquid system and they can be measured independently of the other components of the system. These properties include physical properties of solid and liquid, the size, size distribution and shape of the particles, and the surface properties of the particles in their solution environment. The parameter types have a significant effect on particle behavior in the solid/liquid system, for example on their settling velocity, retaining ability on a filter medium and consistency of the formed cake. It is known that solid particles appear in a number of different forms and sizes and they are rarely either spherical or uniform. Also within industrial processes the particles tend to break which causes even further their irregular form and size. [1]

4.2 Fractionation of slurry and filtration process improvement

Slurry contains solid particles in a number of shapes and sizes. Filtration of slurry in its native form is not always practical or even possible since the slurry particles might block the pores of the filter medium, making it impenetrable [37]. As the cake layer is formed, the particles are agglomerated on top of each other in a random order. The properties of the formed cake and thus the filtration properties are strongly dependent on the type of agglomeration and size distribution of the particles. [38-42]

In order to improve vacuum belt filtration process and reach more desirable cake structure, classification of coarser particles from fine particles to form a pre-coat layer on the filter medium either by gravity settling or hydrocyclones is used [3]. The improving effect of coarser particles on vacuum filtration is described by Wakeman and Tarleton [1], as they propose the increased permeability and faster dewatering of the cake when the mean particle size is doubled. Pre-coating effect on vacuum filter process has also been investigated as the mixture of commercial pre-coating agent and slurry particles [43]. Particle size stratification on a horizontal vacuum belt filter due to gravity settling is described in Figure 11.

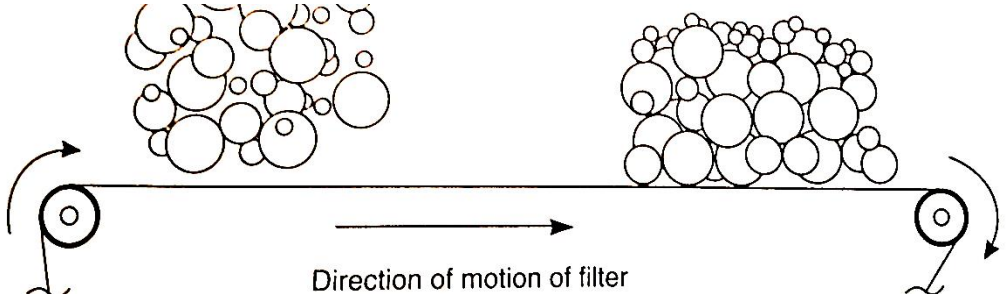

Figure 11. Particle size stratification on a horizontal vacuum belt filter due to gravity settling [3].

Ideal situation would be to have bridging formation of the particles on the filter medium that would prevent the pore blocking and create stable and permeable layer of particles [1]. This is possible when the particle concentration in the feed is heightened, increasing the probability of particle capture at the surface of the filter medium [44]. As the forces between the particles interact, they form a stable and packed bed [38, 39].

4.3 Cake structure, particle packing and porosity

As the fluid passes through a filter cake, particle packing forms a certain volume of voids within the solid material. According to Wakeman and Tarleton [7], higher degree of porosity results in improved permeability independent of the type of particle packing. The relation between porosity degree and permeability, and the effect of particle packing on the structure and properties of bed has been investigated by many researchers. Depending on the properties and amount of coarse particles in the suspension, the porosity value of the formed cake varies.

Particle packing research

Endo *et al.* [45] carried out air and water laboratory scale permeability tests for dust cakes consisting of six different types of powders including monodisperse spheres and various polydisperse non-spherical particles. They found that for both fluids the increased dust cake porosity resulted in lower pressure difference across the bed during filtration as the fluid flow velocity was increased by applying more vacuum underneath the filter material. As water was filtered, the similar trend was achieved also in the case where the bed material varied. [45]

Hwang *et al.* simulated the packing structures of a filter cake [38, 39]. They compared cake structures formed by spherical and spheroidal particles with different types of size distributions. It was found that in case of spheroidal particles, the uniform size distribution type gave a packing structure with a larger pore size when compared to the normal and Rosin-Rammler distribution types. This was because the uniform size distribution type gave the particles more equal size than the other types. The cake structures were also compared with normal distributions as the standard deviation varied. The results unveiled that for both spherical and spheroidal particles, the increase of standard deviation resulted in more irregular packing structure, thus creating more diverse shape and size of pores within the bed. [38] The effect of increased standard deviation on the packing structure of particles is described in Figure 12.

Figure 12. The effect of increased standard deviation on the packing structure change of spherical particles with normal distribution type. Standard deviations (σ) from left to right: 0 m, $2x10^{-6}$ m, $5x10^{-6}$ m. [38]

Hwang *et al.* also presented important aspects regarding the movement of the particles at the cake surface and within the cake [38]. They assumed that the particle is not deposited at the cake surface until it is in contact with at least two stable particles at the same. Otherwise, the particle migrates along the cake surface. Particles are also affected by drag and gravity forces during filtration, which may force them to penetrate deeper into the cake layer, thus creating a more compact cake structure. [38] Simulation of the cake formation by uniform-sized spheroidal particles showed that the packing structure is greatly affected by the length ratio of the major axis to the minor one. It was also observed that the structure of the filter cake looser as the shape of particles departs from spherical form. [39] Forces affecting on particle during cake filtration are described in Figure 13.

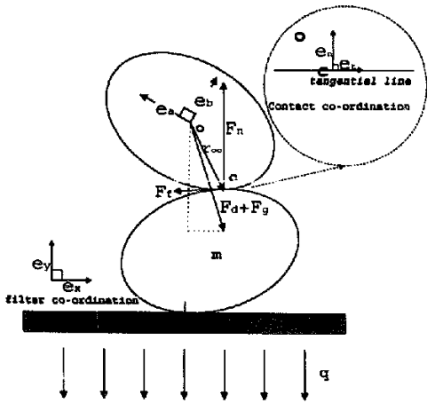

Figure 13. Forces affecting on particles during cake filtration [39].

The effect of particle properties on cake formation has also been investigated by Mota *et al.* [40]. They modelled cakes containing both coarse and fine particles with a wide size distribution and different particle shapes. The approach proposed by the researchers was successfully applied to filtration data obtained in other research experiments. It was concluded that substantial decrease of the cake permeability occurs, when the presence of fine particles in coarse granular bed is more than 10%. [40]

The porosity value of the formed bed depends on the volume fraction amount of small and large sized particles and the relation value of the particle sizes located in different fractions [41], and the particle shapes [42]. Mota *et al.* [41] measured porosity and permeability relationship of mixed beds formed by spherical particles of different sizes. It was found that the increase of the volume fraction of large particles did not increase the porosity value, when the ratio value of large to small particles ranged between 10.22 and 1.985. However, the permeability of the bed increased when the volume of large particles was more than 80%. [41] According to the mathematical model proposed by Yu *et al.* [42], particle shape strongly affects porosity.

Yu and Standish [46] estimated the porosity of particle mixtures by a linear-mixture packing model. The findings regarding the correlation between porosity and the fractional solid volume of large particles were similar to the ones by Mota *et al.* [41]. Random packing structure of spherical particles and the connections among the controlling components are also illustrated by the researchers as shown in Figure 14. [46] The forces between the packed particles are well described also by Thomas and Reichmann [47].

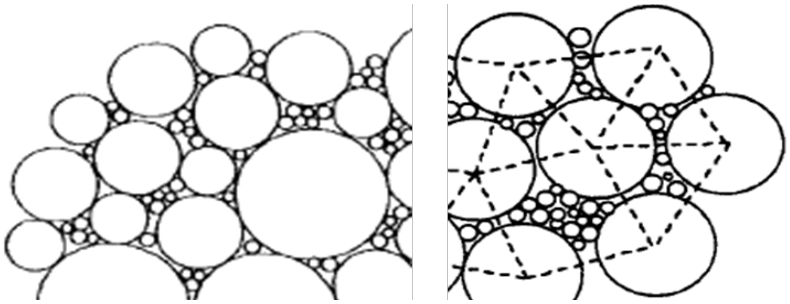

Figure 14. Random packing structure of spheres (left) and connections among the controlling components (right) described by Yu and Standish [46].

Dias *et al.* [48] studied dependence of packing porosity on particle size ratio of particulate binary mixtures. They reported ten-fold increase in porosity fraction when the ratio value of small to large particles was increased by ten-fold. It was concluded that the overall porosity of a binary mixture is determined by the arrangement of different sized particles. According to the researchers, during the packing small and large particles affect each other by displacement, wedging and wall effect. Figure 15 presents the arrangement of small particles between large particles. [48]

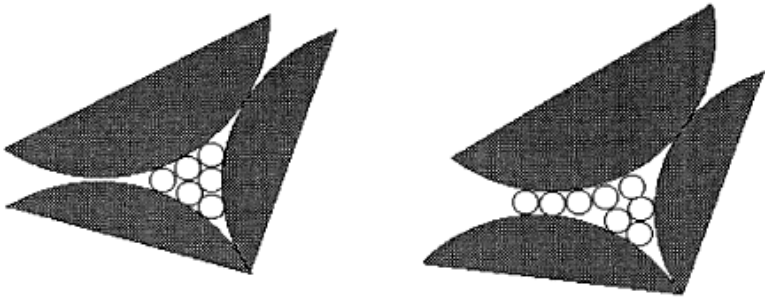

Figure 15. Particle deposition of small particles between large particles described by Dias *et al.* [48]. Small particles fill the free space between the large particles (left), small particles wedge in between the large particles.

Mota *et al.* [49] made two-dimensional simulations of packed beds composed of binary and ternary particle mixtures. Even though porosity was found to be dependent on the volume fraction of the large particles, it was stated that this does not totally determine the porosity of the packed beds. Substantial decrease in porosity was reported when a third fraction of smaller particles was introduced into the binary mixture. [49]

Wakeman [44] carried out research on the influence of particle properties on filtration of incompressible cakes. The effect of particle size on the cake specific resistance was measured. As the porosity was kept constant in all cases, a substantial decline in the resistance was observed when the particle size increased. Once the particle size was doubled from 6.5 µm to 13 µm, it resulted in a clear increase of the obtained filtrate volume. The particle shape was seen to affect the resistance, as the specific surface area of the particles changed. Higher specific surface area of a particle caused higher resistance. The conclusion made out of these

discoveries was that in order to reach an ideal structure for the formed cake, the particles should have a monosize distribution and they should be as large and as spherical as possible. [44]

4.4 Filter aids

In order to improve filtration process by preventing rapid filter medium blinding, and improving filtration rate and filtrate clarity, powders with special properties, so-called filter aids are used [18]. Filter aids are rigid, porous and highly permeable solids that are mainly used to form an extra layer on top of a filter medium or to be mixed with the feed suspension, thus creating a more permeable cake [3]. The two most often used filter aids are diatomite and perlite [18]. Filter aids like natural cellulose fibers and silica can be also used as a combination with other types of filter aids [7].

Filter aids can be used in two ways. Body feed method is based on continuous adding of filter aid to the feed stream [18]. Pre-coating is in question when the filter aids are used to form a layer on a filter medium before the main feed is filtered [50]. The amount of the used pre-coating ranges between 0.5 and 1.0 kg/m^2 [18]. By using filter aids in filtration processes, the overall filtration costs can be reduced [50].

Pre-coating can also occur by the formation of coarser particles of the feed stream on top of the filter medium before the finer ones. This procedure has been applied in horizontal and rotary drum vacuum filtration processes. It has been noted that by using coarser particles as a pre-coat, blinding of the filter cloth by the finer particles can be prevented, better filtrate clarity achieved and applicability of the filter to finer feeds extended. [3] Pre-coating is often used for example in the beverage industry where extremely clear filtrate is required [37].

Filter aid research

Both body feed and pre-coat methods have showed good results in improving filtration processes in several industry segments. Different materials employed have made it possible to reach the desired filtrate qualities and better filtration rates. [51-55]

Composition of filter aids is usually silica or cellulose. The benefits of using silica filter aid are based on its variety of curious shapes, high porosity and precise chemical composition. Moreover, they are chemically quite inert. [7] A good example of preciseness of using silica powder as the filter aid has been observed by Boittelle *et al.* [51]. They discovered that by using 15 μm silica particles as a pre-coat in wine filtration, the filtrate accumulation speed was increased and the turbidity of the filtrate was decreased without any notable loss of the essential chemical components in the filtrate. The same benefits were gained also when polyamide particles were used as the pre-coat material. [51]

Suh *et al.* [52] evaluated the effects of diatomaceous earth, inorganic adsorbent and polymeric flocculant on cake filtration performance during standard vacuum filtration experiments under constant pressure. As the filter aids were added to the

corn gluten meal hydrolysate as body feed, cake compressibility reduction and improved filtrate clarity were reported. It was discovered that the reduction in cake compressibility correlated with the enhanced filtrate flux and clarity. As stated by the researchers, the fine particles of the feed were more easily captured by the less compressible cake layer. [52]

Meeroff and Englehardt [53] carried out ultrafiltration experiments of bitumen/water emulsion. As filtrations with and without filter aid addition were compared, it was reported that bentonite clay addition as the body feed filter aid improved the permeate flux and reduced system fouling. [53]

Vorobiev *et al.* [54] carried out filtration experiments of an aqueous calcium carbonate suspension in the presence of dispersants with and without a pre-coat layer. It was found out that the pre-coat layer composed of aggregated mineral particles lowered the cake specific resistance and protected the filtrate from fine particles of the dispersants suspension and molecules of the dispersant. [54]

Harjula *et al.* [55] tested inorganic ion exchange materials as pre-coat filter materials for the removal of radioactive components from simulated radioactive waste liquids. When the pre-coat filtration experiments were compared to conventional column operation with granular materials, it was observed that the used pre-coats provided high decontamination factors at much higher flow rates. [55]

5 CLASSIFIERS

5.1 Background and theory

In chemical industry, slurries are often treated by classifiers. Classifiers are employed to separate particles of different sizes from each other and divide them into finer and coarse fractions. The separation of the fractions is based on density difference, as the particles are influenced by centrifugal forces. [3]

Classifiers are grouped according to the movement type of solids through the unit, which can be either hydraulic or mechanic. The main purpose of both classifier types is to classify suspended solids into different size fractions. [7] According to Wakeman and Tarleton [7], hydraulic classifiers are mainly used to treat feeds in which particle size range is 50-2000 μm and solid concentration 4-40%. These ranges are similar to the ones in this work, so the focus will be more on hydraulic units.

When calculating the drag between the particle and the liquid in a centrifugal field, the gravitational constant (g) used in gravitational field sedimentation calculations in Stokes' law region, is replaced by the centrifugal acceleration ($r\omega^2$). Thus, the Stokes' law equation is presented as follows [6]:

$$u_d = \frac{d_d^2 r\omega^2(\rho_d - \rho_c)}{18\mu_c} \tag{40}$$

where r Radius of the inner surface of the liquid in a centrifugal field, m

ω Angular velocity in a centrifugal field, rad/s

Solid-liquid separation process has three main flows. The initial feed is divided within a process unit into overflow and underflow, both containing solids and liquids in different ratios. The separation is never fully complete, because the liquid phase always contains some amount of solids and the solid phase always contains some amount of liquid. [3]

Hydrocyclones and sedimenting centrifuges are used in separating solid particles of different sizes into fine and coarse fractions. Along with gravity sedimentation equipment and flotation cells they have been widely used in mineral processing for separation of minerals. [3]

Separation efficiency calculations of the solid material is often based on mass recovery. When classification between fine and coarse material is in question, mass balance equations are used. [3] Mass balances of a separator are described in Figure 16.

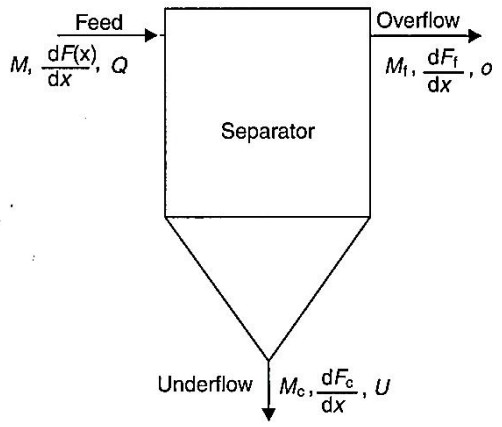

Figure 16. Mass balances of a separator [3].

If accumulation of material in the separator does not exist, the mass balance of a separator is calculated as [3]:

$$M = M_c + M_f \tag{41}$$

where M Mass flow rate of the feed, kg/s

M_c Mass flow rate of the coarse material in the underflow, kg/s

M_f Mass flow rate of the fine material in the overflow, kg/s

Mass balance has to apply also to any size fractions of particle size between x1 and x2:

$$(M)_{x1/x2} = (M_c)_{x1/x2} + (M_f)_{x1/x2} \tag{42}$$

and for each particle size x:

$$(M)_x = (M_c)_x + (M_f)_x \tag{43}$$

Thus, the total mass balance for particles of size x is presented:

$$M\frac{dF}{dx} = M_c\frac{dF_c}{dx} + M_f\frac{dF_f}{dx} \tag{44}$$

where $\frac{dF}{dx}$ Size distribution frequency of the feed

$\frac{dF_c}{dx}$ Size distribution frequency of the coarse material

$\frac{dF_f}{dx}$ Size distribution frequency of the fine material

5.2 Hydrocyclones

Hydrocyclones are used in a number of ways in classification processes. In the case of vacuum belt filtration process, hydrocyclones are used as pre-treatment method to divide the feed stream into underflow and overflow, consisting of coarse and fine

particles respectively. This enables pre-coating the filter medium with coarse particles, thus improving the performance of the filtration process. Improved filtrate clarity and usefulness of the vacuum belt filter to finer feeds without an undesired effect on the cake moisture content can be achieved by the correctly set cut point. [3] Hydrocyclones are mainly employed to treat suspensions with particle size range of 5-200 μm and solid concentration of 2-30%. [7] Hydrocyclone as a pre-treatment method for vacuum belt filtration process is described in Figure 17.

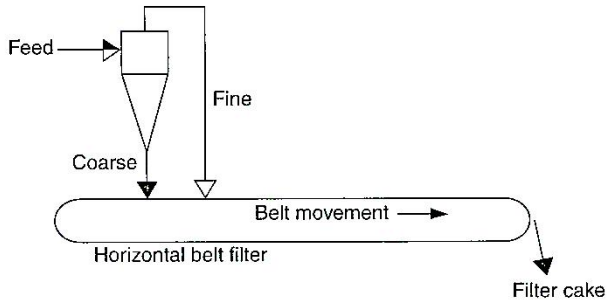

Figure 17. Hydrocyclone as a pre-treatment method for vacuum belt filtration process [3].

The separation phenomenon of hydrocyclones is based on three types of flow velocities that occur within the unit. In order to separate solid particles from the fluid, they are subjected to centrifugal acceleration. The velocity of the flow at any point within the cyclone can be divided into tangential, radial and vertical or axial velocity. [3] The coarser and finer particles are separated into underflow and overflow by the combination of centrifugal forces of between 800 and 50 000g, and a swirling motion. Typical mean velocity of the feed ranges between 10 and 30 m/s [7]. In order to achieve fine separation, pressure difference of 200-350 kPa is used in small-diameter cyclones. [5]

The basic characteristics in hydrocyclone structure are an inverted conical bottom section attached to a cylinder, and the feed, underflow and overflow ports. The feed port is attached to the cylinder, underflow and overflow ports locate in the bottom and top of the unit respectively. [7] Figure 18 describes the flow patterns of a hydrocyclone.

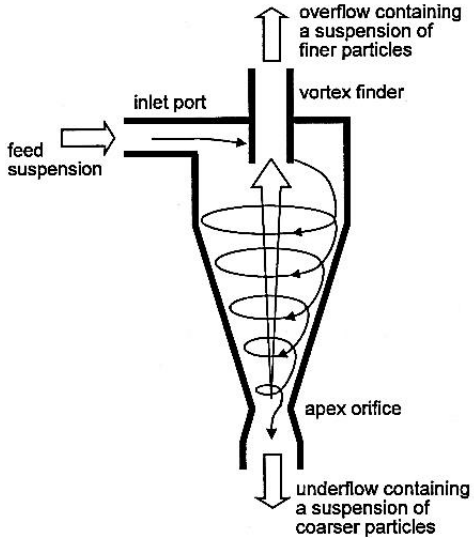

Figure 18. Flow patterns of a hydrocyclone [7].

The structure of hydrocyclones are of two types, narrow angle and wide angle design. The cone angle has a crucial role on behavior of the circulating flows in the process. The geometry difference between the narrow and wide angle units is based on the cone angle, being up to about 25° and 25-180° respectively. Units with narrower angles are usually employed to separate fine particles due to suppression of the flow. [3] Figure 19 describes the design types of hydrocyclones.

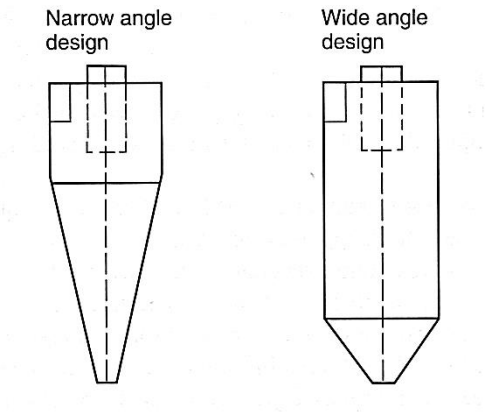

Figure 19. Design types of hydrocyclones [3].

The separation effect of classifiers is based on rotational motion within a process unit. The fluid and the particles are subjected to the force which is the sum of vertical forces due to gravity and centrifugal forces in a horizontal plane. [56] Figure 20 describes the forces acting on element of fluid in a vortex.

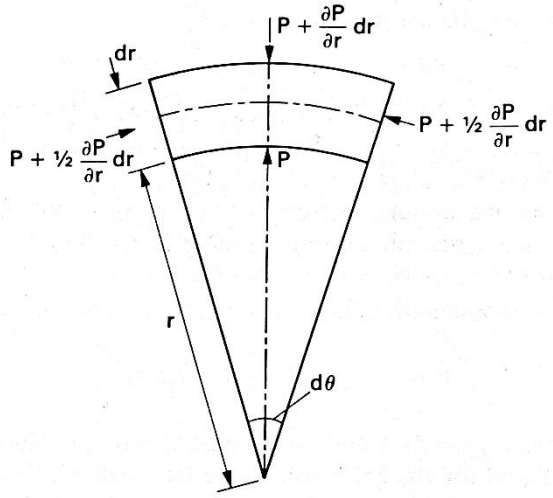

Figure 20. Forces acting on element of fluid in a vortex at radius r and pressure P [56].

5.3 Centrifuges

According to Wakeman and Tarleton [7], centrifuges are divided into two general classes, sedimenting and filtering centrifuges. In this work, the main interest will be on sedimenting phenomenon of centrifuges, so filtering centrifuges are excluded.

The nature of the feed stream and product requirements determine which type of centrifuge is employed. Sedimentation centrifuges are of four main types: tubular bowl, basket solid bowl, disc and scroll discharge. [4] Typically, the particle size in the treated slurries ranges between 0.1-100 μm in the case of tubular bowl, basket solid bowl and disc centrifuge types. In the case of scroll discharge centrifuge, the respective particle size range is 1-5000 μm. [7] When the solid particle size within the treated fluid is above 150 μm, or in the case when clarified liquid or compressible cake is the desired product, sedimentation centrifuge is chosen to perform the process. [4] Two often used centrifuge types are presented in Figure 21.

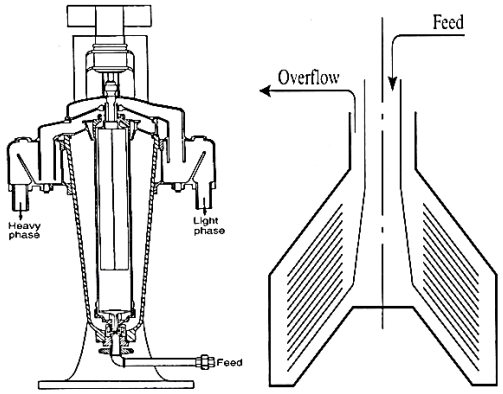

Figure 21. Tubular bowl centrifuge (left) and disc bowl centrifuge (right) [4].

5.4 Gravity thickeners

In solid-liquid separation, gravity thickeners are used to treat large volumes of suspensions. The separation process is based on sedimentation to increase the concentration of suspended solids. Generally, the structure of a thickener consists of a rotating rake placed at the base of a large circular tank. Depending on the consistency of the treated suspension, different types of rakes can be used. [4] Thickener process can be used either continuously or batchwise. After the suspension has been transferred into the tank, settling process takes place. While the settling process, extra additives are sometimes added in the suspension to improve the settling rate. At the point in which the sedimentation has proceeded for an adequate time, the thickened phase is transferred off the tank from the bottom and the remaining clear liquor is collected from the upper part of the tank. [6] Thickeners are typically used to treat suspensions in which the particle size ranges from 0,1 µm to 500 µm. [7] Figure 22 presents the flow directions in a thickener.

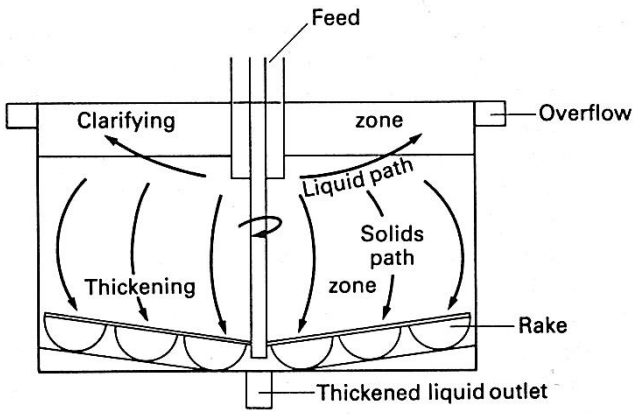

Figure 22. Flow directions in a thickener [6].

The material of thickener tanks of less than 25m diameter is usually steel, whereas a combination of concrete and steel is used for the larger tanks that are from 25m up to 200m in diameter. Mechanical aid to discharge the solids from the bottom is not needed since the mass can be collected exploiting the gravity. [7]

6 FLUID MECHANICS

6.1 Theory

Fluids can be found of two types, gas and liquid. The liquid is an aggregation of closely spaced molecules that cannot resist a shear stress by a static deflection. A fluid affected by any shear stress is in a continuous motion, and is called a continuum when its properties vary continually in space. [19] Two types of liquids can be distinguished according to their viscous stress behavior. Non-Newtonian fluids have a constant viscosity dependent only on temperature. The viscous stress of Newtonian fluids are linearly proportional to the shear strain rate or velocity gradient. [3, 19]

The motion type of flow occurs in many forms. The flow motion can be mainly creeping, laminar or turbulent. The Re number correlates with all motion types. The higher the Re number, the more unsteady flow motion. When the flow is creeping, inertia effects are negligible. Laminar motion describes smooth and steady flow, switching into fluctuating and agitated once it becomes turbulent. This changeover is called transition. When Reynolds number ranges between 0 and 1000, the flow type is laminar. The transition from laminar to turbulence flow occurs when the Re number value is between 1000 and 10000. Turbulent flow is in question when the Re number value is below 10000. [19] Figure 23 describes the changes in flow motion with respect to an increased Reynolds number.

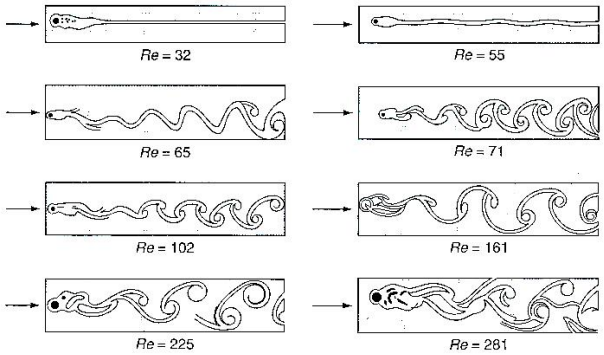

Figure 23. Flow motion change with respect to an increased Re-number [20].

Also, the Archimedes number correlates with the changes in flow motion. The number value increases as the flow type changes from laminar to turbulent. The Archimedes number value is below 32.9 when the flow is at the laminar regime, between 32.9 and $1.04 \cdot 10^5$ at the intermediate regime and above $1.04 \cdot 10^5$ at the turbulent regime. [17]

6.2 Properties of fluid

Gases and liquids differ from each other in terms of cohesive forces related to their behavior. Liquid is composed of relatively close-packed molecules with strong cohesive forces, its volume is considered unchanged and it forms a free surface in gravitational field. [19] In this work gas properties are excluded since the treated fluid is suspension consisting of water and solid magnetite particles.

According to White [20], fluid properties are divided mainly into four categories. Kinematic properties are basically the properties of flow field, and miscellaneous properties depend on for example flow conditions. [20]

1. Kinematic properties (linear velocity, angular velocity, vorticity, acceleration, strain rate)
2. Transport properties (e.g. viscosity)
3. Thermodynamic properties (e.g. pressure, density and temperature)

4. Other miscellaneous properties (e.g. surface tension)

Energy converts to one form to another when a fluid is in motion. There are four main components of which the total energy of a fluid in motion consists: internal, pressure, potential and kinetic energy. [56]

Fluid flow and heat transfer calculations in computational fluid dynamics

According to Versteeg and Malalasekera [57], all fluid properties are functions of space and time in computational fluid dynamics. The fluid is considered as a continuum, and three conservation laws of physics apply in calculations:

- the mass of a fluid is conserved (a.)

- Newton's second law (b.)

- first law of thermodynamics (c.)

a. Mass balance for the fluid element

Rate of increase of mass in fluid element = Net rate of flow of mass into fluid element

b. Rate of increase of momentum of fluid particle = Sum of forces on fluid particle

c. Rate of increase of energy of fluid particle = Net rate of heat added to fluid particle + Net rate of work done on fluid particle

In fluid mechanics, calculations are based on four primary dimensions (mass, length, time and temperature) from which secondary dimensions are derived. [19]

6.3 Multiphase flow

Multiphase flow process is used in many industrial processes. The process is based on the interaction between two or three different phases: gas, liquid or solid. Of these alternatives, five process types can be named: gas-liquid, liquid-liquid, gas-solid, liquid-solid and gas-liquid-solid. Multiphase flow means simultaneous flow of materials that differ from each other in terms of phase and chemical properties. The flow is divided into continuous and dispersed phase, called as primary and secondary phases respectively. [19, 56]

Generally multiphase flow is considered as a very complex process. The geometry of the system and the properties of the components affect the behavior of the material. Since two or more phases interact with each other, certain phenomena of movement between the materials have to be taken into account. Flow pattern is influenced by pressure difference, which is related to slip velocity, the relative velocity of the phases. This subsequently influences the fraction of the pipe volume occupied by a particular phase, the hold up. [56] According to Coulson *et al.* [56], transportation of solid particles in liquids is called hydraulic transport through either vertical or horizontal pipes.

Solid particles in horizontal pipe flow

According to Equation (39) presented by Richardson and Zaki [21], the velocity of a particle relative to the liquid is called the sedimentation velocity or the slip velocity. Coulson *et al.* [56] present that in solid-liquid system the slip velocity of the particles is close to their terminal falling velocity calculated by the Stokes' Law Equation (Equation 28). In vertical upward flow in solid-liquid system where the solid is denser than the liquid, the slip velocity is increased because the lighter phase rises more quickly than the denser phase [56]. When the accelerating force of a particle is exactly balanced by the resistance force, terminal falling velocity is reached [56]. Because of vortex shedding, the settling particles may undergo fluctuating motions. [18]

The concentration of particles towards the bottom of the pipe increases as the flow velocity decreases. During the flow, solid and liquid phases behave differently. Energy transfer to the solid particles is created by the relative velocity between the phases, because the fluid moves faster than solid components. However, the particles lose energy during the flow as they hit the wall of the pipe and are affected by frictional effects. [56]

It is essential to differentiate between the hold up (h_S) and the volume fraction of particles in the discharge (C_s). To find out the rates of movement of the components at the end of the pipe, it is necessary to measure at least one of the following variables [56]:

The slip velocity is presented as

$$u = u'_L - u'_S \tag{45}$$

where u The slip velocity, m/s

u'_S The absolute linear velocity of the particles, m/s

u'_L The absolute linear velocity of the liquid, m/s

The hold-up of the liquid

$$h_L = 1 - h_S \tag{46}$$

where h_L The hold-up of the liquid, -

h_S The hold-up of the solids, -

Other important variables has been found out by the research carried out by Pirie *et al.* [58], where the mixture velocity (u_m) was measured by electromagnetic flowmeter. By using the aforementioned parameters, the value for the volume fraction of particles in the discharge (C_s) can be calculated as follows [56]:

$$C_s = \frac{u_S' h_S}{u_m} = 1 - \frac{u_L'}{u_m}(1 - h_S) \tag{47}$$

The connection between the slip velocities and volumetric concentrations of small and large particles have been investigated by Dutta and Bhattacharyya [59]. They used a voidage model to predict the slip and interface velocities of sedimenting zones for bidisperse solid-liquid systems. As the model predictions were compared with the experimental results, it was found out that the voidage model was able to predict the sedimentation phenomena of a bidisperse system. [59]

The effect of turbulent flow on particle behavior has been investigated by Sarimeseli and Kelbaliyev [60]. They suggested new expressions for the calculations regarding the particle settling and sediment thickness. It was discovered that the total sedimentation velocity of the particles is dependent ia of the turbulent velocity, the viscosity of the medium, the Reynolds number and the relaxation time. The calculations were found to agree with the results of previous experiments. [60]

Fractionation of particles of different sizes in horizontal flow has been investigated in a laboratory scale by using Split-flow thin cell (SPLITT) fractionation technique. The technique has been used for isolating size fractions by Contado *et al.* [61] and Moon *et al.* [62]. It has also been compared with conventional gravitational settling by Tantidanai *et al.* [63]. The basic principle of the fractionation process is based on a horizontal, particle containing fluid flow within a cell. Depending on the process type, the particles can be exposed to a combination of many forces as they move forward within the flow. For example, gravitational and hydrodynamic lift forces can be used to divide the particles into separated fractions. To control the formed fractions and to separate them in the outlet part of the process, splitting planes are assembled within the cell. [61, 63] Figure 24 describes the particle fractionation in Split-flow thin cell process.

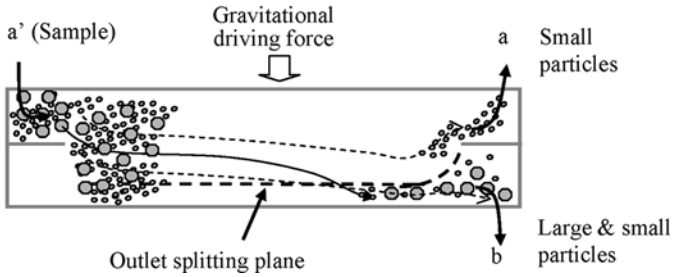

Figure 24. Particle fractionation in Split-flow thin cell (SPLITT) process [63].

EXPERIMENTAL PART

7 OBJECTIVE OF WORK

The objective of this work was to find out how fractionating magnetite slurry particles into separated fine and coarse fractions affect the magnetite slurry cake filtration. The filtration capacity, filtrate flow rate and the essential properties of the cake were measured. Also, it was investigated how magnetite slurry particle settling before the filtration process affect the aforementioned quantities. Both non-fractionated and fractionated magnetite slurry batches were filtered and the results were compared with each other.

8 DEVICES AND METHODS

The experiments were focused on magnetite slurry batch filtration by using constant pressure vacuum filtration by Büchner filtration equipment. In order to gain fine and coarse fractions, magnetite was sieved by using three sieves of different sizes (38 μm, 45 μm and 75 μm). Volumetric particle size distribution of magnetite fractions was analyzed by laser diffraction method by Malvern Mastersizer 3000 with the feed unit Hydro EV. The structure of the cake layers was explored by using Scanning Electron Microscope Hitachi SU3500.

8.1 Magnetite slurry preparation

In the beginning, magnetite barrel was brought to room temperature from outdoor storage to melt for a day. The aim was to prepare magnetite slurry with solid content of nearly 60 w%. The moisture content of the used magnetite was first found out by measuring the weight of two magnetite samples before and after the heating in an oven where the ambient heat was 105 °C. The moisture content of both magnetite samples was found out to be 8.5%. The density of the used magnetite was measured by using pycnometer. The average value of two measurements gave magnetite the density of 4849 $kg \cdot m^{-3}$.

The magnetite slurry was prepared by mixing magnetite and tap water (~20-21 °C, $9.8 \cdot 10^{-4}$ $Ns \cdot m^{-2}$) with a motorized stirrer in a 16 dm^3 tank. While the mixing was in progress, the real solid content of the prepared slurry was measured by taking five slurry samples with a 20 ml syringe within 5-10 cm depth from the surface. To make comparison of the mixing efficiency of magnetite in different size tanks, the same procedure was performed while the slurry was mixed in a 2 dm^3 tank. All the samples were kept overnight in an oven at 105 °C and their weight was measured before and after the heating. The solid content was calculated from all the gained samples from both tanks and the average value was found out to be 56.7 w%. As there was no remarkable difference observed in the solid contents of the samples, the 16 dm^3 tank was chosen for sample preparation as the more practical choice. The density of the 56.7 w% magnetite slurry was determined by taking six slurry samples with a 20 ml syringe within 5-10 cm depth from the surface of the tank. The samples were introduced into a 25 ml graduated cylinder and the weight of the

sample within the measured volume was measured, giving the average density of 1838.8 $kg \cdot m^{-3}$ for the 56.7 w% magnetite slurry. The measurement transcript of these experiments can be found in Appendix I.

The non-fractionated magnetite slurry batches

The non-fractionated magnetite slurry batches for initial filtration experiments were pumped from the tank while the mixing was in progress. The samples were pumped from the tank with the speed of 1700 ml/min into 0.4 dm^3 plastic containers. To set the weight of each sample to be within 801-802 g range, a 20 ml syringe was used to gain the remaining amount of slurry from the tank within 5-10 cm depth from the surface.

The fractionated magnetite slurry batches

The magnetite slurry batches for fraction filtrations were prepared in four stages. At first, 10 kg of magnetite was dried by keeping it in an oven at 105 °C for 48 hours. After this, the magnetite amount was kept in a desiccator for 7 days from then on to keep it dry all the time. For each fraction filtration experiment a magnetite sample was taken from the desiccator to be sieved into separated fine and coarse fractions, using either 38 µm, 45 µm or 75 µm sieves. The obtained fine/coarse fraction w% ratios were 86/14, 69/31, 68/32 and 66/34. Schematic diagram describing the magnetite sample sieving into separate fine and coarse fraction and the used weight ratios between the fractions is shown in Figure 25.

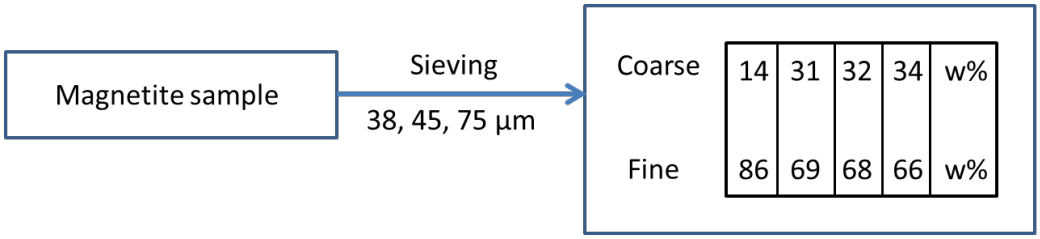

Figure 25. Schematic diagram describing magnetite sample sieving into fine and coarse fractions, and the used weight ratios between the fractions.

The overall weight of magnetite and water of the two separated batches together was adjusted equal to the weight of the non-fractionated slurry batches, being within the range of 801-802 g. The solid content in both fine and coarse fraction batches was kept similar (56.7 w%) to the non-fractionated batches. The remaining magnetite residue from both fine and coarse fractions was used in analyzing the volumetric particle size distributions.

8.2 Büchner filtration

The filtrations were carried out by using Büchner constant vacuum batch filtration equipment. The equipment consisted of filter cell, vacuum pipe with a control valve and a vacuum pressure box. The filter cell consisted of bottom and circular wall part between which the filter medium was placed. The diameter between the inner

parts of the circular wall was 11.2 cm, thus giving the filtration area of 0.00985 m^2. The used filter medium SII 24 - KRRX is shown in Figure 26.

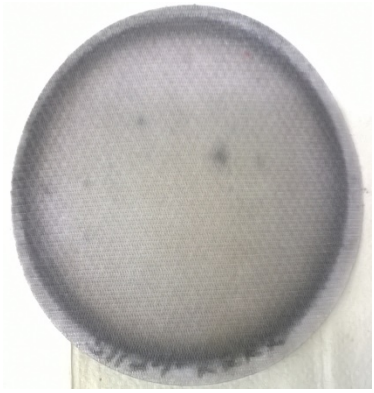

Figure 26. The filter medium used in the experiments, SII 24 – KRRX.

The magnetite slurry to be filtered was poured into the cell, and the filtration started when the control valve was opened. At this point, the slurry deposited on the filter medium was exposed to vacuum pressure created in the box. The filtrate was collected into a container placed on the balance within the box. The used vacuum pressure of the experiments ranged from 0.3 bar to 0.8 bar. The filtration equipment was connected to Labview software, where all the filtration data was recorded once per second. The recorded parameters were the filtrate weight, vacuum pressure and the speed, temperature and pressure of the air flow through the cake. The Büchner constant vacuum pressure filtration equipment parts are shown in Figure 27.

Figure 27. Büchner constant vacuum pressure filtration equipment: the vacuum box with the balance inside (left) and the filter cell (right).

The non-fractionated magnetite slurry filtrations

The non-fractionated magnetite slurry filtrations were carried out to study the filtrate flow rate, cake compressibility and the filtration capacity. The effect of slurry settling time before the filtration on the aforementioned quantities was also investigated. The compressibility factor of the magnetite slurry cake was

determined by performing filtrations at different vacuum pressure differences across the cake, ranging from 0.3 to 0.8 bars. The simplified experiment progress regarding the non-fractionated slurry filtrations is described in Figure 28.

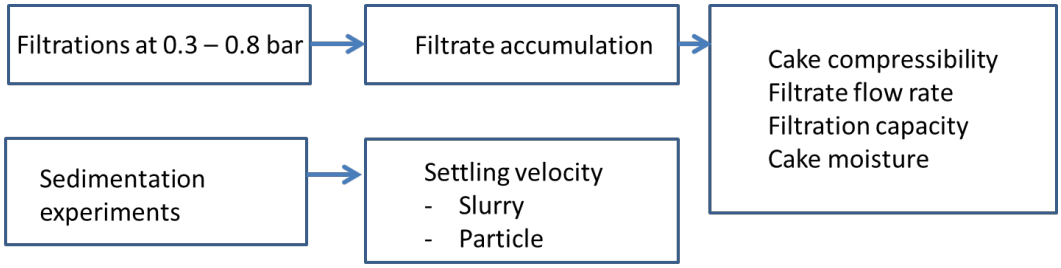

Figure 28. The experiment progress of non-fractionated slurry filtrations.

Repeatability of the filtration experiments was explored by performing the filtrations 2-4 times at each pressure (bar). The two settling effect experiments were carried out once each. The experiments in which 0.5 bar vacuum pressure was applied, were chosen as reference experiments. The gained results were compared to the respective fractionated magnetite slurry filtration results.

Each filtration was performed by pouring the slurry batch into the filter cell, after which the control valve was opened and filtration process started. In the experiments where settling of the slurry was not used, the control valve was opened immediately after pouring the slurry batch into the cell. In the settling effect experiments, the control valve was opened after the desired settling time (1.5 min & 3 min) of the slurry. In each non-fractionated slurry filtration experiment the vacuum pressure was applied for 6-6.5 minutes until the control valve was closed, thus terminating the filtration process. Figure 29 describes the non-fractionated slurry batch filtrations.

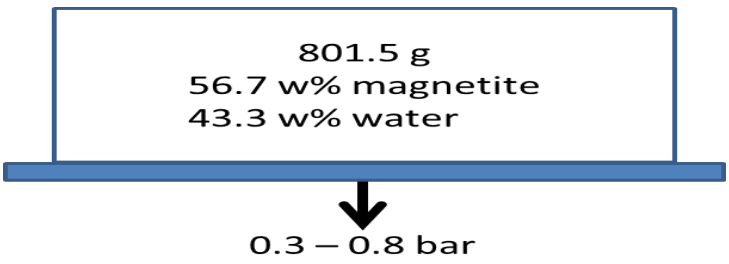

Figure 29. Schematic picture describing non-fractionated slurry batch filtrations. Slurry batch (801.5 g, magnetite concentration 56.7 w%) on the filter medium, vacuum pressure ranging between 0.3 – 0.8 bar below the filter medium.

After filtration, the formed magnetite slurry cake was weighed. The thickness of the cake was measured with a caliper at the center and at four edges. The obtained thickness values were used to calculate the average thickness of the cake. Finally, the cakes were placed into an oven at 105 °C to dry for at least 48 hours. The dried cakes were also weighed in order to calculate the needed quantities.

The fractionated magnetite slurry filtrations

The fractionated magnetite slurry filtrations were carried out to study how the pre-coating of the filter medium by coarse particle fraction affects the filtrate flow rate, cake moisture content and the filtration capacity of the process. The results were compared to the non-fractionated magnetite slurry filtrations. The effect of slurry settling time before the filtration on the aforementioned quantities was also investigated. Repeatability of the filtration experiments was explored by performing the filtrations 2-3 times. The three settling effect experiments were carried out once each. The applied vacuum pressure during all the fraction filtrations was 0.5 bar. The simplified experiment progress regarding the fractionated slurry filtrations is described in Figure 30.

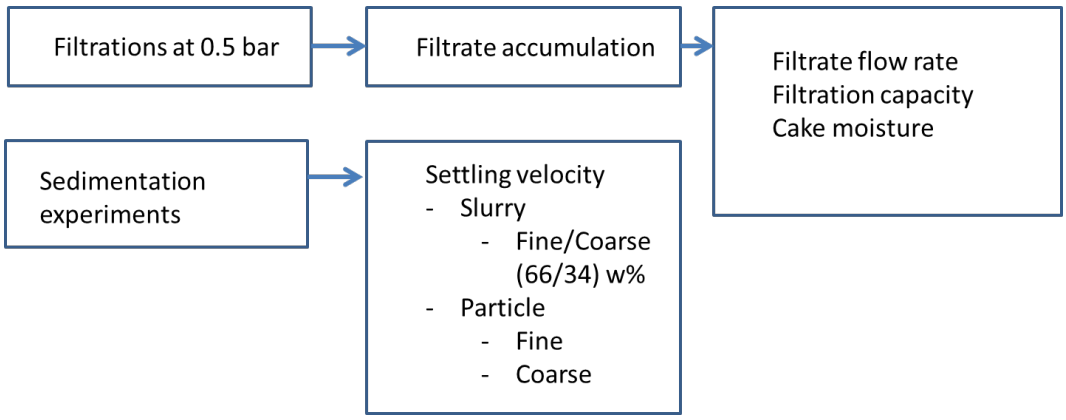

Figure 30. The experiment progress of fractionated slurry filtrations.

Each filtration was performed by pouring first the coarse particle slurry batch into the filter cell to form the pre-coat layer on the filter medium, after which the fine particle slurry batch was introduced on top of the formed coarse pre-coat layer. Figure 31 describes the fractionated slurry batch filtrations.

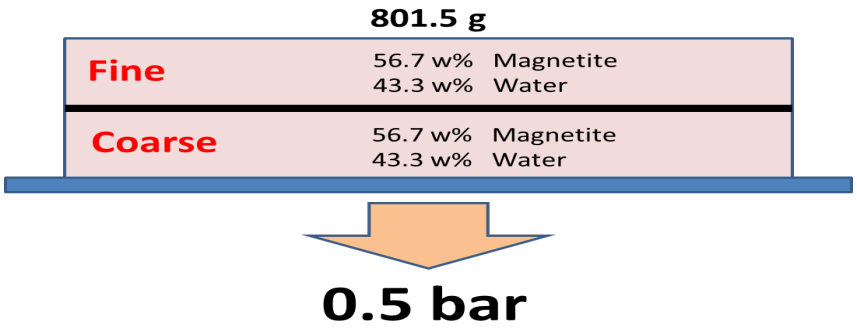

Figure 31. Schematic picture describing fractionated slurry filtrations. Slurry batch (801.5 g with fine and coarse fraction included) on the filter medium, vacuum pressure 0.5 bar below the filter medium.

The control valve was opened immediately after pouring the coarse particle slurry batch into the cell, and closed after a few seconds as the slurry was dewatered. As the overall weight of the first poured slurry batch was substantially lower than that of the second one, filtering of the slurry took only a few seconds in most cases. This caused a rapid change in vacuum pressure, and it took 1.5-2 minutes until the pressure was recovered at the initial level.

The fine particle slurry batch was poured on top of the formed pre-coat layer after this, and the filtration was started again by immediately opening the control valve. After the water layer was seemingly vanished from the cake surface and the filtrate was no more obtained, the filtration process was still carried out for 3 minutes to remove the moisture from the cake. After this, the control valve was closed. The overall filtration process duration of the experiments ranged between 5-7.5 minutes.

In the settling effect experiments, both coarse and fine slurry batches were poured into the filter cell before the control valve was opened. After the coarse particle fraction was poured, it was let to settle for 1.5 minutes. After this, the fine particle fraction was carefully spread on top of it to avoid the breaking of the pre-coat layer. The spreading was done by pouring the slurry on a spoon from where it carefully spilled into the filter cell. The control valve was opened after the fine particle slurry had settled for 1.5 minutes. The overall filtration process duration of the experiments ranged between 6-9.5 minutes.

After the filtrations, each cake and the gained filtrate amount was weighed. The same procedures and quantity calculations were carried out the same way as in the non-fractionated slurry filtrations.

8.3 Magnetite sievings

Each magnetite sample for fractionated slurry filtrations was sieved into fine and coarse fractions. The fine magnetite fraction was collected in a cup attached below the used sieve (38 µm, 45 µm or 75 µm). The magnetite sample was first introduced in a 2 mm sieve above the actual used sieve. These three parts were kept still with a lid fastened into two poles. The combination of the sieves, cup and lid was placed on a vibrating plane that caused the fine magnetite particles pass through the used sieve into the cup below. The coarse particle fraction was thus left on top of the used sieve. The used sieving equipment with the needed parts assembled is shown in Figure 32. Table I describes the obtained fine and coarse fractions and the used sieves in more detail.

Figure 32. The sieving machine with all parts assembled (left), upper and more loose sieve (up right), lower and more dense sieve (down right).

Table I. The sieve batches used in fraction filtrations.

Sieve batch	Sieve, µm	Sieving time, h	F/C w% ratio
s1	45	7.5	69/31
s2	38	7	66/34
s3	75	4	86/14
s4	38	8	66/34
s5	45	10	69/31
s6	75	15	86/14
s7	38	16	68/32
s8	45	8	69/31
s9	75	21	86/14
s10	38	11	66/34
s11	45	4.83	69/31
s14	45	1	66/34
s15	38	3.5	66/34
s16	75	3.75	86/14

It can be seen in Table I, that sieving time ranged substantially between the sievings where the same sieve size and F/C w% ratio was used. This occurred due to sieve pore blocking by the fine magnetite particles over time. Moreover, magnetic properties of the magnetite particles probably caused agglomeration between the particles. This might have slowed down the sieving process even further. The fractions obtained from the sieve batch s2 were used in sedimentation experiments. The sieve batches s12 and s13 were left out. This was due to the unreliable results gained from the fraction filtration experiments in which the fractions from these sieve batches were used.

8.4 Sedimentation experiments

The sedimentation experiments for magnetite slurries were carried out in 500 ml and 100 ml graduated cylinders, diameters of which were 5.9 cm and 2.6 cm

respectively. Settling progress was observed regarding the settling velocity of the slurry. In each experiment the upper interface height of the magnetite particle bed and sedimentation flux were measured as a function of time. As stated by Coulson *et al.* [6], the friction effect of the graduated cylinder wall on the settling behavior does not occur when the ratio of the diameter of the graduated cylinders to the diameter of the slurry particles is greater than 100. Thus, the wall friction effects of the graduated cylinders used in the experiments were considered negligible. Sedimentation flux was calculated with Equation (48):

$$\Psi = \frac{\rho h A_s}{A_s t} = \frac{\rho h}{t} \tag{48}$$

where Ψ Sedimentation flux, kg/m^{2}s

ρ Slurry density, kg/m^3

h Slurry height, m

A_s Sedimentation area, m^2

t Time, s

After the magnetite slurry batch was poured into the cylinder, the initial interface height of the slurry particle bed in the cylinder was marked down. Recording of the interface height change was started immediately after the slurry was vertically mixed with a mixing rod and the rod was pulled out of the cylinder. The magnetite particle bed interface height was measured at several spots, and the time at every spot was marked down. In some of the experiments, the settling progress was also documented by taking photos of several phases during the experiment. In order to ensure the repeatability of the results, the experiments were carried out 3-7 times. Figure 33 describes a magnetite slurry batch sedimentation in a 500 ml graduated cylinder.

Figure 33. Magnetite slurry in a 500 ml graduated cylinder.

8.5 Analyses

Several analyses were carried out to support the gained filtration results. To investigate the volumetric particle size distribution of different cake layers, barrel batch samples and separate fine and coarse fractions, laser diffraction method was used. To explore closer the cake layers and particle deposition, scanning electron microscope was employed to obtain exact pictures.

8.5.1 Volumetric particle size distribution

Each particle analysis sample, weighing 1.5 – 2.5 g, was mixed with 40-50 ml of tap water. The samples were then introduced to a 1000 ml analyzer beaker with a pipette. The beaker was filled with de-ionized water. The sample was then stirred with a motorized stirrer, and the volumetric particle size distribution was measured with laser diffraction for 3-5 times at 15 second intervals. Fraunhofer method was used in the size distribution definition. Each experiment was repeated 2-4 times, and the average value was obtained. As the volumetric particle size distribution was obtained, the gained values of Dx(10), Dx(50), Dx(90) and D[3;2] were used in the calculations.

Cake layers

In order to study the deposition of particles in different cake layers, a sample piece was taken out of the cake with an apple-corer. The sample was divided into three parts that represent the bottom, center and top layers of the cake. All the layer samples had nearly the same weight. Thus it was made sure that each part of the cake layer was represented at equal cross-sectional thickness.

Reference batch and fractions

Volumetric particle size distribution was determined from the barrel magnetite batch to determine the particle properties of the slurries used in the non-fractionated slurry filtrations. To investigate in more detail how different particle size ratios affect the filtration results, the volumetric particle size distribution of every sieved fine and coarse particle fraction was also measured.

8.5.2 Scanning electron microscope

In order to investigate the particle deposition in the cake layers in more detail, scanning electron microscope was used to obtain pictures of different cake layers. Acceleration voltage of 15.0 kV, 25x magnification and detector SE were used. The pictures were obtained from dry cake samples. Deposition of particles across the cake layer and the existence of possible voids were investigated.

In order to investigate the particle shape in the cake layers in more detail, one of the samples was casted into Epofix epoxy resin. Once the sample was dried for several days, the formed piece was sharpened and buffed with Struers Tegrapol equipment. Acceleration voltage of 15.0 kV, 100x magnification, detector BSE-3D and chamber pressure of 80 Pa were used.

9 EXPERIMENTAL RESULTS

Altogether 18 non-fractionated and 13 fractionated slurry batch filtrations were carried out. The effect of fractionation on filtrate flow rates and filtration capacity of the process were studied. Also the moisture content, compressibility and other essential properties of the cake were determined. The effect of settling on the filtration performance was explored. The non-fractionated slurry filtrations carried out at 0.5 bar were used as a reference for the respective fractionated slurry batch filtrations.

9.1 Non-fractionated slurry

At first, 16 filtrations were performed in order to study the filtrate flow rates at different vacuum pressures (0.3 – 0.8 bar) and to calculate the essential properties of the cake. The particle size properties were the same in all non-fractionated slurry filtrations. The volumetric particle size distribution of the non-fractionated slurry is presented by Figure 34 and Table II.

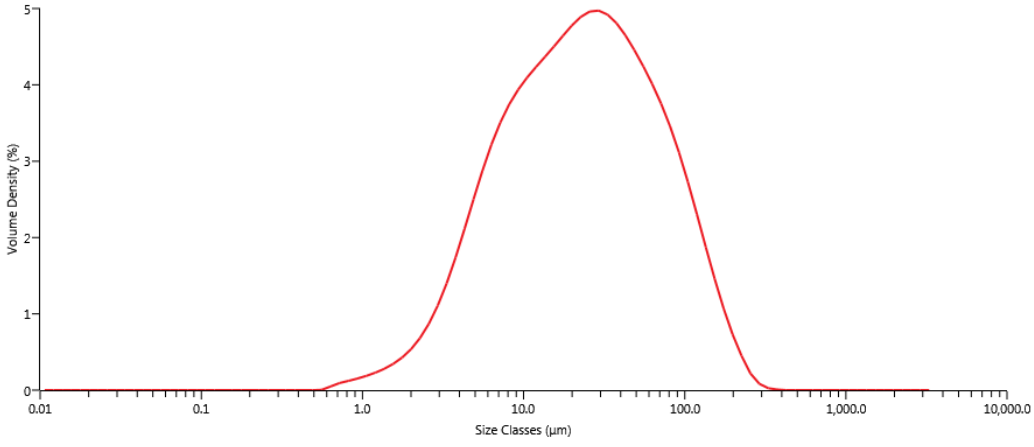

Figure 34. The volumetric particle size distribution of a magnetite barrel sample, representing all non-fractionated magnetite slurry filtrations. The detailed information is presented in Table II.

Table II. The volumetric particle size distribution of the non-fractionated slurries.

Particle size, µm				
Dx(10)	Dx(50)	Dx(90)	D[3;2]	D[4;3]
4.99	23.10	93.90	11.50	38.30

9.1.1 Filtrate flow rate and the cake properties

Non-fractionated magnetite slurry filtrations showed good repeatability. Filtrations carried out in different vacuum pressures were clearly distinguished, as can be seen in Figure 35. As expected, higher vacuum pressure used in the experiment resulted in faster filtering of the slurry. Each filtration was carried out until the accumulation of filtrate was no longer obtained.

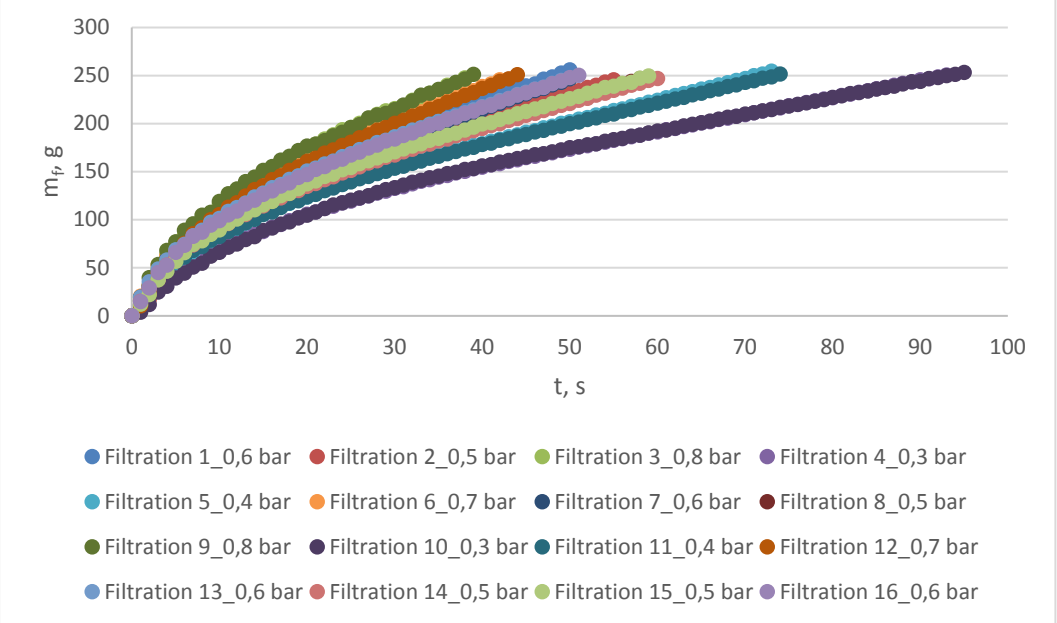

Figure 35. Non-fractionated magnetite slurry filtrate accumulation as the function of time. Slurry magnetite concentration 56.7 w%, density 1838.8 kg·m^{-3}. The applied vacuum pressure difference range 0.3-0.8 bar, filtration area 0.00985 m^2.

In Figure 35 the filtrate accumulation trend is similar to which the theory suggests for constant pressure cake filtration [7, 10, 37]. Similar trends in filtration graphs have also been obtained in other research experiments [64, 65]. The measurement transcript of these experiments can be found in Appendix II. The increased vacuum pressure in the filtrations lowered the cake moisture. This can be easily observed in Figure 36, where the obtained cakes were exposed to vacuum pressures ranging from 0.3 bar to 0.8 bar. The essential properties of the non-fractionated cakes were determined. The obtained values of the average cake specific resistance, filtration capacity, porosity, moisture content and saturation are presented in Table III.

Figure 36. Magnetite slurry cakes obtained at different vacuum pressures. From left to right: 0.3 bar (Filtration 4), 0.5 bar (Filtration 8), 0.7 bar (Filtration 6) and 0.8 bar (Filtration 9).

Table III. The properties of non-fractionated slurry cakes.

Filtration	Δp bar	ε_{cake} -	Cake moisture w%	α_{av} 10^9 kg·m^{-1}	Capacity kg$_{\text{Dry cake}}$·m^{-2}·h^{-1}	S -
1	0.6	0.66	12.0	4.49	3071	0.63
2	0.5	0.73	13.1	5.33	3040	0.61
3	0.8	0.60	10.9	5.14	4232	0.64
4	0.3	0.81	14.3	4.97	1713	0.60
5	0.4	0.79	14.1	5.29	2123	0.60
6	0.7	0.61	11.1	5.51	3702	0.62
7	0.6	0.65	11.8	5.65	3145	0.63
8	0.5	0.74	13.2	4.89	2704	0.61
9	0.8	0.58	10.6	5.91	4078	0.59
10	0.3	0.80	14.1	4.88	1621	0.58
11	0.4	0.80	14.1	5.42	2138	0.61
12	0.7	0.59	10.9	5.32	3799	0.61
13	0.6	0.63	11.5	5.60	3260	0.62
14	0.5	0.75	13.4	5.46	2648	0.59
15	0.5	0.75	13.4	4.78	2699	0.59
16	0.6	0.62	11.4	5.55	2993	0.61

As expected, the increased vacuum pressure resulted in lower porosity and cake moisture. The higher average cake specific resistance and filtration capacity also correlated with the increased vacuum pressure. These findings are similar to what the literature suggests [3, 7]. Saturation was almost the same in all filtrations.

The particle packing of non-fractionated slurry was investigated by carrying out volumetric particle size distribution analyses of the cake layers. Figure 37 and Table IV present the volumetric particle size distribution of bottom (red), center (green) and top (blue) layer of the magnetite slurry cake obtained at the vacuum pressure 0.8 bar (Filtration 9).

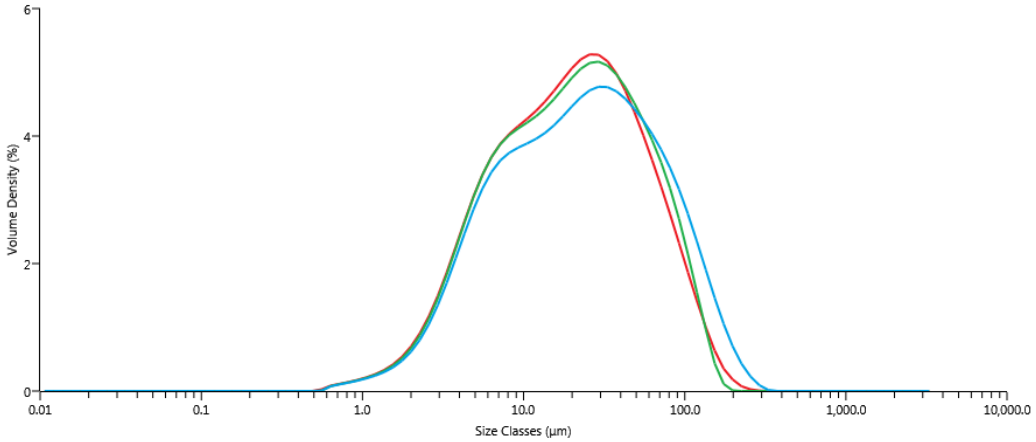

Figure 37. The volumetric particle size distribution of bottom (red), center (green) and top (blue) layers of the non-fractionated cake (Filtration 9). The applied vacuum pressure difference 0.8 bar, filtration area 0.00985 m^2. The detailed information is presented in Table IV.

Table IV. The volumetric particle size distribution of the cake layers from Filtration 9 at 0.8 bar.

	Particle size, µm				
Cake layer	Dx(10)	Dx(50)	Dx(90)	D[3;2]	D[4;3]
Bottom	4.30	19.40	72.00	9.94	30.20
Center	4.36	19.90	73.60	10.10	30.40
Top	4.56	22.60	94.20	10.80	38.00

The volumetric particle size distribution of the layers of the magnetite slurry cake obtained at the vacuum pressure 0.3 bar (Filtration 10) are presented in Figure 38 and Table V. The cake layers in Figure 38 are marked as follows: bottom (red), center (green) and top (blue).

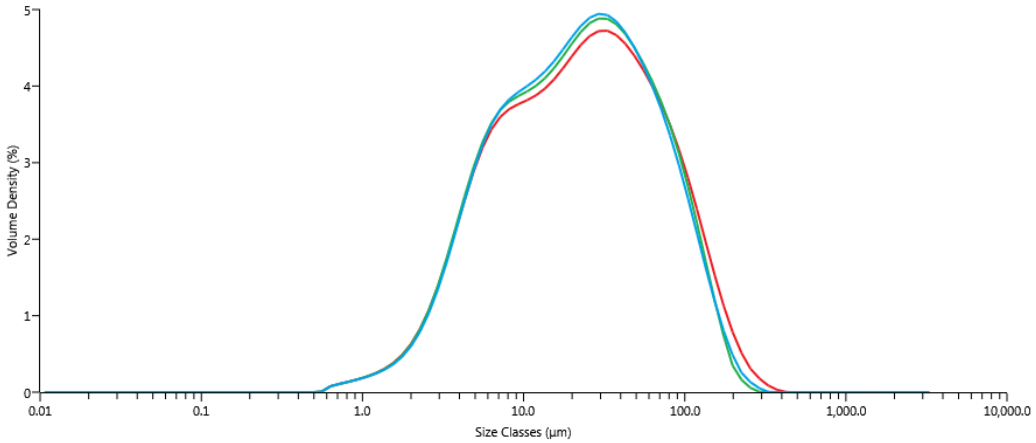

Figure 38. The volumetric particle size distribution of bottom (red), center (green) and top (blue) layers of the non-fractionated cake (Filtration 10). The applied vacuum pressure difference 0.3 bar, filtration area 0.00985 m^2. The detailed information is presented in Table V.

Table V. The volumetric particle size distribution of the cake layers from Filtration 10 at 0.3 bar.

	Particle size, µm				
Cake layer	Dx(10)	Dx(50)	Dx(90)	D[3;2]	D[4;3]
Bottom	4.50	22.90	96.90	10.80	39.10
Center	4.48	21.90	87.10	10.60	35.30
Top	4.56	21.80	86.70	10.70	35.50

The deposition of magnetite particles in the cake layers does not seem to be dependent on the used vacuum pressure. This can be seen when the particle size values in the cake layers are compared between Tables IV and V. It could be assumed that the higher vacuum pressure draws the largest particles towards the bottom layer, but the obtained values suggest on the contrary. This might indicate that once the slurry is poured into the filter cell, the initially reached particle deposition remains unchanged and the particles do not migrate towards the bottom layer of the cake. The incompressibility of the magnetite particles supports this conclusion.

Settling effect

The effect of slurry settling on the filtrate flow rates and the essential properties of the cake was explored by carrying out two filtrations at 0.5 bar, the first with the settling time of 1.5 minutes and the second with the settling time of 3 minutes before filtration. The filtrations were used as a reference for the respective fractionated slurry batch filtrations. The results were also compared to the other non-fractionated slurry filtrations carried out without settling.

It can be seen in Figure 39 that doubling the settling time before filtration did not have a notable effect on the flow rate. Each filtration was carried out until the accumulation of filtrate was no longer obtained.

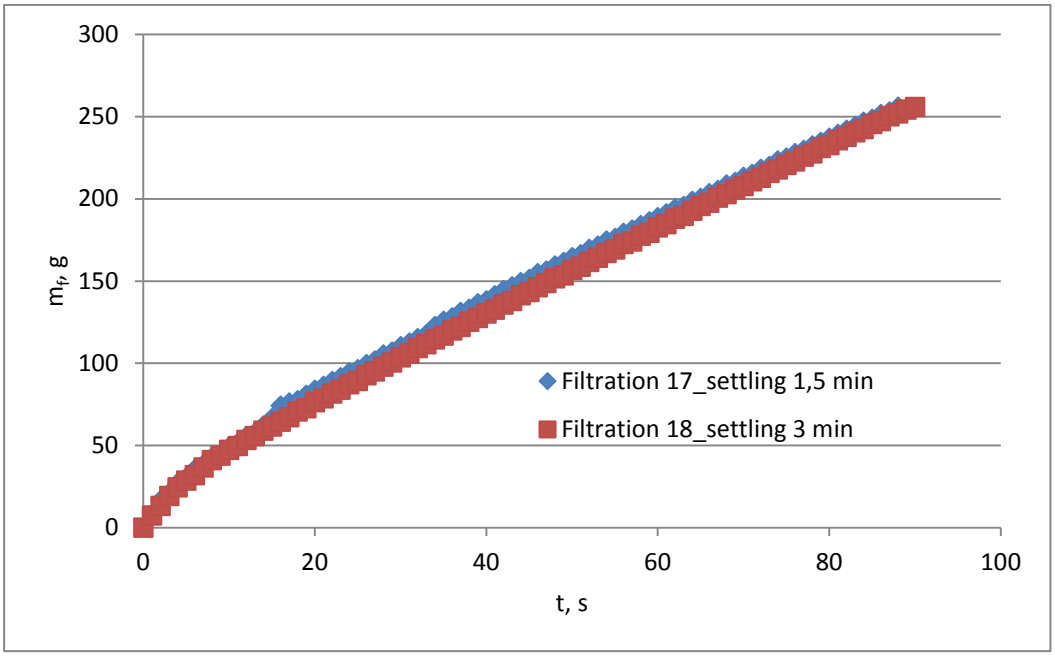

Figure 39. Settled non-fractionated magnetite slurry filtrate accumulation as the function of time. The settling time of 1.5 and 3 minutes before filtration. Slurry magnetite concentration 56.7 w%, slurry density 1838.8 kg·m^{-3}. The applied vacuum pressure difference 0.5 bar, filtration area 0.00985 m^2.

It can be assumed that settling of magnetite slurry makes the formed bed tightly packed quite rapidly, because of the high density of the magnetite particles. This might explain the negligible difference between the filtrate flow rates in Figure 39. The essential properties of the cake obtained from the settling filtrations is presented in Table VI. The measurement transcript of these experiments can be found in Appendix II.

Table VI. The properties of non-fractionated slurry cakes when settling was used, 1.5 minutes (Filtration 17) and 3 minutes (Filtration 18).

Filtration	Δp bar	ε_{cake} -	Cake moisture %	α_{av} 10^9 kg·m^{-1}	Capacity kg$_{\text{Dry cake}}$·m^{-2}·h^{-1}	S -
17	0.5	0.75	13.5	4.68	1862	0.57
18	0.5	0.73	13.1	4.36	1809	0.56

In comparison to the non-settled slurries, settling resulted in lower filtration capacity values. The porosity and cake moisture content remained basically unchanged, whereas the saturation value was a bit lower. Doubling the settling time did not have a significant effect on the aforementioned values.

The effect of settling on particle packing of non-fractionated slurry was investigated by carrying out volumetric particle size distribution analyses of the cake layers. Figures 40 and 41 and Tables VII and VIII present the volumetric particle size distribution of bottom (red), center (green) and top (blue) layer of the magnetite slurry cakes obtained at the vacuum pressure 0.5 bar with settling time of 1.5 min (Filtration 17) and 3 min (Filtration 18) respectively.

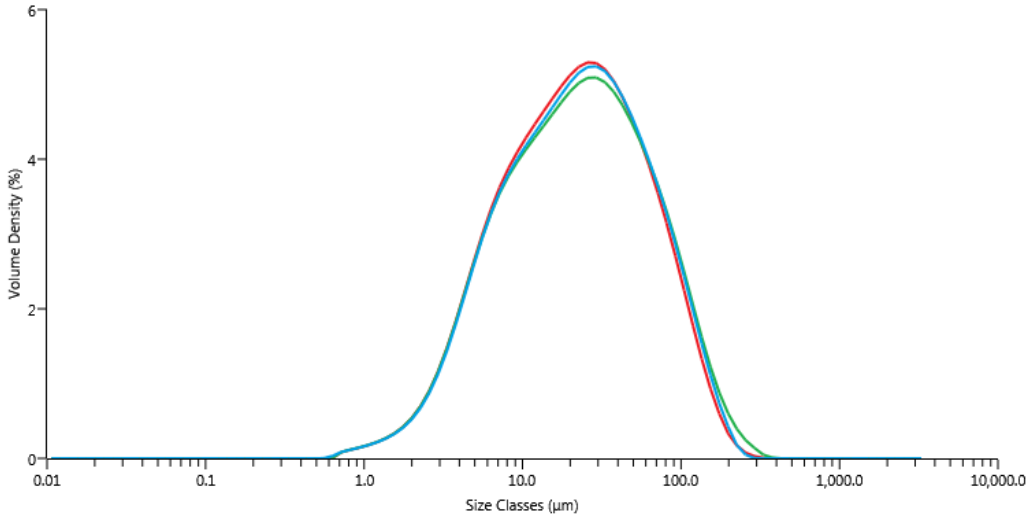

Figure 40. The volumetric particle size distribution of bottom (red), center (green) and top (blue) layers of the non-fractionated cake with the settling time of 1.5 min (Filtration 17). The applied vacuum pressure difference 0.5 bar, filtration area 0.00985 m^2. The detailed information is presented in Table VII.

Table VII. The volumetric particle size distribution of the cake layers from Filtration 17 with the settling time of 1.5 min.

	Particle size, µm				
Cake layer	Dx(10)	Dx(50)	Dx(90)	D[3;2]	D[4;3]
Bottom	4.92	21.50	80.20	11.30	33.70
Center	4.92	22.40	88.70	11.50	36.80
Top	4.98	22.20	84.00	11.50	34.90

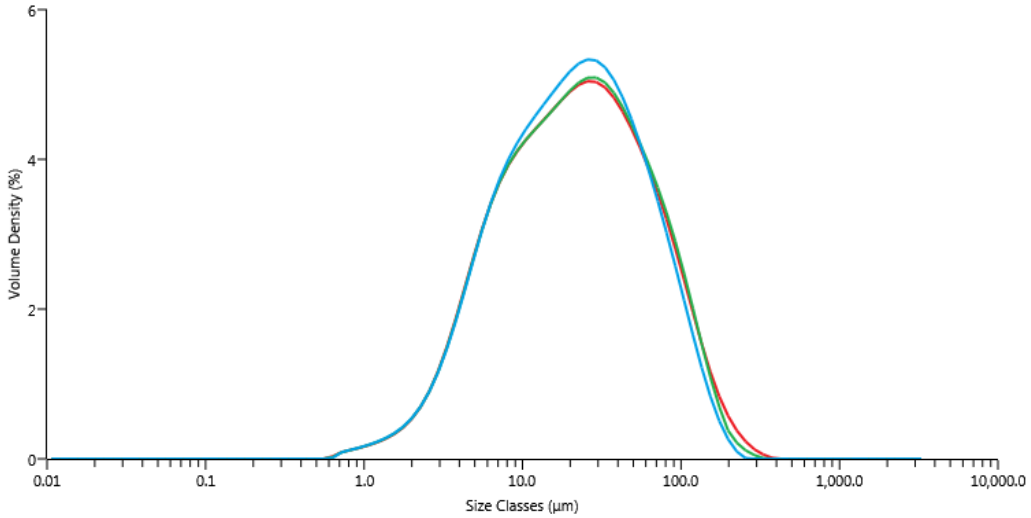

Figure 41. The volumetric particle size distribution of bottom (red), center (green) and top (blue) layers of the non-fractionated cake with the settling time of 3 min (Filtration 18). The applied vacuum pressure difference 0.5 bar, filtration area 0.00985 m^2. The detailed information is presented in Table VIII.

Table VIII. The volumetric particle size distribution of the cake layers from Filtration 18 with the settling time of 3 min.

Cake layer	Particle size, µm				
	Dx(10)	Dx(50)	Dx(90)	D[3;2]	D[4;3]
Bottom	4.87	21.60	86.50	11.20	35.90
Center	4.88	21.70	84.50	11.20	34.90
Top	4.89	20.90	76.80	11.10	32.40

As the magnetite particles are incompressible, the settling effect on particle deposition in the cake layers might be considered quite negligible. When the settling time of 1.5 minutes was used, the particle size in the bottom layer was smaller than in the top layer. Even though the obtained particle sizes were found to be other way around when the settling time of 3 minutes was used, it might be due to random initial particle deposition that varies between each experiment as the slurry is poured into the filter cell.

9.1.2 Cake compressibility

The compressibility of the magnetite slurry cake was defined by the value of power coefficient obtained in Figure 42, defined by Equation (26). The average cake specific resistance values were plotted as the function of the applied vacuum pressure. The values used in Figure 42 are obtained from Table III.

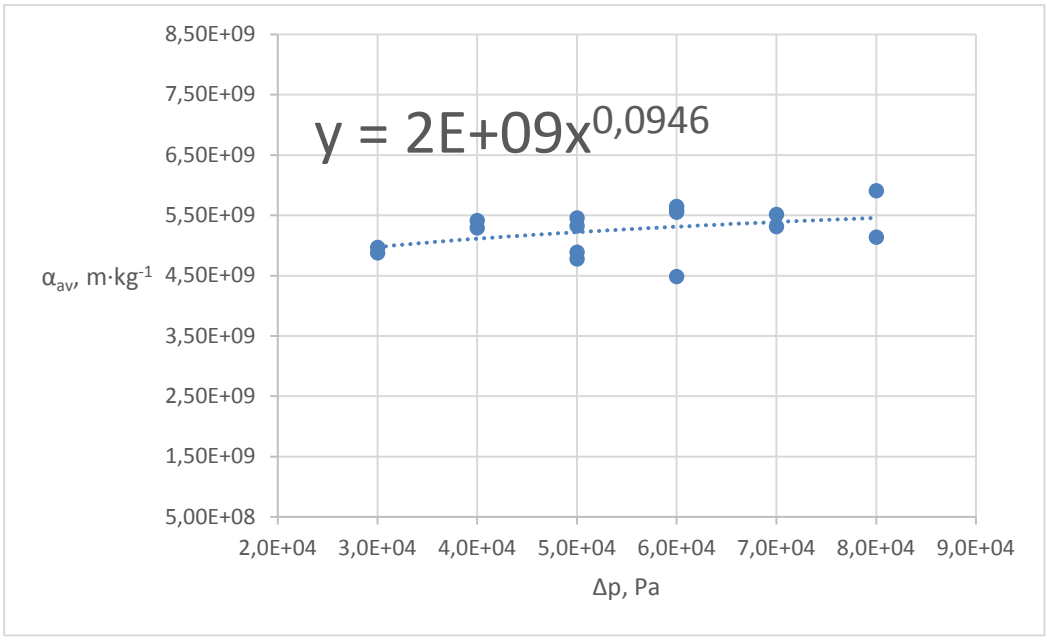

Figure 42. Magnetite slurry cake compressibility. Average cake specific resistance as the function of vacuum pressure difference. Slurry magnetite concentration 56.7 w%, slurry density 1838.8 kg·m^{-3}, slurry batch weight 801.5 g, filtration area 0.00985 m^2.

As expected, the average cake specific resistance slightly increased as the used pressure was increased. However, as the density of the used magnetite in the slurry batches was determined as high as 4849 kg·m^{-3}, it was expected that the cake would be almost incompressible. The obtained value for the coefficient was 0.0946, which indicated that the formed magnetite slurry cake was almost incompressible, as determined in the literature by Wakeman and Tarleton [1]. As the applied vacuum pressure was increased, the trend of the average cake specific resistance increase was found to be similar to the trend reported in other research experiments where dead-end filtration was employed [16, 66, 67].

9.1.3 Sedimentation experiments

Sedimentation of the non-fractionated magnetite slurry was investigated. At first, a 56.7 w% magnetite slurry batch was settled in order to find out the repeatability of the experiments in addition to the sedimentation flux and the slurry interface height change behavior. Then, it was studied how the change of magnetite concentration in the slurry affects the settling behavior. The experiments were carried out in a 500 ml graduated cylinder.

Sedimentation of 56.7 w% magnetite slurry

The results showed good repeatability for the sedimentation experiments carried out with a 56.7 w% magnetite slurry. The experiments were carried out three times. The initial slurry height was 14.25 cm. As can be seen in Figure 43, neither the sedimentation flux nor the slurry interface height change vary significantly between the experiments.

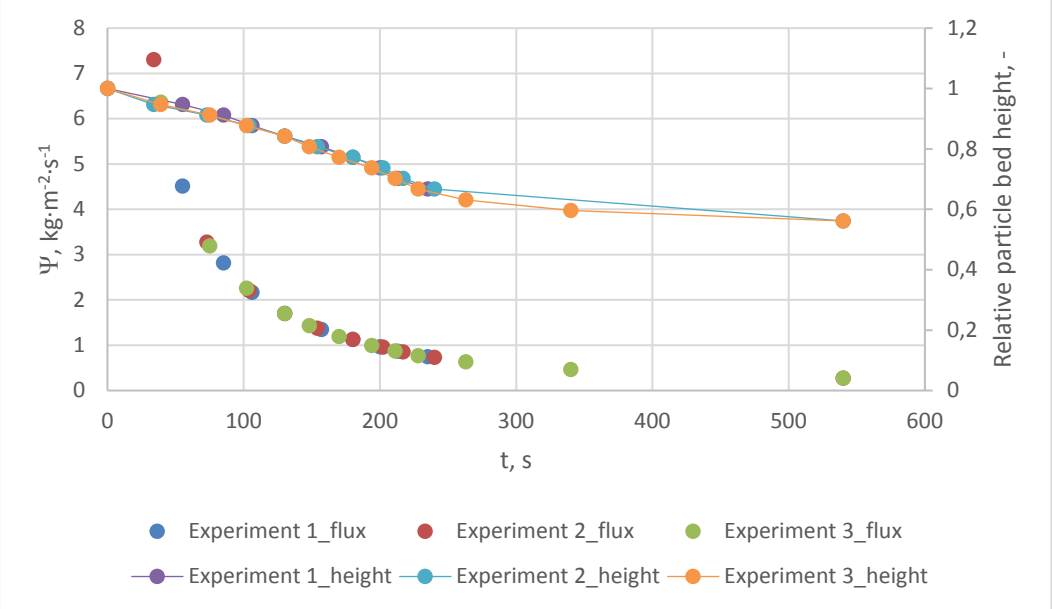

Figure 43. Magnetite slurry sedimentation flux and the upper interface height of the particle bed as the function of time in a 500 ml graduated cylinder (diameter 5.9 cm). Slurry magnetite concentration 56.7 w%, slurry density 1838.8 kg·m^{-3}, batch weight 801.5 g, sedimentation surface area 0.0027 m^2. Initial slurry height 14.25 cm, particle size values: Dx(50) 23.1 µm, D[3;2] 11.5 µm, D[4;3] 38.3 µm. The particle bed height described as the relative value to the initial slurry height.

In Figure 43, sedimentation flux and particle bed height decrease over time. The sediment layer settled at the height of 7 cm after 25 min. In the figure, the settling progress is described until 9 min. As mentioned in the literature [6], separate zones create change in fluid flow behavior during the progress of settling. In this experiment, sedimentation flux decreases substantially already at the early stage of the progress. This phenomenon is most probably caused by the volume displacing return flow as the larger particles fall underneath the finer ones. This would correlate with the theory presented by *Coulson et al.* [6] and gravitational sedimentation simulation presented by *Lu et al.* [36]. Hindered settling was observed, which is described by Mory [17], as the downward movement of a set of particles slows down settling along with time. The measurement transcript of the sedimentation experiments of Figure 43 can be found in Appendix III. Separate zones during the sedimentation experiment were visible, as can be seen in Figure 44.

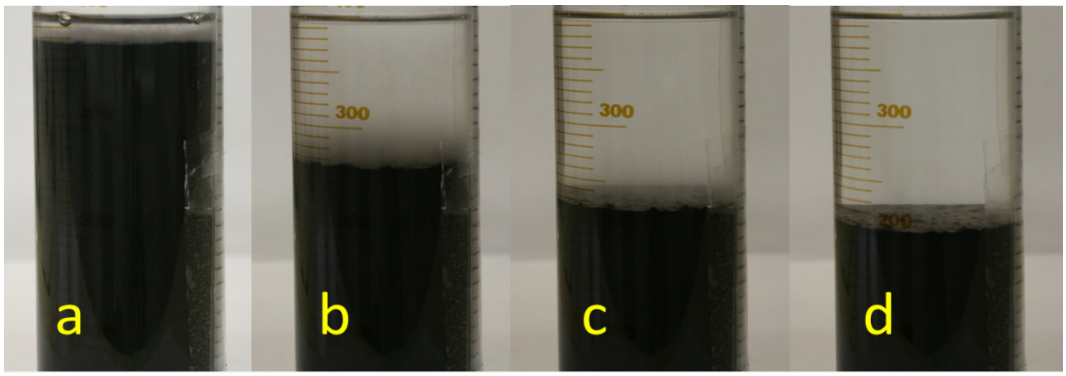

Figure 44. Settling progress during Experiment 3 described in Figure 43. Settling progress at 1min (a), 4min (b), 10min (c) and 35min (d). Three different zones can be distinguished over time: clear liquid, zone of variable composition and sediment [6]. Slurry magnetite concentration 56.7 w%, slurry density 1838.8 kg·m-3, batch weight 801.5 g, sedimentation surface area 0.0027 m2. Initial slurry height 14.25 cm. Slurry settling velocity 0.2 mm/s, particle terminal settling velocity 1.1 mm/s.

In Figure 44, it can be seen that different zones become visible already at the beginning of the sedimentation. As can be seen in the *a* and *b* parts, finer particles rapidly form a layer above the thicker sediment layer. Clear liquid zone naturally becomes larger over time, as the particles settle by the gravitational force and sediment layer becomes more compacted. This is clearly seen during the settling progress, as the parts *b*, *c* and *d* are compared. Overall, the distinguished zones and hindered settling phenomenon correlate well with the theory presented in the literature [6, 17]. Also, the findings are similar to other research experiments where the distinguished zones are described [24, 31, 36].

Using the Stokes' Law Equation (28), the terminal settling velocity for a single particle (23.10 µm) was calculated as 1.1 mm/s. By using the obtained value, the Reynolds number was calculated to define the settling regime with Equation (36). The Archimedes number was also calculated to verify the settling regime with Equation (37). The obtained number values and the defined settling regime are listed in Table IX.

Table IX. The settling regime of the 56.7 w% magnetite slurry (Figure 43).

Re-number (*Equation 36*), -	Ar-number (*Equation 37*), -	Settling regime
0.03	$4.75 \cdot 10^{-7}$	Laminar

As the literature suggests [17, 19], the low values for both Reynolds and Archimedes number define the settling regime as laminar. The overall average slurry settling velocity was measured as 0.2 mm/s. The obtained average slurry settling velocities in mm/s for each experiment are listed in Table X. The velocities were measured until 228-240 seconds after the sedimentation recording was started.

Table X. Average slurry settling velocities of the 56.7 w% magnetite slurry (Figure 43).

Test	Average slurry settling velocity, mm/s
1	0.2
2	0.2
3	0.2

Magnetite concentration effect on settling behavior

In order to study the effect of magnetite slurry concentration on settling velocity, three sedimentation experiments were carried out using the concentrations of 56.7 w%, 45.0 w% and 35.0 w%, with the respective initial slurry heights of 15.5, 18.25 and 20.5 cm. Each experiment was repeated four times. The density values of 45.0 w% and 35.0 w% magnetite slurries were calculated as relative values compared to the measured density value of the 56.7 w% slurry, as the slightly different volume filled by the slurries was taken into account. The effect of magnetite concentration change on the settling behavior of the magnetite slurry is presented in Figure 45.

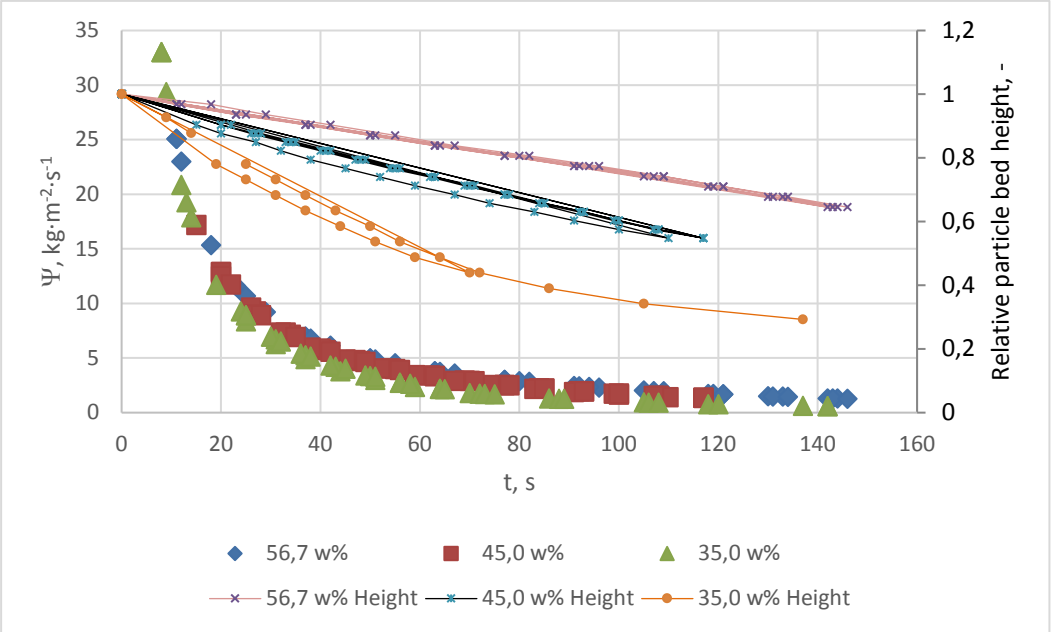

Figure 45. Magnetite slurry sedimentation flux and the upper interface height of the particle bed as the function of time in a 500 ml graduated cylinder (diameter 5.9 cm). Slurry magnetite concentrations 56.7 w%, 45.0 w% and 35.0 w%. Respective slurry densities: 1838.8 kg·m^{-3}, 1561.7 kg·m^{-3} and 1390.3 kg·m^{-3}. Batch weight 801.5 g, sedimentation surface area 0.0027 m^2. Particle size values: Dx(50) 23.1 µm, D[3;2] 11.5 µm, D[4;3] 38.3 µm. Initial slurry heights: 15.50 cm (56.7 w%), 18.25 cm (45.0 w%), 20.50 cm (35.0 w%). The particle bed height described as the relative value to the initial slurry height.

In the case of the 56.7 w% slurry, the settling progress is described until 150 s, at the point of which the sediment layer had settled at the height of 10 cm. The respective times and heights for the 45.0 w% slurry were 110-120 s and 10 cm, and for 35.0 w% slurry 130-150 s and 6 cm. It was discovered that the concentration decrease resulted in the increase of settling velocity, as can be seen in Figure 45. This observation correlates with theory presented by Svarovsky [3]. The difference in both sedimentation flux and slurry interface height over time between the slurries can be distinguished. The findings correlate with theory [6] and other research experiments [27, 28, 32, 33, 68]. The measurement transcript of the sedimentation experiments of Figure 45 can be found in Appendix III.

As the used slurry during the experiments had the same particle size distribution values than in the previous experiment, the settling regime of the experiments was laminar. The overall average slurry settling velocity in mm/s was measured for each slurry: 0.4 mm/s (56.7 w%), 0.7 mm/s (45.0 w%) and 1.1 mm/s (35.0 w%). The obtained average slurry settling velocities in mm/s for each experiment are listed in Table XI. The velocities were measured until 142-146 seconds (56.7 w%), 110-117 seconds (45.0 w%) and 70-142 seconds (35.0 w%) after the sedimentation recording was started. The average settling velocity of the 56.7 w% slurry was higher compared to the previous experiment (Table X) which was probably caused by the different mixing intensity.

Table XI. Average slurry settling velocities of the 56.7 w%, 45.0 w% and 35.0 w% magnetite slurries (Figure 45).

Magnetite concentration, w%	Test	Average slurry settling velocity, mm/s
56.7	1	0.4
	2	0.4
	3	0.4
	4	0.4
45.0	1	0.7
	2	0.7
	3	0.7
	4	0.7
35.0	1	1.4
	2	1.0
	3	1.0
	4	1.0

9.2 Fractionated slurry

In order to study fractionation effect on filtration performance and the properties of the formed filter cake, 13 filtrations were carried out at 0.5 bar. The weight ratios between fine and coarse particle fractions used in the experiments were 86/14, 69/31, 68/32 and 66/34. The filtrate flow rates, filtration capacities and the essential properties of the cake were studied. The volumetric particle size distribution of the obtained fine and coarse fractions, and the exact weights of the filtered fractions are listed in Appendices IV and V respectively. Fraction filtrations 11 and 12 were left out due to the unreliable results. Fraction filtrations 10, 14 and 15 were performed in order to investigate the settling effect before filtration on the filtration performance.

9.2.1 Filtrate flow rate and the cake properties

Fractionated magnetite slurry filtrations were performed by using four different fine/coarse fraction ratios obtained by using three different size sieves. Figure 46 presents the filtrate accumulation as the function of time in the fraction filtrations. In the figure, the numbers from left to right correspond to the number of the performed experiment, the sieve batch number and the sieve hole size in micro meters (μm). The number within the bracket correspond to the fine/coarse fraction ratio (w%). Each filtration was carried out until the accumulation of filtrate was no longer obtained.

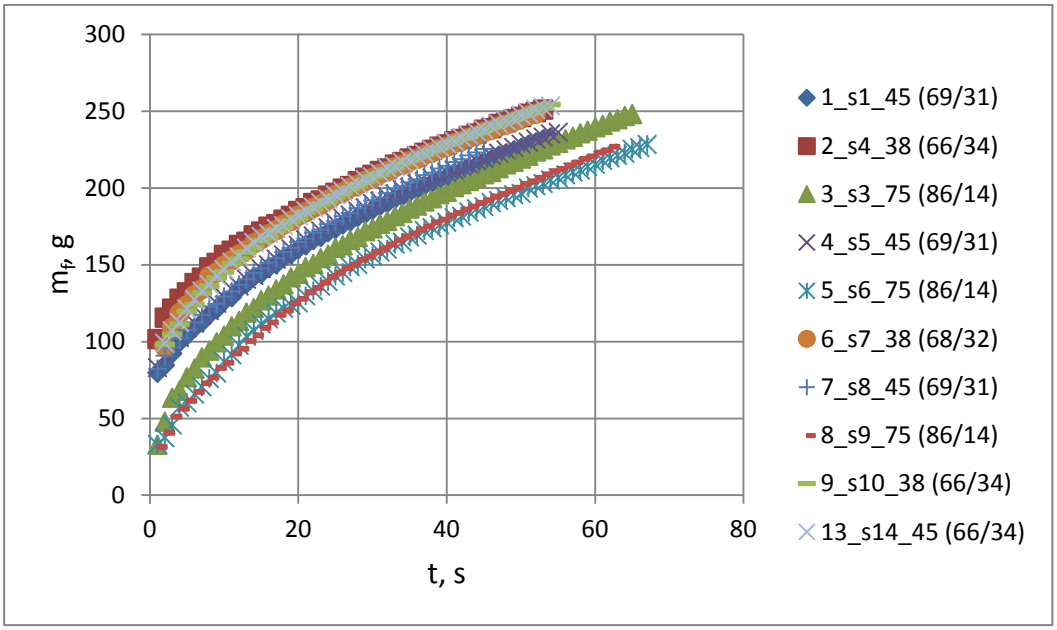

Figure 46. Filtrate accumulation as the function of time in fractionated slurry filtrations. Slurry magnetite concentration 56.7 w%, slurry density 1838.8 kg·m^{-3}. The applied vacuum pressure difference 0.5 bar, filtration area 0.00985 m^2. The particle size and fraction weight information of the fine and coarse fractions in Appendices IV and V.

It can be seen in Figure 46, that the filtrate flow rate was fastest when the fine fraction share of the formed magnetite slurry cake ranged between 66 and 69 w%. The filtrate flow rate was slower when the fine fraction share of the magnetite slurry cake was 86 w%. The particle size ratio between fine and coarse fractions did not substantially affect the filtrate flow rate. This can be concluded for example, when the filtrations 2_s4_38 (66/34) and 13_s14_45 (66/34) are compared. In both cases, the filtrate accumulation graph is almost equal even though the fractions for these experiments were obtained using different size of sieves, 38 µm and 45 µm respectively. The essential properties of the cake were determined. The obtained values of the average cake specific resistance, filtration capacity, porosity, moisture content and saturation of the fractionated cakes are presented in Table XII. The measurement transcript of these experiments can be found in Appendix VI.

Table XII. The properties of fractionated slurry cakes at vacuum pressure 0.5 bar.

Filtration	ε_{cake} -	Cake moisture w%	α_{av} 10^9 kg·m^{-1}	Capacity kg$_{\text{Dry cake}}$·m^{-2}·h^{-1}	S -
1_s1_45 (69/31)	0.81	14.3	8.35	2922	0.55
2_s4_38 (66/34)	0.80	14.1	11.69	2940	0.55
3_s3_75 (86/14)	0.78	13.9	7.37	2447	0.58
4_s5_45 (69/31)	0.82	14.4	9.43	2754	0.55
5_s6_75 (86/14)	0.78	13.8	7.49	2381	0.55
6_s7_38 (68/32)	0.77	13.7	10.64	3095	0.55
7_s8_45 (69/31)	0.79	14.1	9.21	3095	0.55
8_s9_75 (86/14)	0.79	14.0	8.11	2214	0.56
9_s10_38 (66/34)	0.76	13.5	9.61	2902	0.55
13_s14_45 (66/34)	0.80	14.1	9.41	2977	0.53

Compared to the non-fractionated counterpart at the vacuum pressure 0.5 bar, the fractionated slurry cakes showed higher average cake specific resistance values. Porosity, cake moisture and filtration capacity values were mostly a bit higher in the fractionated slurry cakes, whereas saturation values were a bit lower.

Scanning electron microscope analysis

In order to investigate the particle deposition in the cake layers, SEM pictures were obtained. Figure 47 presents the cross-sectional cake layers of the cake obtained from filtration 8_s9_75 (86/14).

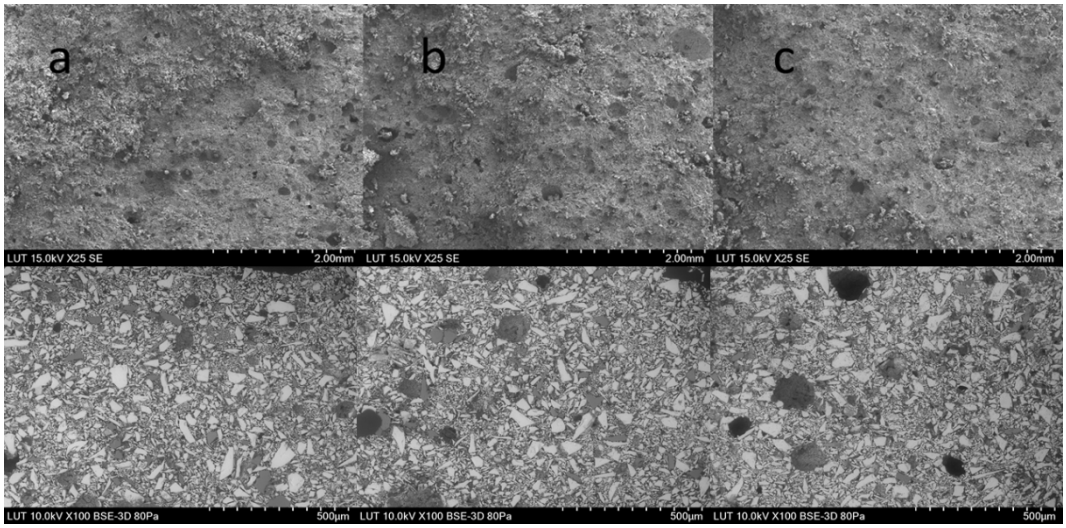

Figure 47. SEM-pictures representing the particle deposition in top, center and bottom layers of the fractionated magnetite slurry cake (filtration 8_s9_75 (86/14)). The pictures above from left to right: a (top), b (center) and c (bottom) of the dry cake sample. Acceleration voltage 15.0 kV, 25x magnification, SE detector. The pictures below from left to right: 11, 6 and 1 mm from the bottom. Acceleration voltage 15.0 kV, 100x magnification, BSE-3D detector, chamber pressure 80 Pa. The sample casted into Epofix epoxy resin. The visible dark spots represent the air bubbles in the sample (pictures below).

In Figure 47, the pictures above from left to right present the cross-sectional pictures taken from top (a), center (b) and bottom (c) layers of the cake from the dry cake sample. Below, the resin sample pictures present the particle deposition in different cake layers. From left to right, the deposition of particles is described from 11mm, 6mm and 1mm from the bottom. As can be seen in Figure 47, the coarser particles do not seem to form a uniform layer at any part of the cake, thus allowing the finer particles to fill the spaces in between them. This type of tight packing might efficiently lower the filtrate flow rate through the cake, by decreasing the overall void space. As described earlier, compared to the non-fractionated slurry filtrations the fractionated slurry filtrations did not show improvement in terms of the filtrate flow rate. The particle deposition described in Figure 47 might give a reason to this observation. According to Svarovsky [3], this type of cake build-up is blinding in the cake itself and it differs from the ideal condition.

Settling effect

The effect of settling on the filtrate flow rates and the essential properties of the cake was explored by carrying out three filtrations, where both coarse and fine fractions were settled for 1.5 minutes before the filtration started at 0.5 bar. The used fine/coarse ratios were 86/14, 69/31 and 66/34. Each filtration was carried out until the accumulation of filtrate was no longer obtained. The filtration graphs are presented in Figure 48.

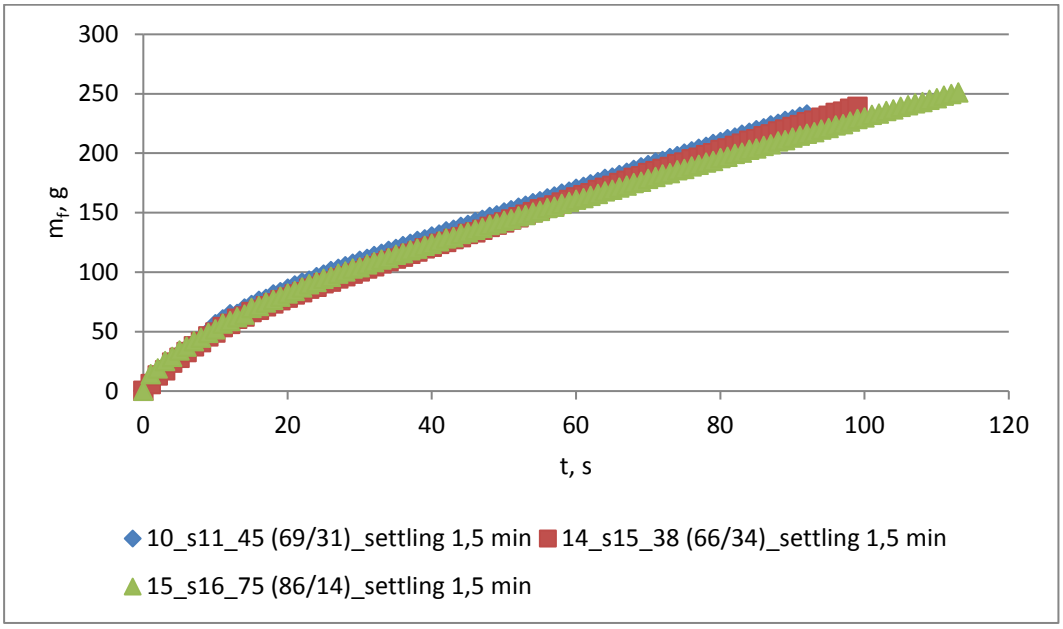

Figure 48. Settled fractionated magnetite slurry filtrate accumulation as the function of time. Both coarse and fine fractions settled for 1.5 minutes before filtration. The fine/coarse fraction ratios (w%): 86/14, 69/31 and 66/34. Slurry magnetite concentration 56.7 w%, slurry density 1838.8 kg·m^{-3}. The applied vacuum pressure difference 0.5 bar, filtration area 0.00985 m^2.

It can be seen in Figure 48, that there is no substantial difference in the filtrate flow rate between the filtrations. When filtrations 10 and 14 are compared, a slight increase in filtrate accumulation can be observed as the coarse fraction amount decreases. Regarding the filtration 15, the exceptional filtrate accumulation trend most probably derives from the uneven spreading of the coarse particle pre-coat layer. The essential properties of the cake obtained from the settling filtrations are presented in Table XIII. The measurement transcript of these experiments can be found in Appendix VI.

Table XIII. The properties of fractionated slurry cakes when settling was used for 1.5 minutes for both fractions.

Filtration	ε_{cake} -	Cake moisture w%	α_{av} 10^9 kg·m^{-1}	Capacity kg$_{Dry\ cake}$·m^{-2}·h^{-1}	S -
10_s11_45 (69/31)	0.81	14.2	7.31	1708	0.55
14_s15_38 (66/34)	0.80	14.2	7.02	1582	0.57
15_s16_75 (86/14)	0.78	13.9	8.41	1426	0.58

Settling effect on the fractionated magnetite slurry cakes did not improve filtration capacity. Porosity, cake moisture content and saturation remained almost unchanged.

9.2.2 Sedimentation experiments

Settling behavior of the fine and coarse fractions both separately and combined were studied. The sedimentation experiments were carried out in a 100 ml graduated cylinder.

Fine and coarse fraction sedimentation

The experiment where the fractions were combined, the fine/coarse ratio of 66/34 w% was used. In each experiment, the slurry magnetite concentration was 56.7 w%. The fractions were obtained from the sieve batch s2, where the hole size was 38 µm. Table XIV presents the particle properties of both fine and coarse fractions obtained from the sieve batch s2.

Table XIV. Volumetric particle size distribution of the coarse and fine magnetite particle fractions obtained from the sieve batch s2 and used in the fraction sedimentation experiments (Figure 49).

	Particle size, µm				
Fraction	Dx(10)	Dx(50)	Dx(90)	D[3;2]	D[4;3]
Coarse	42.10	85.80	180.00	39.60	102.00
Fine	3.80	18.00	60.60	9.02	26.50

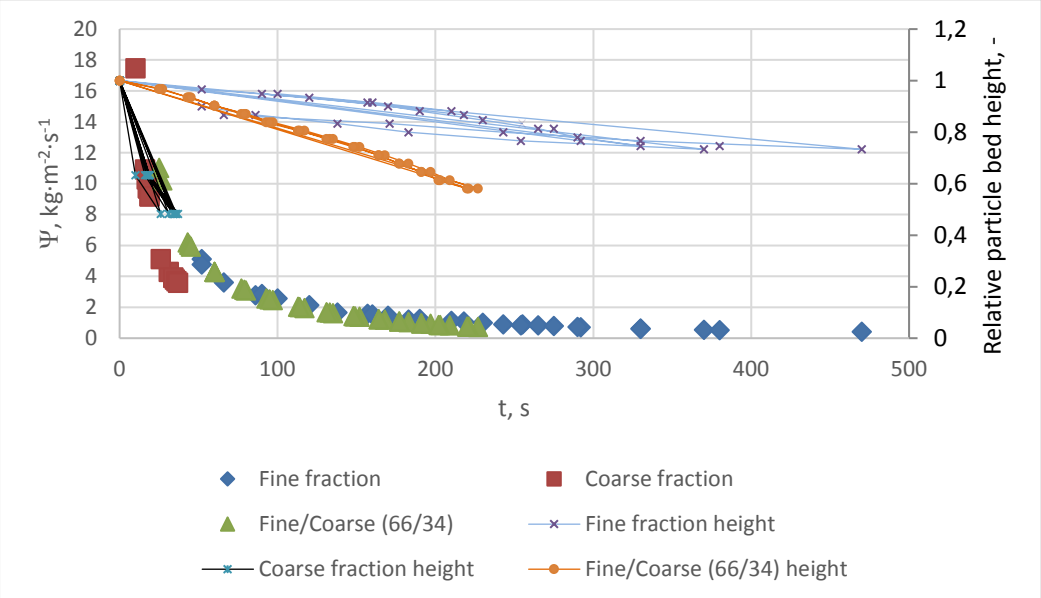

Figure 49. Sedimentation flux and the upper interface height of the particle bed of magnetite fraction slurries as the function of time. Particle size distribution values for the fine and coarse fractions presented in Table XIV. Fine/Coarse w% ratio 66/34. The initial slurry heights: 15.0 cm (Fine & Coarse), 15.5 cm (Fine/Coarse (66/34)). Slurry magnetite concentration 56.7 w%, slurry density 1838.8 kg·m^{-3}, batch weight 150.0 g, sedimentation surface area 0.00051 m^2. The particle bed height described as the relative value to the initial slurry height.

In Figure 49, the settling behavior of slurry batches containing only fine, only coarse and both fine and coarse fractions are described. The initial height for fine and coarse fraction slurries was 15.0 cm, and 15.5 cm for the fine/coarse (66/34) slurry. Each experiment was carried out 3-7 times. In the case of fine fraction settling, the repeatability was not as good as in the other cases. The sediment layer settled at the height of 11 cm after 5-8 minutes. Coarse fraction settled at the height of 7.25 cm after 26-37 seconds. In the case of fine/coarse (66/34) settling behavior, the respective values were 9 cm and 3 minutes 45 seconds (average). A clear difference between coarse and fine fractions can be seen regarding both sedimentation flux and settling velocity. The addition of coarse particle share up to 34 w% increases the settling velocity, and the settling velocity of the slurry consisting mere coarse fraction particles is substantially higher than that of the slurry consisting mere fine fraction particles. This observation correlates well with the other research experiments [32, 33, 36]. Sedimentation flux decreases exponentially in all cases. The measurement transcript of the sedimentation experiments of Figure 49 can be found in Appendix VII.

Using the Stokes' Law Equation (28), the terminal settling velocities for fine (18.0 μm) and coarse (85.8 μm) particles were calculated as 0.7 mm/s and 15.8 mm/s respectively. By using the obtained values, the Reynolds number was calculated to define the settling regime for both fine and coarse fraction slurries with Equation (36). The Archimedes number was also calculated to verify the settling regime with Equation (37). The obtained number values and the defined settling regime for the fine and coarse fractions are listed in Table XV.

Table XV. The settling regime of the fine and coarse fraction 56.7 w% magnetite slurries (Figure 49).

Fraction slurry	Re-number (*Equation 36*), -	Ar-number (*Equation 37*), -	Settling regime
Fine	0.01	$2.25 \cdot 10^{-7}$	Laminar
Coarse	1.38	$2.43 \cdot 10^{-5}$	Laminar

As the Fine/Coarse (66/34) w% slurry consists of both fine and coarse particles, it can be assumed that the settling regime for this slurry is laminar as well. The overall average settling velocity in mm/s was measured for each slurry: 0.1 mm/s (Fine fraction), 2.4 mm/s (Coarse fraction) and 0.3 mm/s (Fine/Coarse 66/34 w%). The obtained average slurry settling velocities in mm/s for each experiment are listed in Table XVI. The velocities were measured until 292-470 seconds (Fine fraction), 26-37 seconds (Coarse fraction) and 220-227 seconds (Fine/Coarse (66/34) w%) after the sedimentation recording was started.

Table XVI. Average slurry settling velocities of the 56.7 w% Fine, Coarse and Fine/Coarse (66/34) magnetite slurries (Figure 49).

Fraction	Test	Average slurry settling velocity, mm/s
Fine	1	0.1
	2	0.1
	3	0.1
	4	0.1
	5	0.1
Coarse	1	2.2
	2	2.5
	3	2.3
	4	3.0
	5	2.3
	6	2.2
	7	2.1
Fine/Coarse	1	0.3
	2	0.3
	3	0.3

9.3 Fractionation effect on magnetite slurry filtrations

Fractionation effect on filtration performance of magnetite slurry was studied by comparing the results obtained from non-fractionated and fractionated slurry filtrations. The changes regarding the filtrate flow rate, cake moisture content and filtration capacity were investigated. Also, the effect of settling on these properties was found out. The non-fractionated reference values are marked as N-F, representing the average value obtained from four non-fractionated slurry filtration experiments (2, 8, 14 and 15) carried out at 0.5 bar.

9.3.1 Filtration time

Higher filtrate flow rate during the filtrations resulted in faster filtration of the cake. Filtration time is considered as the recorded time after which the filtrate was no longer obtained through the cake during the filtration process. At this point, the saturation value of the non-fractionated and fractionated cakes ranged between 0.59-0.61 and 0.53-0.58 respectively.

Figure 50 presents the average filtration time of the non-fractionated (N-F) and fractionated magnetite slurry cakes as the function of fine fraction share of the cake at 0.5 bar vacuum pressure. The fine/coarse fraction w% ratios of the fractionated cakes are marked above, the particle size ratio values between fine and coarse fraction in terms of D[3;2] are marked below.

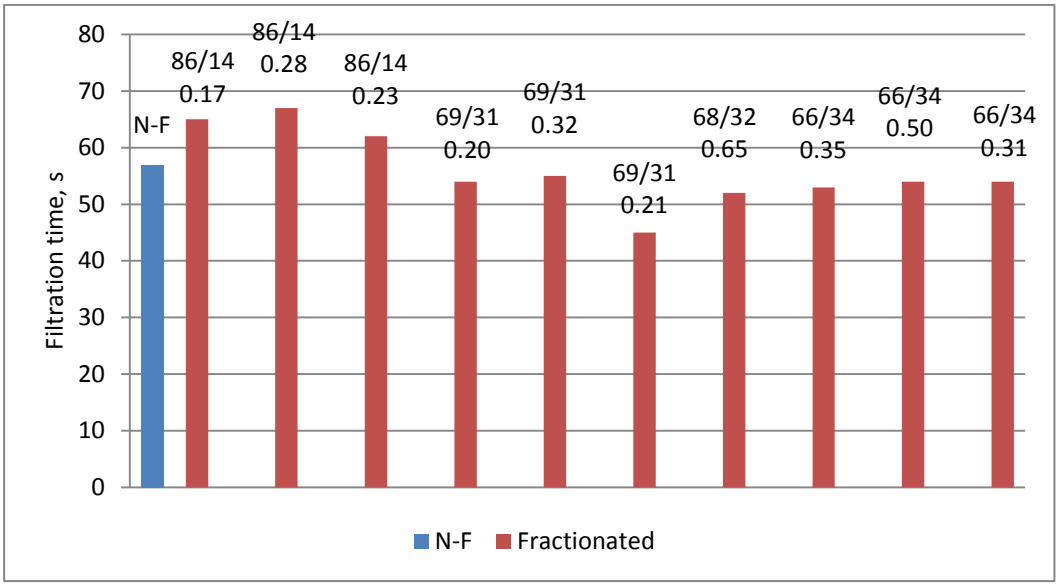

Figure 50. The effect of fine fraction share and fine/coarse fraction particle size ratio values on the filtration time of the non-fractionated and fractionated magnetite slurry cakes. The average filtration time of four non-fractionated slurry cakes (N-F) versus the filtration times of the fractionated slurry cakes. The applied vacuum pressure 0.5 bar, the filtration area 0.00985 m^2. The fine/coarse fraction w% ratio above, below the value of the fine/coarse particle size ratio in terms of D[3;2].

It can be seen in Figure 50, that fastest filtering occurs in the cakes where the fine fraction w% share ranges between 66 and 69. When compared to the non-fractionated cake filtration time, the fractionated cakes were mainly filtered almost as fast. The fractionated cakes with the fine fraction w% share of 86 were filtered slightly slower than the non-fractionated cake. It can be observed in the figure, that the fine/coarse particle size ratio in terms of D[3;2] does not have a notable effect on filtration time. For example, when the fine/coarse fraction w% ratio remains unchanged (66/34) and the D[3;2] ratio value ranges between 0.31 and 0.50, filtration time is almost the same.

Source of error to the results was caused by the slurry sample loss when the slurry batches were poured into the filter cell. This was mainly due to the heavy magnetite particles that were often stuck on the bottom of the container used in pouring the slurry. The particle size ratio values varied slightly even when the same size sieves were used to obtain the fractions. Possible scratches in the sieves might have caused greater value variances at some cases.

Figure 51 presents the filtration times of the non-fractionated and fractionated magnetite slurry cakes as the function of fine/coarse particle size distribution width ratio. The particle size distribution widths for both fractions were calculated with Equation (10).

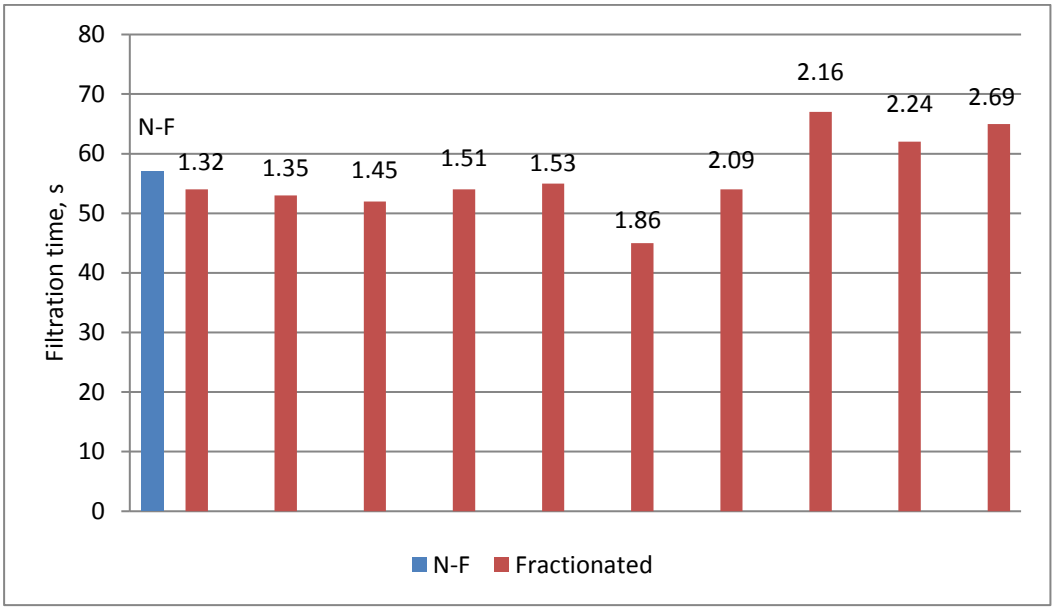

Figure 51. The effect of fine/coarse particle size distribution width ratio on the filtration time of the non-fractionated and fractionated magnetite slurry cakes. The average filtration time of four non-fractionated slurry cakes (N-F) versus the filtration times of the fractionated slurry cakes. The applied vacuum pressure 0.5 bar, the filtration area 0.00985 m^2. The particle size distribution widths calculated using Equation (10).

Figure 51 shows that the filtration time of the fractionated cakes is lower than that of the non-fractionated cake when the fine/coarse particle size distribution width ratio remains around 2 or below that. Filtration time of the fractionated cake is slightly increased when the width value ranges between 2.16 and 2.69. When the width value ranges between 1.32 and 2.09, filtration time of the fractionated cake is slightly faster than that of the non-fractionated cake. This might indicate that faster cake filtration correlates with the decreasing fine/coarse particle size distribution width ratio value, at least up to a certain point.

Settling effect

In Figure 52, the settling effect on the filtration time of the magnetite slurry cake is presented. The settling effect in the case of the non-fractionated and fractionated cakes is described. Regarding the fraction filtrations, the fine/coarse fraction w% ratio and the settling time of the fractions (above), the particle size ratio value between fine and coarse fraction in terms of D[3;2] (middle), and the fine/coarse particle size distribution width ratio value (below) are marked.

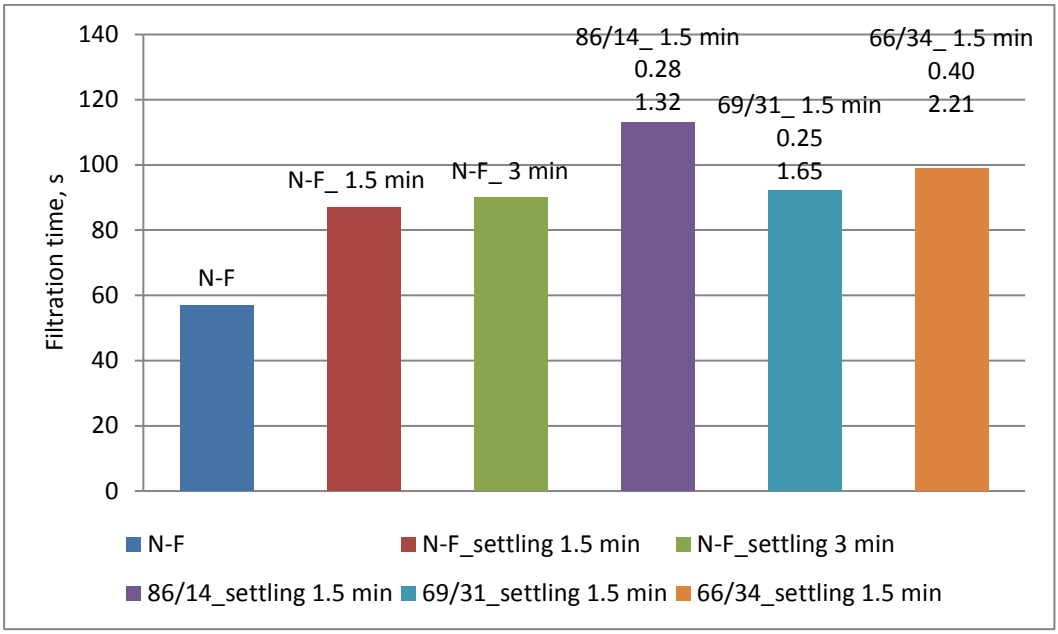

Figure 52. The effect of settling of the magnetite slurry before filtration on the filtration time. The average filtration time of four non-fractionated slurry cake filtrations (N-F), the filtration times of once performed non-fractionated slurry filtrations with the settling times of 1.5 min and 3 min, once performed fractionated slurry filtrations with the settling time of 1.5 min. The applied vacuum pressure 0.5 bar, the filtration area 0.00985 m^2. Regarding the fractionated cake filtrations, the fine/coarse fraction w% ratio is marked above, in the middle the value of the fine/coarse particle size ratio in terms of D[3;2], below the fine/coarse particle size distribution width ratio. The particle size distribution widths calculated using Equation (10).

Figure 52 points out that settling does not speed up the filtration of the magnetite slurry cake. Slower filtration occurred in both cases where the non-fractionated and fractionated slurries were filtered. In the case of the non-fractionated slurry, doubling the settling time before filtration had a negligible effect on the filtration time. In the case of the fractionated slurry, lower fine/coarse particle size ratio value and the fine/coarse particle size distribution width ratio value might correlate with faster filtration. The exceptional value gained from the experiment carried out with the 86/14 fine/coarse fraction w% ratio most probably derives from the uneven pre-coat layer formed by the coarse particles.

9.3.2 Filtration capacity and moisture content of the cake

The effect of fine/coarse fraction w% ratio and particle size ratio on the filtration capacity was investigated in both cases, when the filtrations were carried out with and without settling. Figure 53 shows the filtration capacity as the function of fine fraction share. In the plots, the moisture content of the cake is mentioned above, below the fine/coarse particle size ratio value in terms of D[3;2].

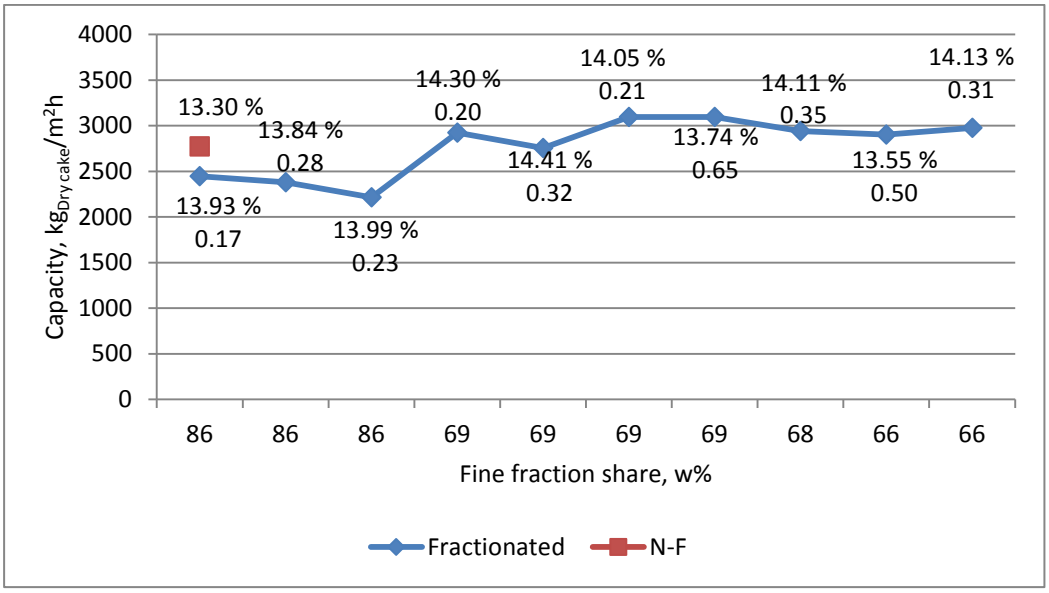

Figure 53. Fine fraction share effect on the filtration capacity. The average value of the filtration capacity of four non-fractionated slurry cake filtrations (N-F) versus the values from fractionated slurry cake filtrations. The applied vacuum pressure 0.5 bar, the filtration area 0.00985 m^2. The value above represents the cake moisture content, the value below represents the fine/coarse fraction particle size ratio value in terms of D[3;2].

Figure 53 shows that minor improvements in the filtration capacity was obtained, when the fine fraction share of the filter cake ranged between 66 w% and 69 w%. The filtration capacity was lower than that of the non-fractionated cake, when the fine fraction share of the fractionated cake was 86 w%. The fine/coarse particle size ratio value in terms of D[3;2] did not affect the filtration capacity significantly. This can be observed when the capacity value remains almost at the same level when the fine fraction share of the filter cake ranges between 66 w% and 69 w%, and the D[3;2] ratio value between the fine and coarse fraction ranges between 0.20 and 0.65. The moisture content of the cake did not vary significantly, as it ranged between 13.30 % and 14.41 % in all cases.

A slightly decreasing trend of the filtration capacity can be seen in Figure 54, as the fine/coarse particle size distribution width ratio increases. The highest filtration capacity values are found when the width ratio ranges between 1.32 and 2.09. The filtration capacity values are lower than that of the non-fractionated cake, when the width ratio values range between 2.16 and 2.69.

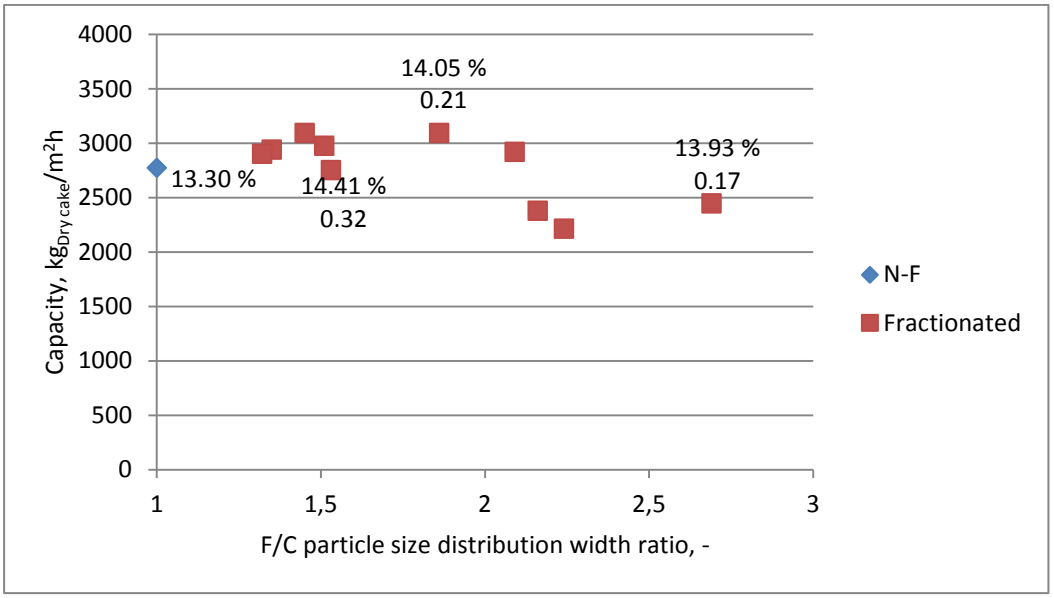

Figure 54. Fine/coarse particle size distribution width ratio effect on the filtration capacity. The average value of the filtration capacity of four non-fractionated slurry cake filtrations (N-F) versus the values from fractionated slurry cake filtrations. The applied vacuum pressure 0.5 bar, the filtration area 0.00985 m^2. At the chosen plots, the value above represents the cake moisture content, the value below represent the fine/coarse fraction particle size ratio in terms of D[3;2]. The particle size distribution widths are calculated using Equation (10).

Settling effect

In Figure 55, settling effect is presented when the filtration capacity is described as the function of fine fraction share of the cake. The values mentioned in the plots are the moisture content of the cake (above), and the fine/coarse fraction particle size ratio in terms of D[3;2] (below). The settling time is not included in the filtration capacity calculations.

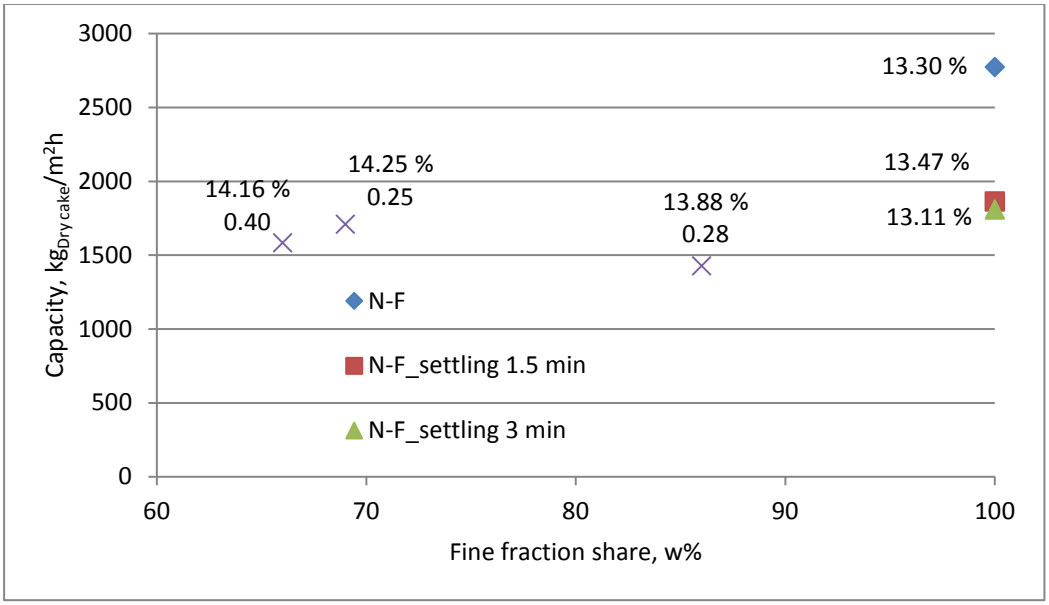

Figure 55. The effect of settling of the magnetite slurry before filtration on the filtration capacity. The average value of the filtration capacity of four non-fractionated slurry cake filtrations (N-F), once performed non-fractionated slurry filtrations with the settling times of 1.5 min and 3 min, once performed fractionated slurry filtrations with the settling time of 1.5 min. The applied vacuum pressure 0.5 bar, the filtration area 0.00985 m^2. Fine/coarse fraction ratios (w%) from left to right: 66/34, 69/31 and 86/14. The value above represents the cake moisture content, the value below represents the fine/coarse fraction particle size ratio in terms of D[3;2].

Settling of either non-fractionated magnetite slurries or coarse and fine fractions before filtration did not improve the filtration capacity, as can be observed in Figure 55. Doubling the settling time of non-fractionated slurry resulted in a slight filtration capacity decrease, which might be due to the tighter packing of particles over time. Regarding the fraction filtrations, filtration capacity seems to increase slightly when the fine fraction share increases, if the exceptional result is not taken into account at 86 w% fine fraction share. The moisture content of the cake remains almost unchanged ranging between 13.11 % and 14.25 %, even though the filtration capacity varies. The particle size ratio values do not correlate clearly with the filtration capacity, which might be explained by the tight particle packing during settling.

In Figure 56, settling effect is presented when the filtration capacity is described as the function of fine/coarse particle size distribution width ratio. The values mentioned in the plots are the moisture content of the cake (above), and the fine/coarse fraction particle size ratio in terms of D[3;2].

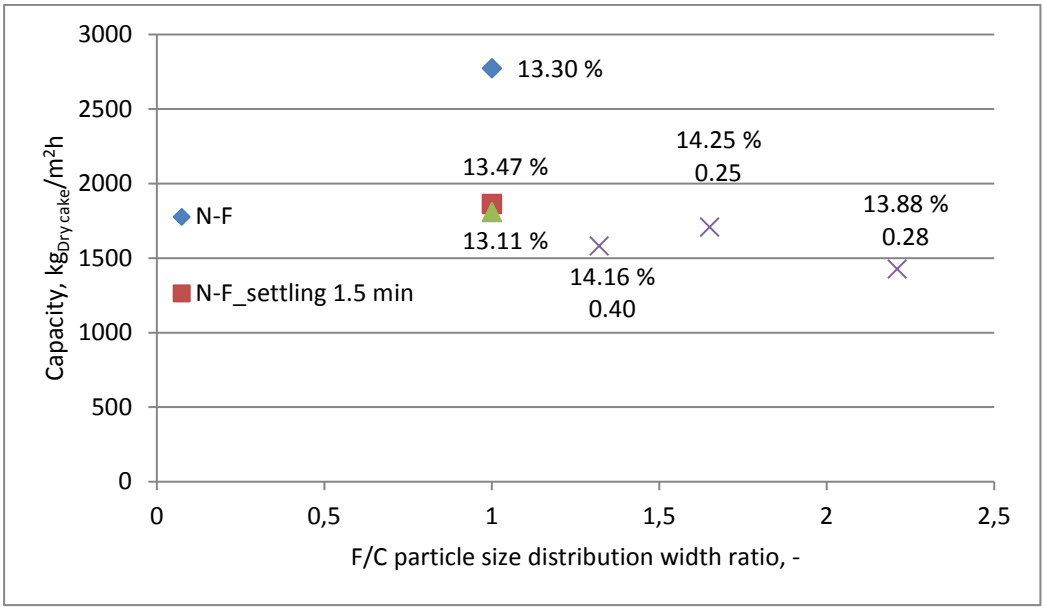

Figure 56. The effect of settling of the magnetite slurry before filtration on the filtration capacity. The average value of the filtration capacity of four non-fractionated slurry cake filtrations (N-F), once performed non-fractionated slurry filtrations with the settling times of 1.5 min and 3 min, once performed fractionated slurry filtrations with the settling time of 1.5 min. The applied vacuum pressure 0.5 bar, the filtration area 0.00985 m^2. Fine/coarse fraction ratios (w%) from left to right: 66/34, 69/31 and 86/14. The value above represents the cake moisture content, the value below represents the fine/coarse fraction particle size ratio in terms of D[3;2]. The particle size distribution widths are calculated using Equation (10).

It is possible, that the fine/coarse particle size distribution width ratio value explains the filtration capacity behavior. In Figures 54 and 56, the highest filtration capacity value seems to correlate with the fine/coarse particle size distribution width ratio within the same range, between 1.45 and 2.0. In the settling experiments, the particle size ratio values do not significantly correlate with the filtration capacity as can be seen in Figures 55 and 56. The capacity value does not vary notably between the experiments, which is most probably caused by the rapid and tight packing of the magnetite particles in all cases. Compared to the results gained from the non-fractionated slurry filtrations, settling of neither the non-fractionated slurry nor the separated coarse and fine fractions improved the filtration capacity.

9.3.3 Air flow and cake moisture correlation

As the filtrate was no longer obtained, the air flow through the cake at this stage was measured. In order to find explaining parameters for the final cake moisture content, Figures 57 and 58 are presented.

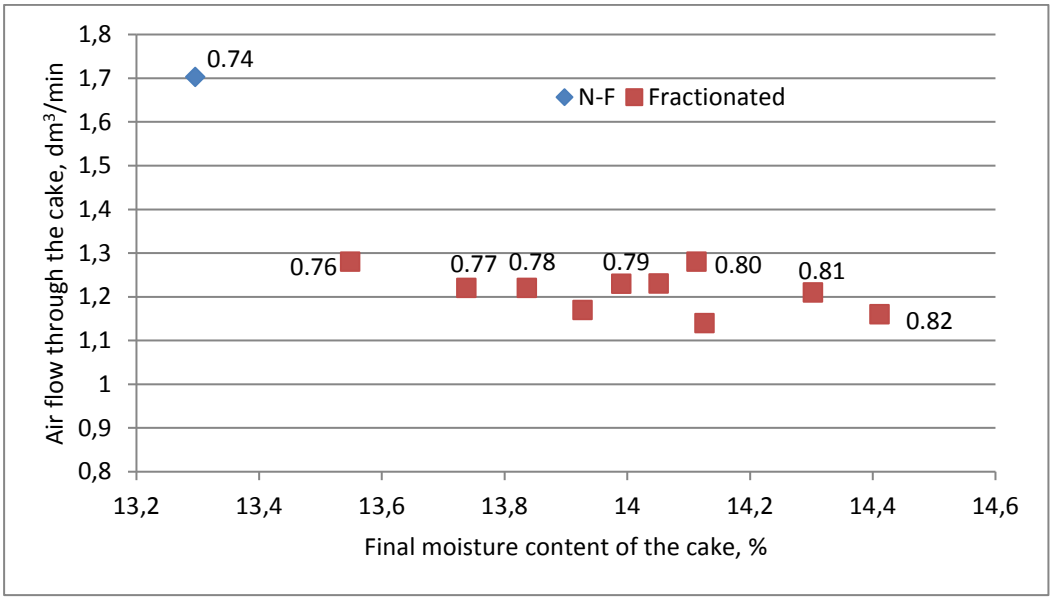

Figure 57. Air flow rate through the cake as the function of final moisture content of the cake when the filtrate was no longer obtained. The average value of four non-fractionated slurry cake filtrations (N-F) versus the values from fractionated slurry cake filtrations. The applied vacuum pressure 0.5 bar, the filtration area 0.00985 m^2. At the chosen plots, the values represent the porosity of the cake.

Final moisture content of the cake did not vary significantly between the performed filtrations. However, slight differences were discovered. In Figure 57, it can be seen that the air flow rate through the cake at the end point of filtration is higher for the non-fractionated cake, compared to all fractionated cakes. The higher air flow rate through the cake at this point mainly explains the lower moisture content. This is because the increased value for air flow correlates with higher dewatering effect of the cake, as explained by Wakeman [44]. It can be observed in Figure 57 that the higher cake porosity correlates with the higher final moisture content of the cake. Figure 58 presents the air flow through the cake as the function of the final moisture content of the cake, when settling was used before filtrations.

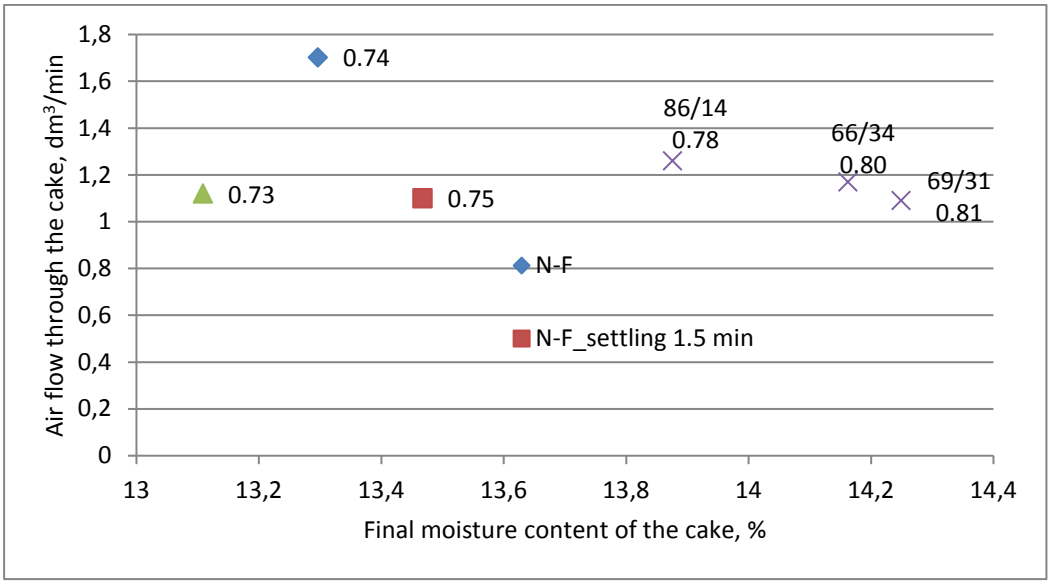

Figure 58. Air flow rate through the settled cake as the function of final moisture content of the cake when the filtrate was no longer obtained. The average value of four non-fractionated slurry cake filtrations (N-F) versus the values from fractionated slurry cake filtrations. The applied vacuum pressure 0.5 bar, the filtration area 0.00985 m^2. The values of the plots represent the fine/coarse fraction w% share (above) and the cake porosity (below).

In the settling effect experiments the final moisture content of the cake did not vary a lot either as can be seen in Figure 58. In both Figures 57 and 58 it can be seen that the increasing porosity correlates with the increasing final moisture content of the cake. The air flow rate through the cake at the end point of filtration was almost the same with all the fractionated cakes. Both Figures 57 and 58 show that fractionation of the magnetite slurry cake results in higher cake moisture content. Only in the case where the non-fractionated slurry was settled for 3 minutes before filtration, slightly lower cake moisture content was achieved.

10 CONCLUSIONS AND FUTURE WORK

The aim of the work was to investigate how fractionating the particles into fine and coarse fractions affect the filtrate flow rate, filtration capacity and cake moisture content when magnetite slurry was filtered at constant vacuum pressure. The experiments revealed that particle fractionation did not significantly improve the filtration performance.

The slurry cakes in which the fine fraction w% share ranged between 66 and 69 resulted in faster filtration than the non-fractionated slurry cake. In the case where the fine fraction share was 86 w%, filtration was slower. It was also discovered that fine/coarse fraction particle size ratio in terms of D[3;2] did not have a significant effect on filtration time of the fractionated cakes. Filtration of the slurry cake was fastest when the fine/coarse particle size distribution width ratio value ranged between 1.32 and 2.09. Filtration was slower when the respective ratio value ranged between 2.16 and 2.69. Compared to the non-fractionated slurry cake filtration time, settling of both non-fractionated and fractionated slurry cakes resulted in slower filtration.

The filtration capacity was observed to be slightly improved when the fine fraction w% share was between 66 and 69. As the fine fraction w% share was 86, the filtration capacity was lower than in the non-fractionated slurry filtrations. The fine/coarse fraction particle size ratio in terms of D[3;2] ranged between 0.2 and 0.65 when the filtration capacity was higher compared to the non-fractionated cake filtrations. When the fine/coarse particle size distribution width ratio was between 1.32 and 2.09, the filtration capacity was higher compared to the non-fractionated cake filtrations. Settling of neither non-fractionated nor fractionated slurry improved the filtration capacity.

The moisture content of the cake did not vary a lot between the filtrations, as the value ranged between 13.30 % and 14.41 %. Compared to the average moisture content value of the non-fractionated cake, none of the fractionated cakes had lower cake moisture content. It was observed that increased cake porosity resulted in higher cake moisture content. Settling of the slurry before filtration resulted mostly in higher cake moisture content. Only in the case when the non-fractionated slurry was settled for 3 minutes, the cake moisture content was slightly lower in comparison to the initial reference value. It could be assumed, that the high average cake specific resistance caused by the fine fraction resulted in lower filtrate flow rate through the slurry cake and thus higher cake moisture content.

Sedimentation experiments were carried out in order to gain data for possible future studies regarding multiphase simulation of magnetite slurry in horizontal pipe flow fractionation. It was observed that the magnetite slurry concentration decrease, particle size increase and relative coarse fraction w% increase resulted in increased settling velocity of the upper interface of the magnetite particle bed.

For other future experiments, it is suggested that particle size and volumetric particle size distribution width ratio values would be investigated in more detail in order to reach more improved magnetite slurry filtration performance. It is known

that pre-coating has been proved to improve the filtration process in many cases. Thus, regarding the less dense materials, it is recommended to explore how the filtrate flow rate, filtration capacity and cake moisture content are affected by the means used in this work.

REFERENCES

1. Wakeman, R.J., Tarleton, E.S, *Solid/Liquid Separation: Principles of Industrial Filtration*, 1. edition, Elsevier Advanced Technology, Great Britain, 2005
2. Chen, G., Yue P.L., Mujumdar, A.S., 2002. Sludge dewatering and drying, *Drying Technology*, vol 20(4&5), 883-916.
3. Svarovsky, L., *Solid-Liquid Separation*, fourth edition, Butterworth-Heinemann, Great Britain, 2000
4. Sinnott, R. K., 2005. Chemical Engineering Vol. 6, fourth edition, Oxford: Butterworth-Heinemann
5. Ruthven, D.M., 1997, Encyclopedia of Separation Technology, Volume 2, A Kirk-Othmer Encyclopedia, John Wiley & Sons, Inc., New York
6. Coulson, J. M., Richardson, J. F., Backhurst, J. R., Harker, J. H., 1991. Chemical Engineering Vol. 2, fourth edition, Oxford: Pergamon Press Ltd
7. Wakeman, R.J., Tarleton, E.S, *Filtration: equipment selection, modelling and process simulation*, first edition, Elsevier Advanced Technology, Great Britain, 1999
8. Tsang, K.R., Vesilind, P.A., 1990. Moisture Distribution in Sludges, *Water Science & Technology*, vol 22, 135-142.
9. Vesilind, P.A., 1994. The Role of Water in Sludge Dewatering, *Water Environmental Research*, vol 66, 4-11.
10. Rushton, A., Ward, A.S, Holdich, R.G, *Solid-Liquid Filtration and Separation Technology*, 2. edition, WILEY-VCH Verlag GmbH, Weinheim, Germany, 2000
11. Holdich, R. G., 2002. Fundamentals of Particle Technology, 1st ed., Shepshed: Midland Information Technology and Publishing
12. Richardson, J. F., Harker, J. H., Backhurst, J. R., 2002. Chemical Engineering Vol.2, 5th ed., Oxford: Butterworth-Heinemann
13. Allen, T., Powder Sampling and Particle Size Determination, Elsevier B.V., Amsterdam, 2003

14. Jancovic, A., Sinclair, S., 2006. The shape of product size distributions in stirred mills, *Minerals Engineering*, vol 19, 1528-1536.

15. Mendret, J., Guigui, C., Schmitz, P., Cabassud, C., 2009. In situ dynamic characterization of fouling under different pressure conditions during dead-end filtration: Compressibility properties of particle cakes, *Journal of Membrane Science*, vol 333, 20-29.

16. Le-Clech, P., Marselina, Y., Ye, Y., Stuetz, R.M., Chen, V., 2007. Visualisation of polysaccharide fouling on microporous membrane using different characterization techniques, *Journal of Membrane Science*, vol 290, 36-45.

17. Mory, M., 2011. Fluid Mechanics for Chemical Engineering, ISTE Ltd, London

18. Green, D.W., Perry, R.H., 2007. Perry's chemical engineering handbook, 8th edition, Mcgraw-Hill

19. White, F. M., 2003. Fluid Mechanics, fifth edition, McGraw-Hill Companies, New York

20. White, F. M., 2006. Viscous Fluid Flow, third edition, McGraw-Hill Companies, New York

21. Richardson, J.F., Zaki, W.N., 1954. Sedimentation and fluidization, *Trans. Inst. Chem. Eng.*, vol 32, 35-53.

22. Krishnamoorthy, P., 2010. Sedimentation model and analysis for differential settling of two – particle – size suspensions in the Stokes region, *International Journal of Sediment Research*, vol 25, 119-133.

23. Franca, S.C.A., Massarani, G., Biscaia Jr., E.C., 1999. Study on batch sedimentation simulation – establishment of constitutive Equations, *Powder Technology*, vol 101, 157-164.

24. Holdich, R.G., Butt, G., 1997. Solid/liquid separation by sedimentation, *Proceedings of the Institution of Mechanical Engineers*, vol 211, 43-52.

25. Koo, S., 2008. Sedimentation velocity of bidisperse suspensions, *Journal of Industrial and Engineering Chemistry*, vol 14, 679-686.

26. Davis, J. F., Maffia, G.J., 1995. Collagen dispersions for liquid-solid separations in water treatment and sludge dewatering. *Separations Technology*, vol 5, pp. 147-152.

27. Bux, J., Peakall, J., Biggs, S., Hunter, T. N., 2015. *In situ* characterization of a concentrated colloidal titanium dioxide settling suspension and associated bed development: Application of an acoustic backscatter system. *Powder Technology*, vol 284, pp. 530-540.

28. Tseng, W. J., Li, S-Y., 2003. Effect of polysaccharide polymer on sedimentation and rheological behavior of aqueous $BaTiO_3$ suspensions. *Materials Processing Technology*, vol 142, pp. 408-414.

29. Tseng, W. J., Wu, C. H., 2003. Sedimentation, rheology and particle-packing structure of aqueous Al_2O_3 suspensions. *Ceramics International*, vol 29, pp. 821-828.

30. Yoshida, H., Nurtono, T., Fukui, K., 2005. A new method for the control of dilute suspension sedimentation by horizontal movement. *Powder Technology*, vol 150, pp. 9-19.

31. Fitch, B., 1962. Sedimentation process fundamentals. *Trans. Am. Inst. Min. Engng*, 223, 129.

32. Heath, A.R., Bahri, P.A., Fawell, P.D., Farrow, J.B., 2006. Polymer Flocculation of Calcite: Relating the Aggregate Size to the Settling Rate, *Aiche Journal*, vol 52, Issue 6, 1987-1994.

33. Turian, R.M., Ma, T.W., Hsu, F.L.G., Sung, D.J., 1997. Characterization, settling, and rheology of concentrated fine particulate mineral slurries, *Powder Technology*, vol 93, 219-233.

34. Tomkins, M.R., 2005. Hindered settling of sand grains, *Sedimentology*, vol 52, 1425-1432.

35. Chen, G.W., Chang, I.L., Hung, W.T., Lee, D.J., 1996. Regimes for zone settling of waste activated sludges, *Water Research*, vol 30, 1844-1850.

36. Lu, W-M., Tung, K-L., Pan, C-H., Hwang, K-J., 1998. The Effect of Particle Sedimentation on Gravity Filtration. *Separation Science and Technology*, vol 33(12), pp. 1723-1746.
37. Sparks, T., Solid-liquid filtration, 2012, Elsevier Ltd., Oxford Encyclopedia, John Wiley & Sons, Inc., New York
38. Hwang, K-J., Wu, Y-S., Lu, W-M., 1997. Effect of the size distribution of spheroidal particles on the surface structure of a filter cake. *Powder Technology*, vol 91, pp. 105-113.
39. Hwang, K-J., Wu, Y-S., Lu, W-M., 1996. The surface structure of cake formed by uniform-sized rigid spheroids in cake filtration. *Powder Technology*, vol 87, pp. 161-168.
40. Mota, M., Teixeira, J.A., Bowen, W.R., Yelshin, A., 2003. Interference of coarse and fine particles of different shape in mixed porous beds and filter cakes. *Minerals Engineering*, vol 16, pp. 135-144.
41. Mota, M., Teixeira, J.A., Bowen, W.R., Yelshin, A., 2001. Binary spherical particle mixed beds: Porosity and permeability relationship measurement, *Trans. Filt. Soc.*, vol 1(4), 101-106.
42. Yu, A.B., Zou, R.P., Standish, N., 1996. Modifying the Linear Packing Model for Predicting the Porosity of Nonspherical Particle Mixtures, *Ind. Eng. Chem. Res.*, vol 35, 3730-3741.
43. SHIJIAZHUANG GONGDA CHEM IND EQUIP CO LT (SHIJ-Non-standard). Sludge drying method for solid-liquid separation of domestic sewage by using precoated vacuum-type drum filter, where precoating agent is commercial precoating agent or mixture of commercial precoating agent and recovered sludge particles. Guo H., Zhang J., Patent Number(s): CN102491614-A. Derwent Primary Accession Number: 2012-J04798 [70].
44. Wakeman, R., 2007. The influence of particle properties on filtration. *Separation and Purification Technology*, vol 58, pp. 234-241.
45. Endo, Y., Chen, D-R., Pui D. Y.H., 2001. Air and water permeation resistance across dust cakes on filters—effects of particle polydispersity and shape factor. *Powder Technology*, vol 118, pp. 24-31.

46. Yu, A.B., Standish, N., 1991. Estimation of the Porosity of Particle Mixtures by a Linear-Mixture Packing Model, *Ind. Eng. Chem. Res.*, vol 30, 1372-1385.

47. Thomas, J., Reichmann, B., 2002. In-situ-Messung der Kompressibilität, Permeabilität und des Fliessverhaltens von hochdispersen Filterkuchen mit einer Press-Scherzelle, *Chemie Ingenieur Technik*, vol 74, 76-81.

48. Dias, R.P., Teixeira, J.A., Mota, M.G., Yelshin, A.I., 2004. Particulate Binary Mixtures: Dependence of Packing Porosity on Particle Size Ratio, *Ind. Eng. Chem. Res.*, vol 43, 7912-7919.

49. Mota, M., Teixeira, J.A., Yelshin, A., 1999. Image analysis of packed beds of spherical particles of different sizes, *Separation and Purification Technology*, vol 15, 59-68.

50. McKetta, J.J., Cunningham, W.A., Encyclopedia of Chemical Processing and Design, 21, Marcel Dekker, Inc., New York, 1984

51. Boittelle, C., Poupot, C., Milisic, V., Mietton-Peuchot, M., 2008. Advances in the Precoat Filtration Process, *Separation Science and Technology*, vol 43, 1701-1712.

52. Suh, C.W., Kim, S.E., Lee, E.K., 1997. Effects of filter additives on cake filtration performance, *Korean Journal of Chemical Engineering*, vol 14(4), 241-244.

53. Meeroff, D.E., Englehardt, J.D., 2001. Precoat filtration and ultrafiltration of emulsified bitumen from water, *Journal of Environmental Engineering*, vol, 46-53.

54. Vorobiev, E., Mouroko-Mitoulou, T., Soua, Z., 2004. Precoat filtration of a deflocculated mineral suspension in the presence of a dispersant, *Colloids and Surfaces A: Physicochemical Engineering Aspects*, vol 251, 5-17.

55. Harjula, R., Lehto, J., Paajanen, A., Tusa, E., Yarnell, P., 2004. Use inorganic ion exchange materials as precoat filters for nuclear waste effluent treatment, *Reactive & Functional Polymers*, vol 60, 85-95.

56. Coulson, J. M., Richardson, J. F., Backhurst, J. R., Harker, J. H., Chemical Engineering Vol. 1, fourth edition, Oxford: Pergamon Press Ltd

57. Versteeg, H. K., Malalasekera, W., 2007. An Introduction to Computational Fluid Dynamics, second edition, Pearson Education Limited

58. Pirie, R. L., Davies, T., Khan, A. R. and Richardson, J. F.: 2nd International Conf. on Flow Measurement – BHRA, London (1988), Paper F3, 187. Measurement of liquid velocity in multiphase flow by salt injection method.

59. Dutta, B.K., Bhattacharyya, S., 2009. An effective voidage model for sedimentation of bidisperse solid suspension, *Chemical Engineering and Processing*, vol 48, 1382-1389.

60. Sarimeseli, A., Kelbaliyev, G., 2004. Sedimentation of solid particles in turbulent flow in horizontal channels. *Powder Technology*, vol 140, pp. 79-85.

61. Contado, C., Dondi, F., Beckett, R., Giddings, J. C., 1997. Separation of particulate environmental samples by SPLITT fractionation using different operating modes. *Analytica Chimica Acta*, vol 345, pp. 99-110.

62. Moon, M. H., Kim, H-J., Kwon, S-Y., Lee, S-J., Chang, Y-S., Lim, H., 2004. Pinched Inlet Split Flow Thin Fractionation for Continuous Particle Fractionation: Application to Marine Sediments for Size-Dependent Analysis of PCDD/Fs and Metals. *Analytical Chemistry*, vol 76, 3236-3243.

63. Tantidanai, N., Veerasai, W., Beckett, R., 2006. Comparison of Gravitational SPLITT Fractionation with Gravitational Settling for Separating Micron Size Particles. *Separation Science and Technology*, vol 41, pp. 3003-3025.

64. Koenders, M.A., Wakeman, R.J., 1996. The initial stages of compact formation from suspensions by filtration, *Chemical Engineering Science*, vol 51, No. 16, 3897-3908.

65. Tarleton, E.S., Willmer, S.A., 1997. The effects of scale and process parameters in cake filtration, *Chemical Engineering Research & Design*, vol 75, 497-507.

66. Murase, T., Iwata, M., Kato, I., Lee, W-D., Shirato, M., 1988. Determination of specific resistance of highly compressed cake by use of expression data, *Journal of Chemical Engineering of Japan*, vol 21, Issue 2, 204-206.

67. Wetterling, J., Mattsson, T., Theliander, H., 2014. Effects of surface structure on the filtration properties of microcrystalline cellulose, *Separation and Purification Technology*, vol 136, 1-9.

68. Matsson, T., Martinez, E.L., Sedin, M., Theliander, H., 2013. Local solidosity of microcrystalline cellulose during dead-end filtration and sedimentation. *Chemical Engineering Research and Design*, vol 91, 1155-1162.

APPENDICES

Magnetite density (ρ_{water}=0.99820 g·cm^{-3}, T_{water}=19.8 °C)

Measurement	Magnetite density, kg·m^{-3}
1	4820
2	4878
	4849

Magnetite batch moisture content

Sample	Initial magnetite weight, g	Final magnetite weight, g	Moisture content, %
1	268.58	245.64	8.54
2	329.96	301.87	8.51

Magnetite slurry solid content

Sample	Mixing tank, dm^3	Initial sample weight, g	Final sample weight, g	Solid content, %
1	2	38.30	21.66	56.55
2	2	37.34	21.07	56.43
3	2	38.00	21.49	56.55
4	2	37.07	20.97	56.57
5	2	36.11	20.41	56.52
6	16	38.80	22.05	56.82
7	16	39.87	22.66	56.82
8	16	39.46	22.38	56.71
9	16	42.19	23.97	56.82
10	16	38.54	21.92	56.87
				56.67

The density of the 56.7 w% magnetite slurry

Measurement	Volume, ml	Weight, g	Density, kg·m^{-3}
1	25.50	46.85	1837.3
2	25.25	45.90	1817.8
3	25.50	46.77	1834.1
4	25.75	47.69	1852.0
5	24.60	45.28	1840.7
6	25.75	47.66	1850.9
			1838.8

Sample number	Δp, bar	$V_{Pores\ in\ the\ cake}$, m^3	Average cake thickness, m	$V_{Wet\ cake}$, m^3	$V_{Dry\ cake}$, m^3
1	0.6	5.60E-05	0.01377	1.36E-04	8.49E-05
2	0.5	6.38E-05	0.01461	1.44E-04	8.74E-05
3	0.8	5.26E-05	0.01402	1.38E-04	8.83E-05
4	0.3	7.20E-05	0.01509	1.49E-04	8.89E-05
5	0.4	6.85E-05	0.01465	1.44E-04	8.62E-05
6	0.7	5.34E-05	0.01428	1.41E-04	8.77E-05
7	0.6	5.73E-05	0.01435	1.41E-04	8.87E-05
8	0.5	6.55E-05	0.01477	1.45E-04	8.85E-05
9	0.8	5.05E-05	0.01501	1.48E-04	8.74E-05
10	0.3	6.79E-05	0.01479	1.46E-04	8.51E-05
11	0.4	7.12E-05	0.01498	1.47E-04	8.93E-05
12	0.7	5.34E-05	0.01490	1.47E-04	9.00E-05
13	0.6	5.68E-05	0.01485	1.46E-04	9.01E-05
14	0.5	6.75E-05	0.01530	1.51E-04	8.96E-05
15	0.5	6.75E-05	0.01533	1.51E-04	8.98E-05
16	0.6	5.37E-05	0.01438	1.42E-04	8.61E-05
17	0.5	6.90E-05	0.01617	1.59E-04	9.14E-05
18	0.5	6.72E-05	0.01654	1.63E-04	9.18E-05

Sample number	Δp, bar	$m_{Filtrate}$, kg	$m_{Wet\ cake}$, kg	$m_{Dry\ cake}$, kg	$V_{Filtrate}$, m^3
1	0.6	0.28236	0.46760	0.41155	2.82E-04
2	0.5	0.28250	0.48782	0.42404	2.83E-04
3	0.8	0.29222	0.48092	0.42829	2.92E-04
4	0.3	0.27616	0.50298	0.43097	2.76E-04
5	0.4	0.27803	0.48663	0.41814	2.78E-04
6	0.7	0.29189	0.47865	0.42530	2.92E-04
7	0.6	0.28629	0.48739	0.43009	2.86E-04
8	0.5	0.28179	0.49451	0.42902	2.82E-04
9	0.8	0.29786	0.47435	0.42389	2.98E-04
10	0.3	0.27277	0.48029	0.41242	2.73E-04
11	0.4	0.27589	0.50401	0.43285	2.76E-04
12	0.7	0.29823	0.48979	0.43644	2.98E-04
13	0.6	0.28806	0.49380	0.43698	2.88E-04
14	0.5	0.28206	0.50218	0.43464	2.82E-04
15	0.5	0.27871	0.50305	0.43556	2.79E-04
16	0.6	0.29205	0.47122	0.41750	2.92E-04
17	0.5	0.27636	0.51213	0.44316	2.76E-04
18	0.5	0.27931	0.51243	0.44526	2.79E-04

Sample number	Δp, bar	c, $m_{Dry\ cake} \cdot V^{-1}_{Filtrate}$	Filtration time, s	Filtration time, h
1	0.6	1457.54	49	0.014
2	0.5	1501.03	51	0.014
3	0.8	1465.64	37	0.010
4	0.3	1560.58	92	0.026
5	0.4	1503.94	72	0.020
6	0.7	1457.06	42	0.012
7	0.6	1502.29	50	0.014
8	0.5	1522.48	58	0.016
9	0.8	1423.12	38	0.011
10	0.3	1511.97	93	0.026
11	0.4	1568.92	74	0.021
12	0.7	1463.43	42	0.012
13	0.6	1516.98	49	0.014
14	0.5	1540.95	60	0.017
15	0.5	1562.77	59	0.016
16	0.6	1429.55	51	0.014
17	0.5	1603.56	87	0.024
18	0.5	1594.14	90	0.025

Sedimentation of the 56.7 w% magnetite slurry (Experiment set 1)

1. test			2. test			3. test		
t, s	h, cm	Ψ, kg·m^{-2}·s^{-1}	t, s	h, cm	Ψ, kg·m^{-2}·s^{-1}	t, s	h, cm	Ψ, kg·m^{-2}·s^{-1}
0	14.25		0	14.25		0	14.25	
55	13.50	4.51	34	13.50	7.30	39	13.50	6.37
85	13.00	2.81	73	13.00	3.27	75	13.00	3.19
106	12.50	2.17	104	12.50	2.21	102	12.50	2.25
130	12.00	1.70	130	12.00	1.70	130	12.00	1.70
157	11.50	1.35	154	11.50	1.37	148	11.50	1.43
180	11.00	1.12	180	11.00	1.12	170	11.00	1.19
200	10.50	0.97	202	10.50	0.96	194	10.50	1.00
213	10.00	0.86	217	10.00	0.85	211	10.00	0.87
235	9.50	0.74	240	9.50	0.73	228	9.50	0.77

Sedimentation of the 56.7 w% magnetite slurry (Experiment set 2)

1. test			2. test			3. test		
t, s	h, cm	Ψ, $kg \cdot m^{-2} \cdot s^{-1}$	t, s	h, cm	Ψ, $kg \cdot m^{-2} \cdot s^{-1}$	t, s	h, cm	Ψ, $kg \cdot m^{-2} \cdot s^{-1}$
	15.50			15.50			15.50	
18	15.00	15.32	11	15.00	25.08	12	15.00	22.99
29	14.50	9.19	23	14.50	11.59	25	14.50	10.67
42	14.00	6.13	37	14.00	6.96	37	14.00	6.96
55	13.50	4.51	50	13.50	4.96	50	13.50	4.96
67	13.00	3.57	63	13.00	3.79	63	13.00	3.79
82	12.50	2.80	77	12.50	2.99	77	12.50	2.99
96	12.00	2.30	91	12.00	2.42	92	12.00	2.40
109	11.50	1.94	105	11.50	2.01	107	11.50	1.98
121	11.00	1.67	118	11.00	1.71	119	11.00	1.70
133	10.50	1.45	130	10.50	1.49	131	10.50	1.47
144	10.00	1.28	142	10.00	1.29	143	10.00	1.29

4. test		
t, s	h, cm	Ψ, $kg \cdot m^{-2} \cdot s^{-1}$
	15.50	
11	15.00	25.08
23	14.50	11.59
38	14.00	6.77
51	13.50	4.87
64	13.00	3.74
80	12.50	2.87
94	12.00	2.35
109	11.50	1.94
121	11.00	1.67
134	10.50	1.44
146	10.00	1.26

Sedimentation of the 45.0 w% magnetite slurry (Experiment set 2)

1. test			2. test			3. test		
t, s	h, cm	Ψ, kg·m^{-2}·s^{-1}	t, s	h, cm	Ψ, kg·m^{-2}·s^{-1}	t, s	h, cm	Ψ, kg·m^{-2}·s^{-1}
20	16.50	12.88	20	16.50	12.88	15	16.50	17.18
27	16.00	9.25	26	16.00	9.61	20	16.00	12.49
34	15.50	7.12	33	15.50	7.34	27	15.50	8.97
41	15.00	5.71	40	15.00	5.86	32	15.00	7.32
48	14.50	4.72	47	14.50	4.82	38	14.50	5.96
55	14.00	3.98	54	14.00	4.05	45	14.00	4.86
63	13.50	3.35	62	13.50	3.40	52	13.50	4.05
70	13.00	2.90	69	13.00	2.94	59	13.00	3.44
77	12.50	2.54	77	12.50	2.54	67	12.50	2.91
85	12.00	2.20	84	12.00	2.23	74	12.00	2.53
93	11.50	1.93	92	11.50	1.95	83	11.50	2.16
100	11.00	1.72	99	11.00	1.74	91	11.00	1.89
108	10.50	1.52	108	10.50	1.52	100	10.50	1.64
117	10.00	1.33	117	10.00	1.33	110	10.00	1.42

4. test		
t, s	h, cm	Ψ, kg·m^{-2}·s^{-1}
22	16.50	11.71
28	16.00	8.92
35	15.50	6.92
42	15.00	5.58
49	14.50	4.62
56	14.00	3.90
63	13.50	3.35
71	13.00	2.86
78	12.50	2.50
145	12.00	1.29
93	11.50	1.93
100	11.00	1.72
107	10.50	1.53
117	10.00	1.33

Sedimentation of the 35.0 w% magnetite slurry (Experiment set 2)

1. test			2. test			3. test		
t, s	h, cm	Ψ, $kg \cdot m^{-2} \cdot s^{-1}$	t, s	h, cm	Ψ, $kg \cdot m^{-2} \cdot s^{-1}$	t, s	h, cm	Ψ, $kg \cdot m^{-2} \cdot s^{-1}$
18	19		9	19	29.35	8	19	33.02
29	18		14	18	17.88	12	18	20.86
42	17			17			17	
19	16	11.71	25	16	8.90	24	16	9.27
25	15	8.34	31	15	6.73	30	15	6.95
31	14	6.28	37	14	5.26	36	14	5.41
37	13	4.88	43	13	4.20	42	13	4.30
44	12	3.79	50	12	3.34	49	12	3.40
51	11	3.00	56	11	2.73	56	11	2.73
59	10	2.36	64	10	2.17	64	10	2.17
70	9	1.79	72	9	1.74	73	9	1.71
			86	8	1.29	88	8	1.26
			105	7	0.93	106	7	0.92
			137	6	0.61	118	6,5	0.77
						142	6	0.59

4. test		
t, s	h, cm	Ψ, $kg \cdot m^{-2} \cdot s^{-1}$
8	19	33.02
13	18	19.25
	17	
25	16	8.90
32	15	6.52
38	14	5.12
45	13	4.02
51	12	3.27
58	11	2.64
65	10	2.14
75	9	1.67
89	8	1.25
108	7	0.90
120	6,5	0.75
142	6	0.59

1_s1_45 (69/31)	Particle size, µm					PSD width, -
Coarse	Dx(10)	Dx(50)	Dx(90)	D[3;2]	D[4;3]	(Dx(90)-Dx(10))/Dx(50)
	37,6	76	136	41,9	81,3	1,29

1_s1_45 (69/31)	Particle size, µm					PSD width, -
Fine	Dx(10)	Dx(50)	Dx(90)	D[3;2]	D[4;3]	(Dx(90)-Dx(10))/Dx(50)
	3,84	15,3	45,3	8,45	20,6	2,71

2_s4_38 (66/34)	Particle size, µm					PSD width, -
Coarse	Dx(10)	Dx(50)	Dx(90)	D[3;2]	D[4;3]	(Dx(90)-Dx(10))/Dx(50)
	11,2	73	159	24,2	86,8	2,02

2_s4_38 (66/34)	Particle size, µm					PSD width, -
Fine	Dx(10)	Dx(50)	Dx(90)	D[3;2]	D[4;3]	(Dx(90)-Dx(10))/Dx(50)
	3,8	15,6	46,5	8,51	21,6	2,74

3_s3_75 (86/14)	Particle size, µm					PSD width, -
Coarse	Dx(10)	Dx(50)	Dx(90)	D[3;2]	D[4;3]	(Dx(90)-Dx(10))/Dx(50)
	75,2	132	230	54,2	148	1,17

3_s3_75 (86/14)	Particle size, µm					PSD width, -
Fine	Dx(10)	Dx(50)	Dx(90)	D[3;2]	D[4;3]	(Dx(90)-Dx(10))/Dx(50)
	4,04	17,5	59,3	9,14	25,5	3,16

4_s5_45 (69/31)	Particle size, µm					PSD width, -
Coarse	Dx(10)	Dx(50)	Dx(90)	D[3;2]	D[4;3]	(Dx(90)-Dx(10))/Dx(50)
	18	80,3	161	26,8	90,4	1,78

4_s5_45 (69/31)	Particle size, µm					PSD width, -
Fine	Dx(10)	Dx(50)	Dx(90)	D[3;2]	D[4;3]	(Dx(90)-Dx(10))/Dx(50)
	3,8	15,6	46,4	8,49	21	2,73

5_s6_75 (86/14)	Particle size, µm					PSD width, -
Coarse	Dx(10)	Dx(50)	Dx(90)	D[3;2]	D[4;3]	(Dx(90)-Dx(10))/Dx(50)
	52,4	131	243	34,3	141	1,45

5_s6_75 (86/14)	Particle size, µm					PSD width, -
Fine	Dx(10)	Dx(50)	Dx(90)	D[3;2]	D[4;3]	(Dx(90)-Dx(10))/Dx(50)
	4,11	20,1	67,4	9,68	28,8	3,15

6_s7_38 (68/32)	Particle size, µm					PSD width, -
Coarse	Dx(10)	Dx(50)	Dx(90)	D[3;2]	D[4;3]	(Dx(90)-Dx(10))/Dx(50)
	4,57	49	92,9	12,8	48	1,80

6_s7_38 (68/32)	Particle size, µm					PSD width, -
Fine	Dx(10)	Dx(50)	Dx(90)	D[3;2]	D[4;3]	(Dx(90)-Dx(10))/Dx(50)
	3,77	14,9	42,7	8,28	19,9	2,61

7_s8_45 (69/31)	Particle size, µm					PSD width, -
Coarse	Dx(10)	Dx(50)	Dx(90)	D[3;2]	D[4;3]	(Dx(90)-Dx(10))/Dx(50)
	44,6	90,5	175	41,7	101	1,44

7_s8_45 (69/31)	Particle size, µm					PSD width, -
Fine	Dx(10)	Dx(50)	Dx(90)	D[3;2]	D[4;3]	(Dx(90)-Dx(10))/Dx(50)
	3,87	16,1	47	8,63	21,4	2,68

8_s9_75 (86/14)	Particle size, µm					PSD width, -
Coarse	Dx(10)	Dx(50)	Dx(90)	D[3;2]	D[4;3]	(Dx(90)-Dx(10))/Dx(50)
	64,9	134	258	40,5	149	1,44

8_s9_75 (86/14)	Particle size, µm					PSD width, -
Fine	Dx(10)	Dx(50)	Dx(90)	D[3;2]	D[4;3]	(Dx(90)-Dx(10))/Dx(50)
	3,96	19,2	65,8	9,37	27,8	3,22

9_s10_38 (66/34)	Particle size, µm					PSD width, -
Coarse	Dx(10)	Dx(50)	Dx(90)	D[3;2]	D[4;3]	(Dx(90)-Dx(10))/Dx(50)
	5,97	65,3	142	17,5	71,3	2,08

9_s10_38 (66/34)	Particle size, µm					PSD width, -
Fine	Dx(10)	Dx(50)	Dx(90)	D[3;2]	D[4;3]	(Dx(90)-Dx(10))/Dx(50)
	3,87	16,1	48,3	8,67	22,1	2,76

10_s11_45 (69/31)	Particle size, µm					PSD width, -
Coarse	Dx(10)	Dx(50)	Dx(90)	D[3;2]	D[4;3]	(Dx(90)-Dx(10))/Dx(50)
	40,6	86,7	176	35	101	1,56

10_s11_45 (69/31)	Particle size, µm					PSD width, -
Fine	Dx(10)	Dx(50)	Dx(90)	D[3;2]	D[4;3]	(Dx(90)-Dx(10))/Dx(50)
	4,02	16,4	46,4	8,89	21,4	2,58

13_s14_45 (66/34) *Coarse*	Particle size, µm					PSD width, -
	Dx(10)	Dx(50)	Dx(90)	D[3;2]	D[4;3]	(Dx(90)-Dx(10))/Dx(50)
	26,9	78,7	162	27,9	91,3	1,72

13_s14_45 (66/34) *Fine*	Particle size, µm					PSD width, -
	Dx(10)	Dx(50)	Dx(90)	D[3;2]	D[4;3]	(Dx(90)-Dx(10))/Dx(50)
	3,97	15,7	44,8	8,63	20,7	2,60

14_s15_38 (66/34) *Coarse*	Particle size, µm					PSD width, -
	Dx(10)	Dx(50)	Dx(90)	D[3;2]	D[4;3]	(Dx(90)-Dx(10))/Dx(50)
	8	71,3	159	21,5	84	2,12

14_s15_38 (66/34) *Fine*	Particle size, µm					PSD width, -
	Dx(10)	Dx(50)	Dx(90)	D[3;2]	D[4;3]	(Dx(90)-Dx(10))/Dx(50)
	3,88	16	48,7	8,62	22,4	2,80

15_s16_75 (86/14) *Coarse*	Particle size, µm					PSD width, -
	Dx(10)	Dx(50)	Dx(90)	D[3;2]	D[4;3]	(Dx(90)-Dx(10))/Dx(50)
	58,6	130	239	35,8	141	1,39

15_s16_75 (86/14) *Fine*	Particle size, µm					PSD width, -
	Dx(10)	Dx(50)	Dx(90)	D[3;2]	D[4;3]	(Dx(90)-Dx(10))/Dx(50)
	4,19	21,4	69,9	10,1	29,9	3,07

			Fine fraction (F)		Coarse fraction (C)		
Filtration	Sieve batch (µm)	(F/C), w%	$F_{magn.}$, g	F_{water}, g	$C_{magn.}$, g	C_{water}, g	Σ Batch, g
1_s1_45	1 (45)	69/31	319	244	135	103	802
			Σ Fine, g	Magn. w%	*Σ Coarse, g*	Magn. w%	
			563	56,7	238	56,7	
			Fine fraction (F)		Coarse fraction (C)		
Filtration	Sieve batch (µm)	(F/C), w%	$F_{magn.}$, g	F_{water}, g	$C_{magn.}$, g	C_{water}, g	Σ Batch, g
2_s4_38	4 (38)	66/34	298	228	156	119	802
			Σ Fine, g	Magn. w%	*Σ Coarse, g*	Magn. w%	
			526	56,7	275	56,7	
			Fine fraction (F)		Coarse fraction (C)		
Filtration	Sieve batch (µm)	(F/C), w%	$F_{magn.}$, g	F_{water}, g	$C_{magn.}$, g	C_{water}, g	Σ Batch, g
3_s3_75	3 (75)	86/14	399	304	56	43	802
			Σ Fine, g	Magn. w%	*Σ Coarse, g*	Magn. w%	
			703	56,7	98	56,7	
			Fine fraction (F)		Coarse fraction (C)		
Filtration	Sieve batch (µm)	(F/C), w%	$F_{magn.}$, g	F_{water}, g	$C_{magn.}$, g	C_{water}, g	Σ Batch, g
4_s5_45	5 (45)	69/31	314	240	141	108	802
			Σ Fine, g	Magn. w%	*Σ Coarse, g*	Magn. w%	
			553	56,7	248	56,7	
			Fine fraction (F)		Coarse fraction (C)		
Filtration	Sieve batch (µm)	(F/C), w%	$F_{magn.}$, g	F_{water}, g	$C_{magn.}$, g	C_{water}, g	Σ Batch, g
5_s6_75	6 (75)	86/14	391	299	63	48	802
			Σ Fine, g	Magn. w%	*Σ Coarse, g*	Magn. w%	
			690	56,7	112	56,7	

			Fine fraction (F)		Coarse fraction (C)		
Filtration	Sieve batch (µm)	(F/C), w%	$F_{magn.}$, g	F_{water}, g	$C_{magn.}$, g	C_{water}, g	Σ Batch, g
6_s7_38	7 (38)	68/32	309	236	145	111	802
			Σ Fine, g	Magn. w%	*Σ Coarse, g*	Magn. w%	
			545	56,7	256	56,7	
			Fine fraction (F)		Coarse fraction (C)		
Filtration	Sieve batch (µm)	(F/C), w%	$F_{magn.}$, g	F_{water}, g	$C_{magn.}$, g	C_{water}, g	Σ Batch, g
7_s8_45	8 (45)	69/31	314	239	141	108	802
			Σ Fine, g	Magn. w%	*Σ Coarse, g*	Magn. w%	
			553	56,7	249	56,7	
			Fine fraction (F)		Coarse fraction (C)		
Filtration	Sieve batch (µm)	(F/C), w%	$F_{magn.}$, g	F_{water}, g	$C_{magn.}$, g	C_{water}, g	Σ Batch, g
8_s9_75	9 (75)	86/14	392	300	62	48	802
			Σ Fine, g	Magn. w%	*Σ Coarse, g*	Magn. w%	
			692	56,7	110	56,7	

			Fine fraction (F)		Coarse fraction (C)		
Filtration	Sieve batch (µm)	(F/C), w%	$F_{magn.}$, g	F_{water}, g	$C_{magn.}$, g	C_{water}, g	Σ Batch, g
9_s10_38	10 (38)	66/34	299	229	155	119	802
			Σ Fine, g	Magn. w%	*Σ Coarse, g*	Magn. w%	
			528	56,7	274	56,7	
			Fine fraction (F)		Coarse fraction (C)		
Filtration	Sieve batch (µm)	(F/C), w%	$F_{magn.}$, g	F_{water}, g	$C_{magn.}$, g	C_{water}, g	Σ Batch, g
10_s11_45	11 (45)	69/31	313	239	141	108	802
	Settling 1.5 min both fractions		*Σ Fine, g*	Magn. w%	*Σ Coarse, g*	Magn. w%	
			553	56,7	249	56,7	

			Fine fraction (F)		Coarse fraction (C)		
Filtration	Sieve batch (µm)	(F/C), w%	$F_{magn.}$, g	F_{water}, g	$C_{magn.}$, g	C_{water}, g	Σ Batch, g
13_s14_45	14 (45)	66/34	301	230	154	118	802
			Σ Fine, g	Magn. w%	*Σ Coarse, g*	Magn. w%	
			530	56,7	271	56,7	
			Fine fraction (F)		Coarse fraction (C)		
Filtration	Sieve batch (µm)	(F/C), w%	$F_{magn.}$, g	F_{water}, g	$C_{magn.}$, g	C_{water}, g	Σ Batch, g
14_s15_38	15 (38)	66/34	301	230	153	117	802
	Settling 1.5 min both fractions		*Σ Fine, g*	Magn. w%	*Σ Coarse, g*	Magn. w%	
			531	56,7	270	56,7	
			Fine fraction (F)		Coarse fraction (C)		
Filtration	Sieve batch (µm)	(F/C), w%	$F_{magn.}$, g	F_{water}, g	$C_{magn.}$, g	C_{water}, g	Σ Batch, g
15_s16_75	16 (75)	86/14	391	299	64	49	802
	Settling 1.5 min both fractions		*Σ Fine, g*	Magn. w%	*Σ Coarse, g*	Magn. w%	
			689	56,7	112	56,7	

Sample number	$V_{Pores\ in\ the\ cake}$, m^3	Average cake thickness, m	$V_{Wet\ cake}$, m^3	$V_{Dry\ cake}$, m^3
1_s1_45 (69/31)	7,20E-05	0,01655	1,63E-04	8,90E-05
2_s4_38 (66/34)	7,00E-05	0,01620	1,60E-04	8,79E-05
3_s3_75 (86/14)	7,04E-05	0,01584	1,56E-04	8,97E-05
4_s5_45 (69/31)	6,98E-05	0,01576	1,55E-04	8,55E-05
5_s6_75 (86/14)	7,01E-05	0,01666	1,64E-04	9,00E-05
6_s7_38 (68/32)	7,01E-05	0,01690	1,66E-04	9,08E-05
7_s8_45 (69/31)	6,23E-05	0,01450	1,43E-04	7,86E-05
8_s9_75 (86/14)	6,11E-05	0,01416	1,39E-04	7,74E-05
9_s10_38 (66/34)	6,72E-05	0,01642	1,62E-04	8,84E-05
10_s11_45 (69/31)	7,14E-05	0,01638	1,61E-04	8,87E-05
13_s14_45 (66/34)	7,23E-05	0,01737	1,71E-04	9,07E-05
14_s15_38 (66/34)	7,07E-05	0,01584	1,56E-04	8,83E-05
15_s16_75 (86/14)	7,10E-05	0,01593	1,57E-04	9,09E-05

Sample number	$m_{Filtrate}$, kg	$m_{Wet\ cake}$, kg	$m_{Dry\ cake}$, kg	$V_{Filtrate}$, m^3
1_s1_45 (69/31)	0,25935	0,50368	0,43164	2,59E-04
2_s4_38 (66/34)	0,26959	0,49630	0,42626	2,70E-04
3_s3_75 (86/14)	0,26896	0,50542	0,43503	2,69E-04
4_s5_45 (69/31)	0,26188	0,48413	0,41436	2,62E-04
5_s6_75 (86/14)	0,26475	0,50636	0,43630	2,65E-04
6_s7_38 (68/32)	0,27427	0,51035	0,44024	2,74E-04
7_s8_45 (69/31)	0,25847	0,44317	0,38090	2,58E-04
8_s9_75 (86/14)	0,26214	0,43660	0,37552	2,62E-04
9_s10_38 (66/34)	0,27581	0,49587	0,42869	2,76E-04
10_s11_45 (69/31)	0,26131	0,50131	0,42988	2,61E-04
13_s14_45 (66/34)	0,27165	0,51204	0,43971	2,72E-04
14_s15_38 (66/34)	0,26388	0,49908	0,42840	2,64E-04
15_s16_75 (86/14)	0,26777	0,51191	0,44088	2,68E-04

Sample number	c, $m_{Dry\ cake} \cdot V^{-1}_{Filtrate}$	Filtration time, s	Filtration time, h
1_s1_45 (69/31)	1649,86	54	0,015
2_s4_38 (66/34)	1608,41	53	0,015
3_s3_75 (86/14)	1606,46	65	0,018
4_s5_45 (69/31)	1529,98	55	0,015
5_s6_75 (86/14)	1609,27	67	0,019
6_s7_38 (68/32)	1656,89	52	0,014
7_s8_45 (69/31)	1362,09	45	0,013
8_s9_75 (86/14)	1356,84	62	0,017
9_s10_38 (66/34)	1538,42	54	0,015
10_s11_45 (69/31)	1645,10	92	0,026
13_s14_45 (66/34)	1653,84	54	0,015
14_s15_38 (66/34)	1623,47	99	0,028
15_s16_75 (86/14)	1646,49	113	0,031

Sedimentation of the 56.7 w% fine fraction magnetite slurry (particle Dx(50)=18 μm)

1. test			2. test			3. test		
t, s	h, cm	Ψ, $kg \cdot m^{-2} \cdot s^{-1}$	t, s	h, cm	Ψ, $kg \cdot m^{-2} \cdot s^{-1}$	t, s	h, cm	Ψ, $kg \cdot m^{-2} \cdot s^{-1}$
0	15		0	15		0	15	
52	14,5	5,13		14,5			14,5	
120	14	2,15		14			14	
170	13,5	1,46	52	13,5	4,77		13,5	
218	13	1,10	86	13	2,78	66	13	3,62
255	12,5	0,90	138	12,5	1,67	171	12,5	1,34
	12		183	12	1,21	243	12	0,91
292	11,5	0,72	254	11,5	0,83	330	11,5	0,64
			370	11	0,55	470	11	0,43

4. test			5. test		
t, s	h, cm	Ψ, $kg \cdot m^{-2} \cdot s^{-1}$	t, s	h, cm	Ψ, $kg \cdot m^{-2} \cdot s^{-1}$
0	14,75		0	14,75	
	14,5			14,5	
90	14	2,86	100	14	2,57
157	13,5	1,58	160	13,5	1,55
190	13	1,26	210	13	1,14
230	12,5	1,00		12,5	
265	12	0,83	275	12	0,80
290	11,5	0,73		11,5	
330	11	0,61	380	11	0,53

Sedimentation of the 56.7 w% coarse fraction magnetite slurry (particle Dx(50)=85.8 μm)

1. test			2. test			3. test		
t, s	h, cm	Ψ, $kg \cdot m^{-2} \cdot s^{-1}$	t, s	h, cm	Ψ, $kg \cdot m^{-2} \cdot s^{-1}$	t, s	h, cm	Ψ, $kg \cdot m^{-2} \cdot s^{-1}$
0	15		0	15		0	15	
18	9,5	9,70	16	9,5	10,92	17	9,5	10,28
35	7,25	3,81	31	7,25	4,30	34	7,25	3,92

4. test			5. test			6. test		
t, s	h, cm	Ψ, $kg \cdot m^{-2} \cdot s^{-1}$	t, s	h, cm	Ψ, $kg \cdot m^{-2} \cdot s^{-1}$	t, s	h, cm	Ψ, $kg \cdot m^{-2} \cdot s^{-1}$
0	15		0	15		0	15	
10	9,5	17,47	18	9,5	9,70	19	9,5	9,19
26	7,25	5,13	34	7,25	3,92	36	7,25	3,70

7. test		
t, s	h, cm	Ψ, $kg \cdot m^{-2} \cdot s^{-1}$
0	15	
19	9,5	9,19
37	7,25	3,60

Sedimentation of the Fine/Coarse (66/34) w% fraction magnetite slurry (magnetite concentration 56.7 w%)

1. test			2. test			3. test		
t, s	h, cm	Ψ, $kg \cdot m^{-2} \cdot s^{-1}$	t, s	h, cm	Ψ, $kg \cdot m^{-2} \cdot s^{-1}$	t, s	h, cm	Ψ, $kg \cdot m^{-2} \cdot s^{-1}$
	15,5			15,5			15,5	
27	15	10,22	25	15	11,03		15	
43	14,5	6,20	44	14,5	6,06	45	14,5	5,93
60	14	4,29	60	14	4,29	60	14	4,29
80	13,5	3,10	77	13,5	3,22	79	13,5	3,14
97	13	2,46	93	13	2,57	95	13	2,52
117	12,5	1,96	113	12,5	2,03	114	12,5	2,02
135	12	1,63	133	12	1,66	131	12	1,68
152	11,5	1,39	149	11,5	1,42	148	11,5	1,43
168	11	1,20	164	11	1,23	164	11	1,23
183	10,5	1,06	177	10,5	1,09	177	10,5	1,09
197	10	0,93	191	10	0,96	191	10	0,96
209	9,5	0,84	203	9,5	0,86	202	9,5	0,86
227	9	0,73	221	9	0,75	220	9	0,75